Nonlinear Dynamics of Railway Wheelsets Incorporating Randomness

By: Jing Yu

Supervised by: Dr. Meilan Liu

Co-Supervised by: Dr. Alexander Sedov

A Thesis submitted to the Faculty of Graduate Studies

in partial fulfillment of the requirements for the

Master of Science in Engineering Degree in

Control Engineering

Lakehead University

July, 2007

Your file Votre référence
ISBN: 978-0-494-31843-0
Our file Notre référence
ISBN: 978-0-494-31843-0

ABSTRACT

The thesis is to investigate the dynamic behavior of a single-axle railway wheelset and identify its chaotic behavior by means of time history, phase portrait, Lyapunov exponents, information dimension, bifurcation diagram and control strategy.

The thesis has its analytical and computational components. For the analytical component, several mathematical models of a single-axle rail vehicle wheelset are presented in order to compare their features for similarities and differences. These models present different contact theories of creep force, and have different parametric values. In addition, Model III does not consider gravitational stiffnesses and gyroscopic couple. As a result, directly comparing simulation results of these models makes it difficult to interpret results and to draw conclusions. Therefore, these models need to be expanded so that issues can be isolated and investigated accordingly. Randomness is introduced and becomes an integral part of the models. The latter step is necessary because any physical system is realistically operating under stochastic conditions. Randomness is introduced by the means of pseudo-random numbers whose characteristic is also discussed. For the computational component, the time history and phase portrait of the wheelset models and their combinations are used to examine the models for similarities and differences. The focus, however, is to employ Lyapunov exponents, information dimensions and bifurcation diagrams to study the effect of randomness in forward speed, or lateral clearance (dead band), or both forward speed and dead band, on the chaotic behavior of

the single-axle wheelset. Results obtained show that Model IIb is the best model; Model III is also a good choice, especially when lacking wheelset data. Numerical simulations indicate that chaotic motion depends upon forward speed, yaw stiffness and the level of randomness. Increasing forward speed and the level of randomness seem to lead to chaos in the wheelset which may further lead to chaos in the railway vehicle system. However, increasing yaw stiffness can suppress the chaotic oscillations.

Toward the goal of chaos suppression, two control strategies are investigated: semi-active control and active control. Simulation results show that both can suppress chaos and control bifurcation pattern of the wheelset. Finally, the thesis concludes with some recommendations for future work.

ACKNOWLEDGMENTS

I would like to express my appreciation to my supervisor Dr. Meilan Liu, for her patient advice and many discussions during the course of my research and for her guidance in organizing the material presented in this thesis. Especially, her encouragement and counsel at critical moments during my studies are greatly appreciated. Appreciation is also due to Dr. Alexander Sedov, my co-supervisor, who also provided valuable input into the preparation of this thesis. Special thanks go to the examiners, Dr. Hao Bai (internal) and Dr. Shudong Yu (external), for devoting their effort and time to review and make suggestions to my work and helping me to finalize the details. I also wish to express my gratitude to Dr. Xiaoping Liu and Dr. Abdelhamid Tayebi for their valuable lectures that introduced me to the modern control concepts. Finally, I acknowledge the encouragement, patience, and support of my family.

This work was partially supported by my advisor through her Discovery Grant funded by the Natural Sciences and Engineering Research Council (NSERC) of Canada.

TABLE OF CONTENTS

LIST OF TABLES

LIST OF FIGURES

LIST OF APPENDICES

Chapter 1

INTRODUCTION

1.1 Background

The history of the usage of rail vehicles in Europe dates back to the 18th century with the development of first wooden and then steel railed wagon-ways on which carts were drawn with horses. These wagon-ways evolved into tramways. Flanged wheels were introduced to rail vehicles in 1789 by William Jessup, as was told by Reference [1.1]. In the early 19th century steam power was introduced to these vehicles. Eventually the steam locomotives replaced the horses as the source of propulsion power. The growth of the railways and the transportation network that they provided facilitated the industrial revolution.

It has been known for more than a century that railway vehicles lose their lateral stability above a certain critical speed, which depends on many parameters [1.2]. The railway industry has made great effort to investigate this problem with the aim of building vehicles that can run at higher and higher speeds on the railway lines while maintaining their lateral stability. In recent years, minimization of wheel and rail wear has also become an important consideration in the design process. Wheel and rail wear has been shown to be linked to the dynamic behavior of railway vehicles [1.3-1.4].

The dynamics of railway vehicles have been of practical interest for many decades. The review paper by Shabana and Sany [1.5] provided an excellent examination of a

number of fundamental issues of railroad vehicle dynamics. They included: (1) flexibility effects due to rail and track flexibility, flexibility of suspensions, and flexibility of car body and joints; (2) wheel and rail interaction due to the rolling and slipping contact between the profiled surfaces of the wheel and rail; and (3) modeling considerations such as linear versus nonlinear models, linearization, effects due to pre-mature linearization, and so on. They concluded that "the interaction between railroad vehicle and track is an important area of study in railroad research". They also found that the use of computer multi-body simulations "requires consideration of many factors such as truck (or bogie) suspensions, side-bearing clearance, the roll mass moment of inertia, the car body mass, the truck mass, the type of lading, the track extreme roughness, the vehicle resonant speed, the maximum peak-to-peak roll angle, the possible buff or draft force from adjacent cars, coupler type, the induced dynamics from track and adjacent cars, track gauge, and track spacing."

The early research on the dynamic stability of railway vehicles seems to date back to the 1960s and to work by DePater [1.6], Matsudaira [1.7] and Wickens [1.8]. Such early work led to a new wave of investigations, as attested in articles by Cooperrider [1.4], by Huilgol [1.9] which appeared to be the first bifurcation analysis of a free running wheelset, and so on. On the other hand, by 19922 Carter [1.10] had developed the two-dimensional theory of rolling contact with friction for application to railway vehicle dynamics. Carter gave an exact closed-form solution for the relation between longitudinal creep and tangential force. Johnson [1.11] extended Carter's two dimensional rolling contact theory

to a three-dimensional one dealing with two rolling spheres. Johnson's theory included the longitudinal and lateral creepages, however spin creep was not considered. Later, Vermeulen and Johnson [1.12] extended the work in [1.11] to pure creepage between two arbitrary smooth half-spaces. Again, spin creep was excluded. Wickens [1.8] examined the instability of profiled wheels rather than purely conical wheels. He derived the equations of motion of elastically restrained wheelset and studied the stability under varying parameters.

The hunting behavior of conventional railway trucks was examined by Cooperrider [1.13]. Hunting refers to the swaying motion of a railway vehicle (Figure 1.1). It is caused by the coning action (Figure 1.2) on which the directional stability of the vehicle depends. As shown in Figure 1.2, lateral displacement causes the left and right wheels to ride with different radii, resulting in the wheelset to turn to left or to right. The swaying motion is at times large enough to cause the wheel flange to impact upon the rail. Above a certain critical speed, the swaying motion can be violent, damaging track and wheels, and potentially causing derailment. Cooperrider determined the influence of nonlinear effects on stability and the characteristics of the hunting motion, and described the effects of flange contact, wheel slip and Coulomb friction by some nonlinear expressions. A theoretical model for wheelset force and displacement relations in tread and flange contact was analyzed by Sweet and Sivak [1.14]. The analysis included a number of issues such as nonlinear geometric constraints for the wheel-rail contact, and creep forces in the contact

plane due to wheel and rail differential velocities. Lohe and Huilgol discovered an asymmetric oscillation using a numerical simulation [1.15].

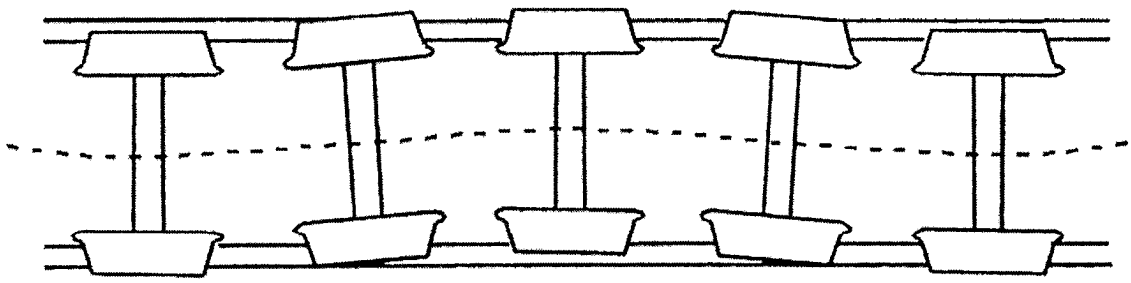

Figure 1.1 Hunting or swaying motion of rail vehicles

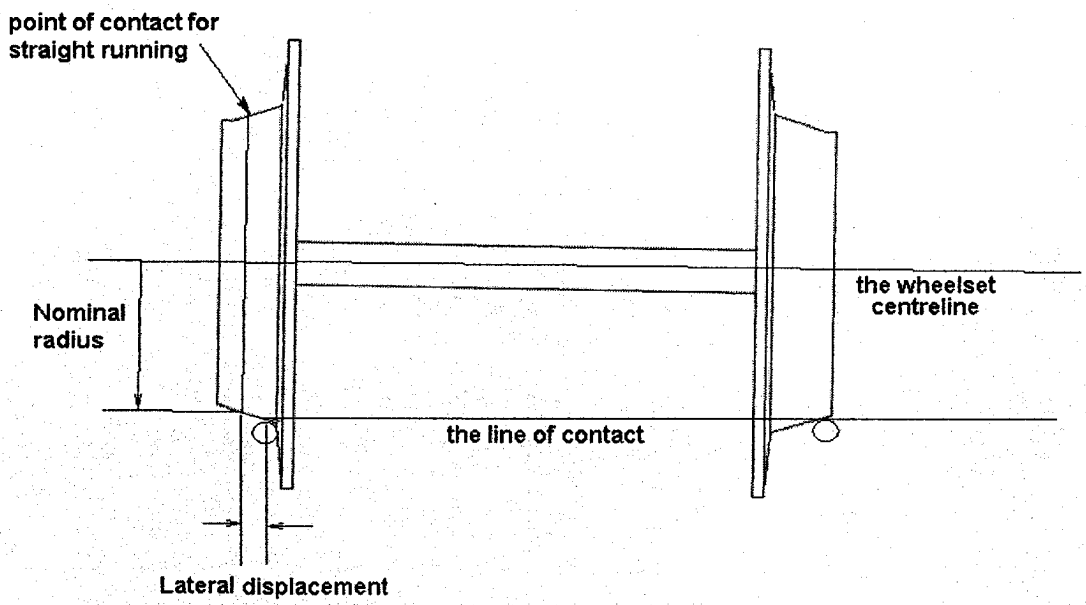

Figure 1.2 Railway wheel coning action

Railway vehicles have also been known to experience chaotic motion. The chaotic motion of a railway wheelset, with wheels having cylindrical tires, moving at a constant forward velocity, was investigated by Meizard and DePater [1.16]. They found two kinds of principal motion: one in which flange contact took place at only one rail and the other in which flange contact occurred at both rails. Or simply put, there was a bifurcation. Using

Vermeulen and Johnson's contact theory, Knudsen et al. [1.17] analyzed a model of suspended rolling railway wheelset. They examined the effect of speed and suspension on the dynamics of the wheelset. The results were presented in the forms of time series and bifurcation diagrams. Knudsen's work was continued by Silvsaard and True [1.18] who identified the periodic windows in the selected forward speed region.

A number of recent publications looked at the interaction between rail vehicle, rail track and passengers with ride comfort as the primary interest. For example, Carlbom [1.19] investigated the interaction by combining the two dynamical systems, car body and bogies, and car body and passengers. The entire car body was modeled by ANSYS. Passengers were treated as single-degree-of-freedom models, and seats and seat cushions were included in the model as well. The software package GENSYS then pieced together the car body, passengers and so on.

Controlling bifurcation as well as chaos in dynamical systems has seen rapid advances in the past decade. For example, bifurcation control was achieved by some controllers that were designed to control the bifurcation route that led to chaos [1.20-1.21]. Different techniques have been developed for the control of chaotic dynamical systems. References [1.22-1.23] employed a small amplitude control law in a restricted region of the state space, thereby stabilizing a pre-existing equilibrium or periodic orbit. Classical control methods were used by many [1.24-1.28]. Non-local linear or nonlinear feedback was utilized [1.29-1.30] to stabilize nominal equilibrium points. A new recursive back-stepping nonlinear controller was proposed [1.31] where a comparison was made

between the proposed controller and the pole placement control design. Finally, methods involving semi-active and active controls of the primary longitudinal stiffness were developed to raise the critical velocity of the wheelset [1.32].

1.2 Objectives

The investigation reported in this thesis is motivated by the continued need to improve ride quality and to reduce wear and damage to the vehicles and track. One of the demonstrated problems in this area is that railway vehicles, under certain conditions, experience erratic motions, or chaotic behavior. Chaotic vibration is accompanied by large dynamic loads between the vehicle and track which can damage the vehicle and track as well as contribute to passenger discomfort. Therefore, from the perspective of practical engineering applications, understanding and identifying the causes of chaotic behaviors in railway vehicles will assist engineers in the task of minimizing undesirable behaviors, hence reducing material wear and damage, and enhancing ride quality. A better ride quality translates into passengers enjoying the rail ride, or goods being transported with minimal damage.

Chaotic motions arise in nonlinear dynamic systems. Nonlinear dynamics remains an area of intense research. A proper modeling of rail vehicles with accurate quantification of their dynamic responses and identification of the causes of possible chaotic behaviors remain important and challenging tasks.

Specifically, this thesis investigates the dynamics of a simplified railway freight vehicle running on an ideal straight track and on a single-axle wheelset. The single-axle wheelset is chosen because it is the fundamental element in railway vehicles. Second, due to weight reduction demands there is a growing interest in the railway industry to replace the conventional two-axle truck (bogie) by the single-axle wheelset. In addition, once the single-axle wheelsets are well understood, it will make easier the task of investigating the two-axle counterpart. Therefore, the objectives of the present study are, (1) to compare existing mathematical models of single-axle wheelsets; (2) to identify the differences in the models and the resulting differences in the predicted dynamic behaviors; (3) to introduce randomness to the models by means of pseudo-random numbers; (4) to gain understanding of the dynamic behaviors of the wheelsets, and understanding of the effect of randomness on the systems; (5) to identify any damage-inducing conditions, operating or otherwise; and (6) to implement control strategies to circumvent hunting instability.

It should be pointed out that the necessity of introducing randomness to the wheelset models comes from the fact that a wheelset, similar to any other physical system, operates under not-so-deterministic conditions. It is nearly impossible to expect, for example, the wheelset to travel with constant, thus deterministic, speed. The uneven wear between wheel flanges and sides of the rails causes varying lateral clearance or dead band. There also exists uneven wear between the wheels and tops of the rails that will cause the contact profile of the wheels to deviate from the expected conical shape form.

1.3 Organization of the Thesis

The thesis consists of six chapters. Chapter 1 is the introduction. In Chapter 2, mathematical models are described. The corresponding equations of motion are then verified and presented. Chapter 3 deals with pseudo-random number generation and Monte Carlo simulation. Chapter 4 presents the fundamentals of chaotic motion, and then proceeds with numerical results pertaining to Lyapunov exponents and information dimensions. Chapter 5 deals with control strategies. The final chapter, Chapter 6, presents the conclusions and recommendations for future work.

1.4 Terminologies

Relevant terminologies are introduced here.

Axle: a central shaft on which a set of rotating wheels are mounted.

Wheelset: an axle and two wheels that are mounted on the axle (Figure 1.3)

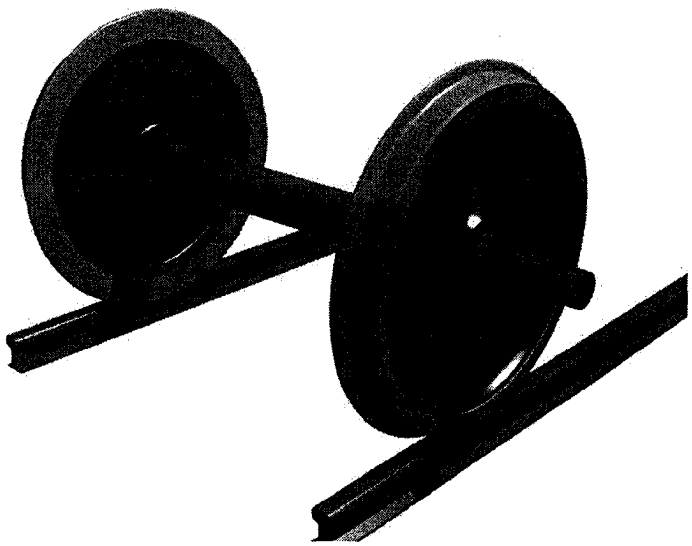

Figure 1.3 Railway wheelset

Bogie (in the U.K.) or **Truck** (in the U.S.): a structure underneath a train to which wheel axles and wheels are attached. Typically there are single-axle trucks (Figure 1.4), two-axle trucks (Figure 1.5) and triple-axle trucks (Figure 1.6).

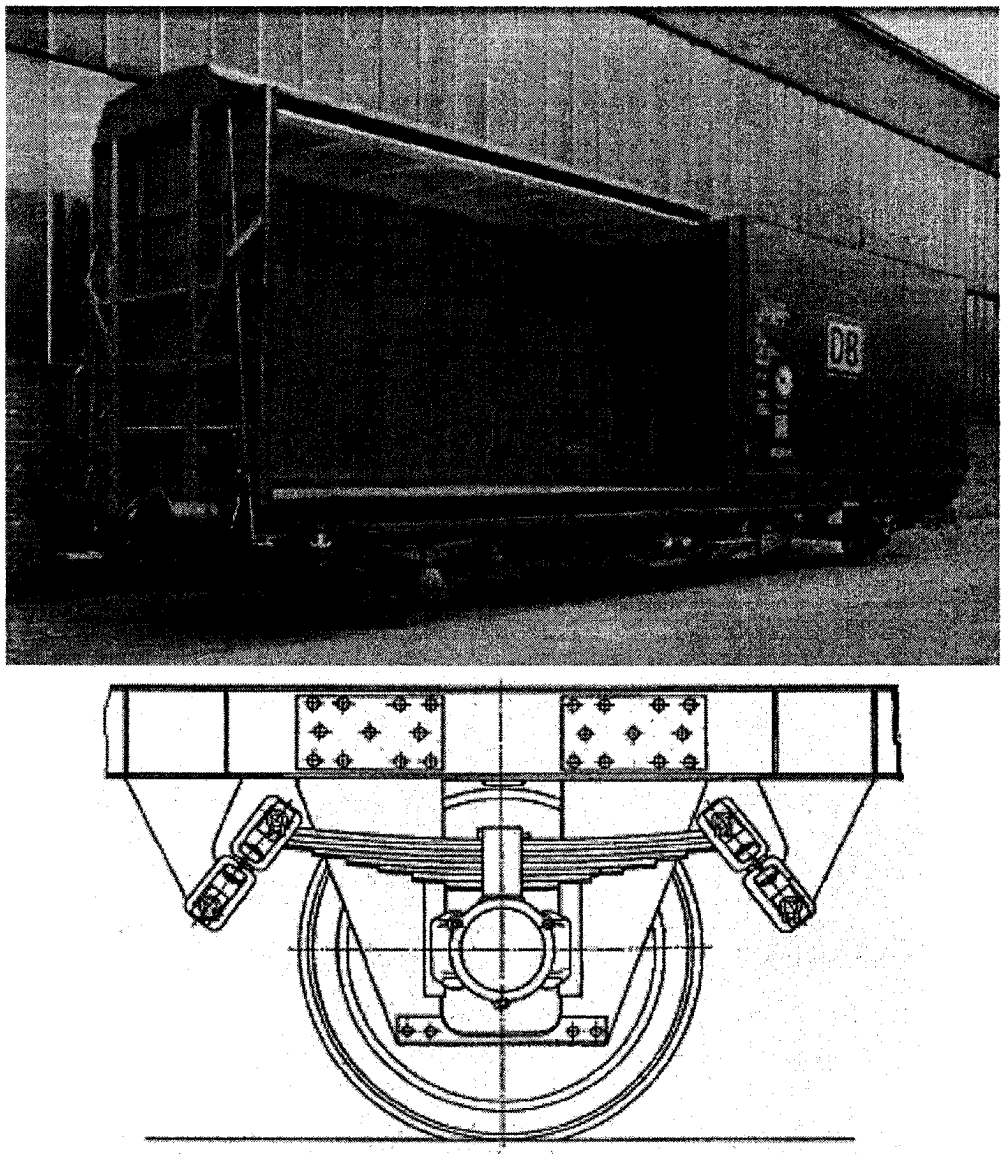

Figure 1.4 (Top) A box car supported by single-axle trucks ; (Bottom) Major components in a single-axle truck

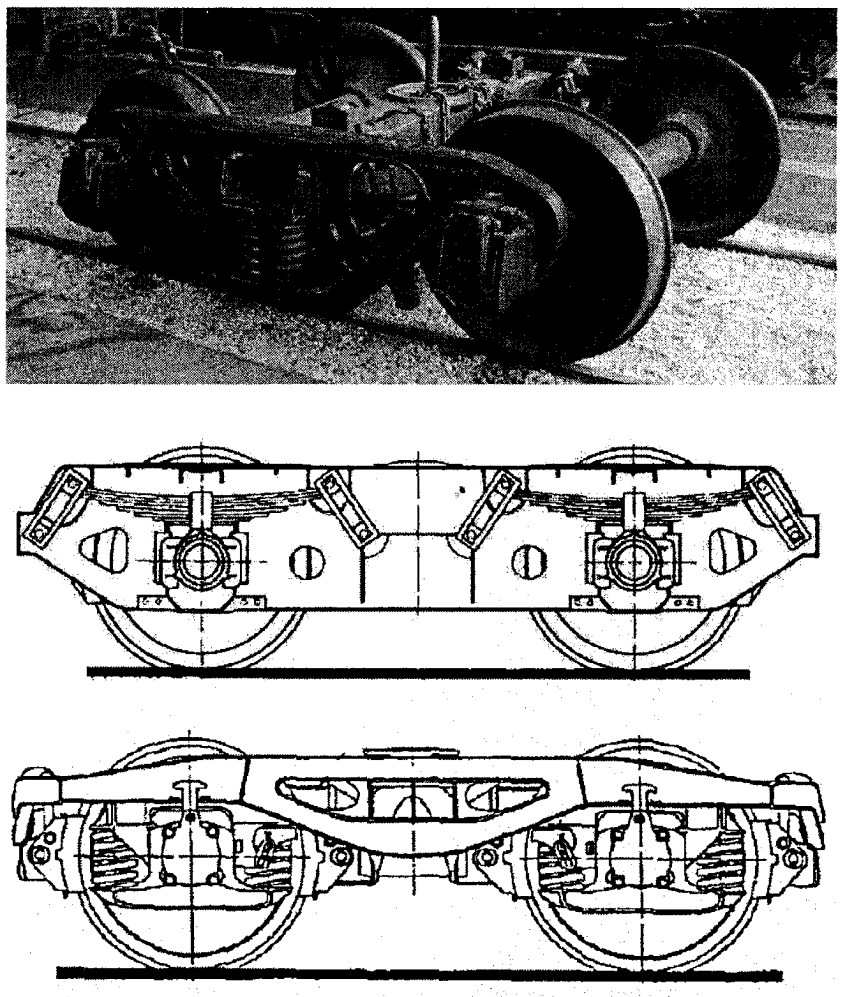

Figure 1.5 (Top) A two-axle truck; (Bottom) Two configurations of a two-axle truck

Figure 1.6 A triple-axle truck

Primary Suspension and **Secondary Suspension**: Secondary suspension system is located between the car body and truck frame, and is to support the axle load that transfers to the truck frame; Primary suspension connects the truck frame and wheelset, transferring loads from the truck frame to rail wheels (Figure 1.7).

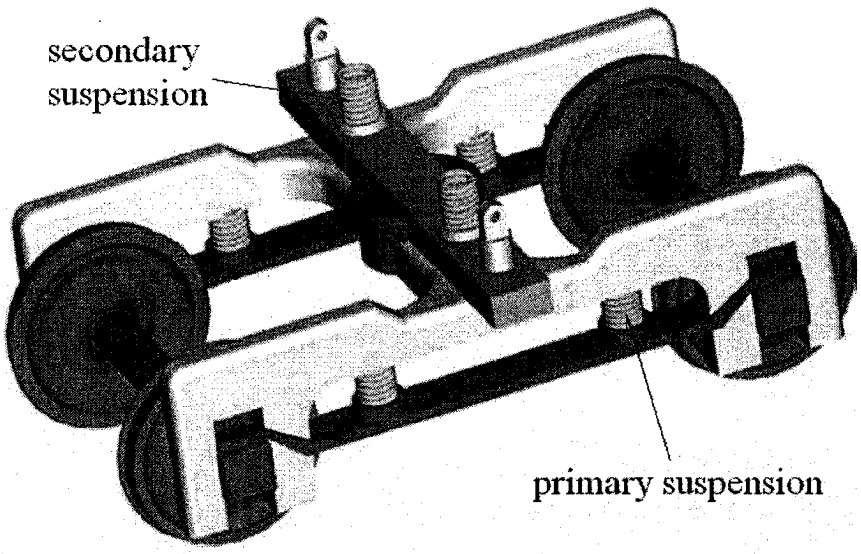

Figure 1.7 Primary and secondary suspensions

Other suspensions (spring and damper combinations) are also used. Figure 1.8 shows the suspensions in a single-axle truck.

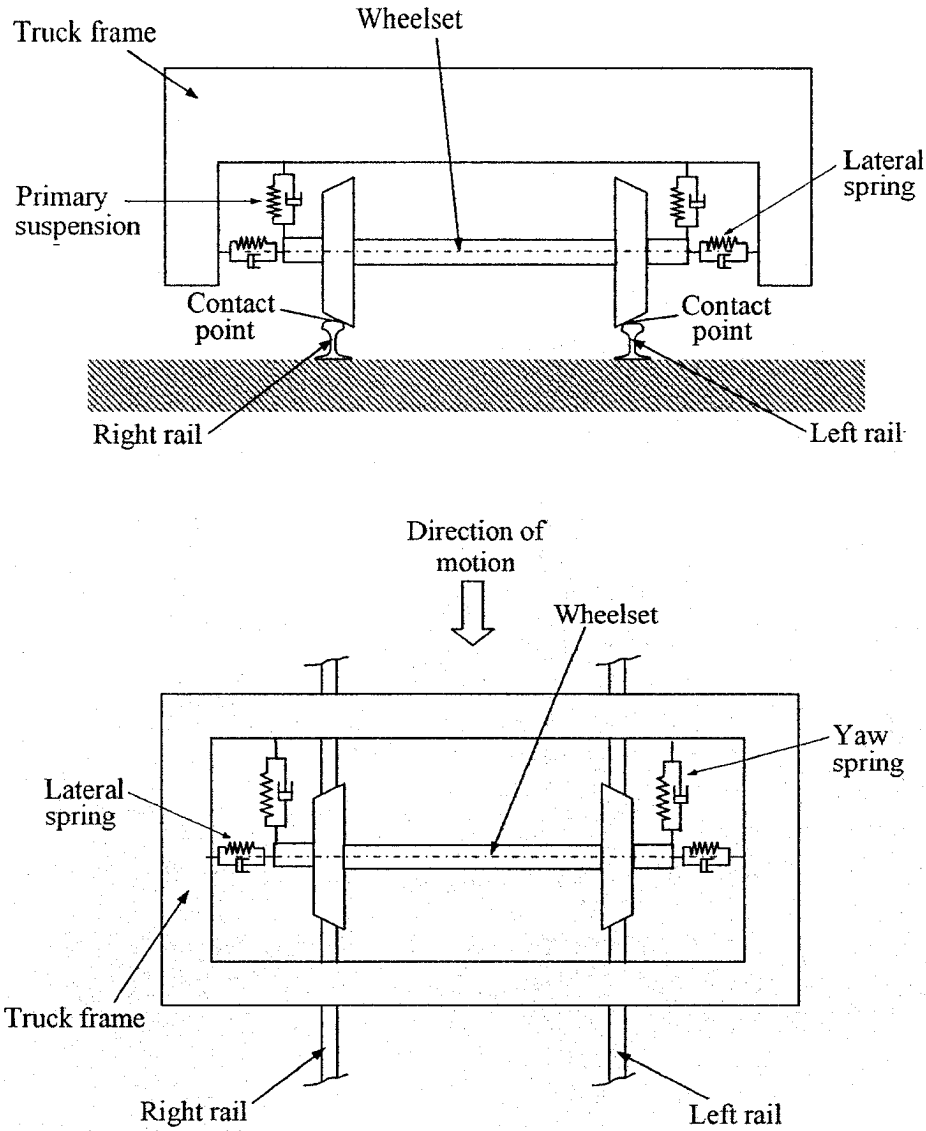

Figure 1.8 Suspensions in a single-axle truck
(Top) Front view; (Bottom) Top view

Chapter 2

MATHEMATICAL MODELS OF A SINGLE-AXLE RAILWAY WHEELSET

In this chapter, several mathematical models of the single-axle rail vehicle wheelset are presented in order to compare their features for similarities and differences. These models will later be used in Chapters 4 and 5. The wheelset is an important dynamic component of the rail vehicle because it is responsible for the wheel-rail interaction.

2.1 Preamble

Various assumptions are made in developing the mathematical models. The applicability of the models depends on these assumptions. Their implications must be clearly understood in interpreting the results obtained from the models. The assumptions or restrictions common to all these models are:

(1) The vehicles are traveling on a perfectly aligned, horizontal, straight track;

(2) The wheels always remain in contact with the rails;

(3) The vehicle components are perfectly rigid, and their elasticity is lumped in the suspension elements;

(4) External forces such as aerodynamic loads are not included;

(5) The axles run freely in the journal bearings without bearing friction or applied torques due to traction or braking; and

(6) Perturbations in the motions of the vehicle components about a steady state are small so that all terms greater than first order in the perturbed coordinates may be neglected in the equations of motion.

It is noted that the truck or bogie is the component through which the weight of the railcar body and its contents, the so-called axle load, is transmitted to the rails. The truck frame supports the axle load through the secondary suspension system which is located between the car body and the truck frame. Wheelsets are connected to the truck frame via the primary suspension. Locomotives, passenger cars, and freight cars have different truck and suspension configurations. For example, passenger trucks have relatively rigid truck frame. Primary suspension elements such as coil springs, air springs, or elastomeric pads are typically present. On the other hand, the frame of a freight truck is less rigid. There is no primary suspension. Dry friction is used intentionally in the secondary suspension. Overall, the suspension elements provide stiffness and damping to the system.

2.2 Wheel-Rail Interaction

As seen from discussions above, the wheelset supports the weight of the railcar body. Considering the wheelset as a free body and taking into account Assumption (4) in the previous section, the "only" external load is the reaction force applied by the rails onto the wheels, the so-called wheel-rail interaction. This interaction includes the normal force and creep force. The latter is so termed because it is caused by creepage which is the microslip between the wheel-rail contact surfaces. In simplistic terms, creep force is the dry friction

and creepage the relative motion. The creep force is chiefly responsible for the dynamics of the wheelset, which in turn is fundamental to the control of rail-wheel wear, vehicle stability and ride comfort. In the present study, two wheel-rail rolling contact theories are used: the Vermeulen and Johnson nonlinear contact theory [2.1] and the Kalker linear theory [2.2].

To appreciate the difference between the two theories, it may be helpful to properly introduce creepage. When two rigid bodies are rotated, or moved, or rotated and moved, relative to one another, the contact point will shift from its original position. The resulting velocities of the two bodies at the contact point may not be equal. When the velocities are equal, the rigid bodies are said to undergo pure rolling; otherwise, they are said to undergo rolling with sliding or creep. So creep or creepage is the deviation of actual rolling contact condition from pure rolling. In the case of wheel-rail contact, creepage is defined in both the longitudinal and lateral directions, and about the common normal to the contact point, hence the longitudinal, lateral and spin creepages, respectively (Figure 2.1).

The Vermeulen and Johnson theory includes the longitudinal and lateral creepages, but the spin creepage is left out. The shape and size of the contact patch are determined by the Hertz theory. On the other hand, the Kalker theory is believed to be the most successful method of determining creep force. It considers all three creepages. The drawback is that the computational time is large. It is therefore deemed not suitable for real time simulation. Since the present study does not concern itself with real time simulation, both theories are appropriate. Details of the Vermeulen and Johnson theory can be seen in Section 2.3.3,

Eqs. (2.17) through (2.20) in particular. The Kalker theory can be found in Appendix A, see Eqs. (A45) and (A46).

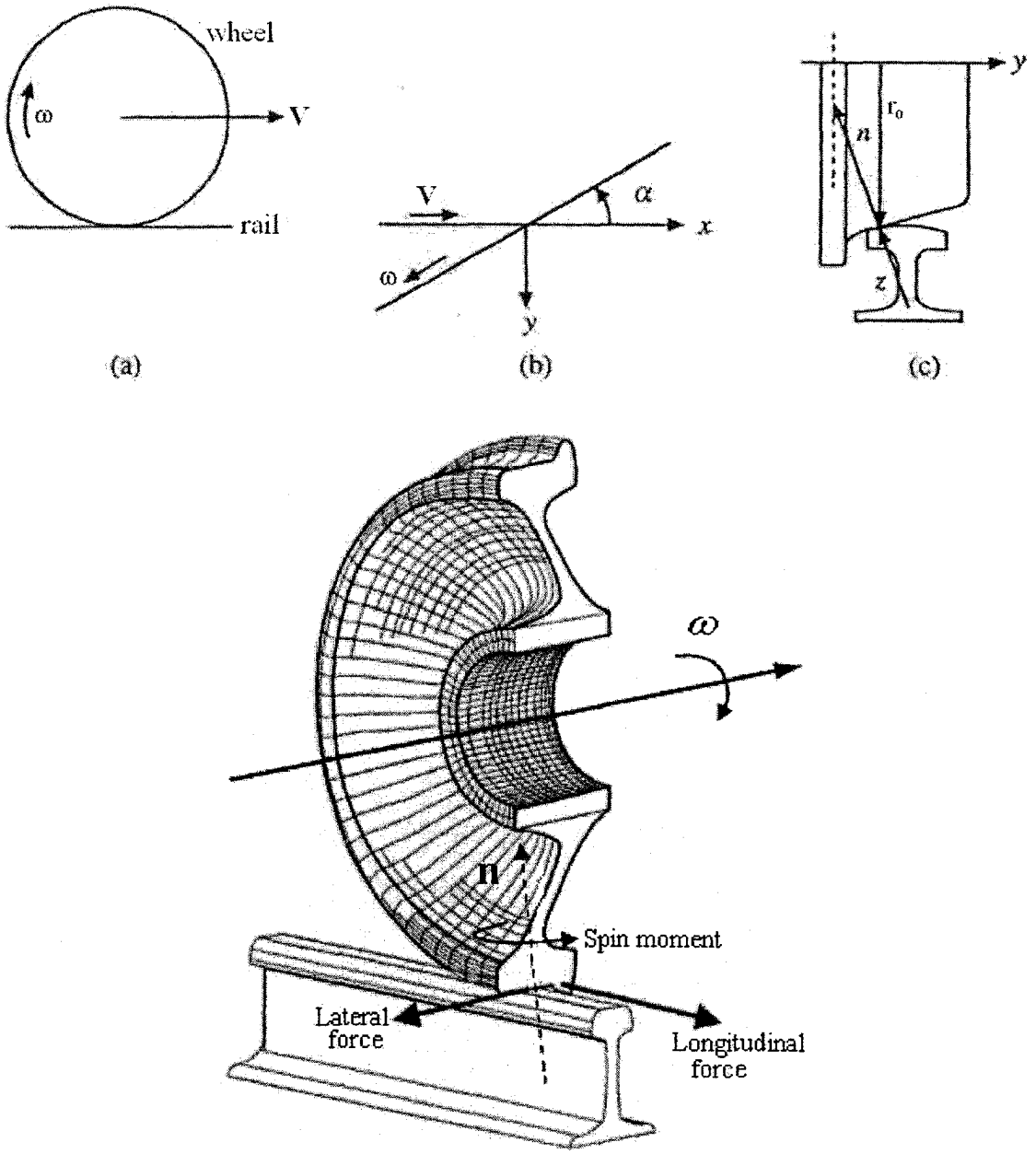

Figure 2.1 Creepages (a) Longitudinal; (b) Lateral; (c) Spin; (d) 3D view

2.3 Equations of Motion for Single-Axle Wheelsets

2.3.1 Model I

First, a brief description of the coordinate systems used is in order. As seen in Figure 2.2(a), the coordinate system x''', y''', z''' is called the equilibrium axes in which Newton's laws of motion can apply. The coordinate system x'', y'', z'' is an intermediate coordinate frame that is rotated by an angle ψ about the z''' axis. The coordinate system x', y', z' is referred to as the body axes which can translate and rotate with the wheelset body. Further details of these axes systems and the transformation amongst them can be seen in Appendix A.

The single-axle wheelset is represented by the free-body diagram (FBD) of Figure 2.2(b). A description of forces and moments appearing in the FBD is given in Table 2.1.

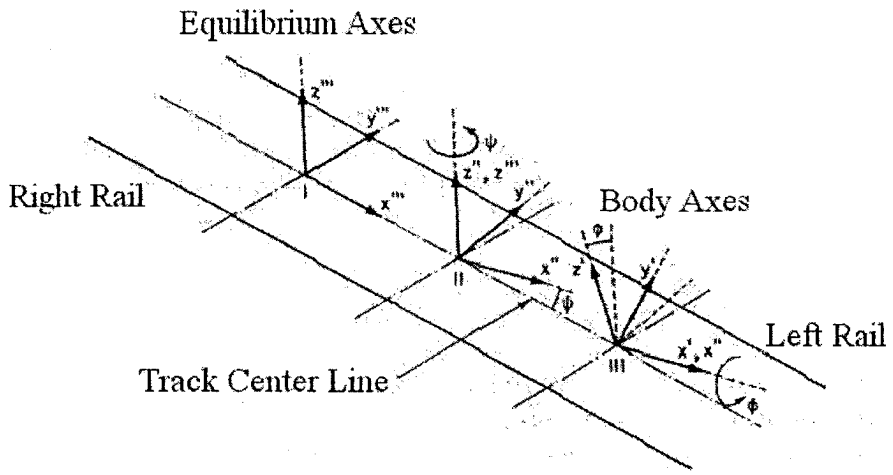

Figure 2.2(a) Axes systems

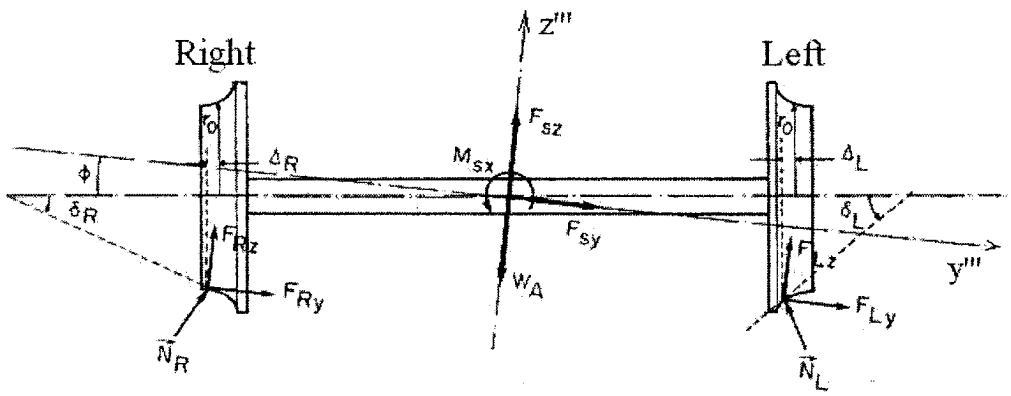

Fig 2.2(b) Free-body diagram of a single-axle wheelset – Viewed from x''' [2.3]

Table 2.1 Definition of Forces and Moments

Forces variables	Definition
$\mathbf{F_L}$, $\mathbf{F_R}$	creep forces at left and right contact points, respectively
$\mathbf{M_L}$, $\mathbf{M_R}$	creep moments at left and right contact points, respectively
$\mathbf{F_s}$	suspension forces
$\mathbf{M_s}$	suspension moments
W_A	axle load
$\mathbf{N_L}$, $\mathbf{N_R}$	normal forces at left and right contact points, respectively

Table 2.2 Description of Variables

Variable	Description
x	longitudinal displacement of the wheelset's mass center
y	lateral displacement of the wheelset's mass center
z	vertical displacement of the wheelset's mass center
φ	roll displacement about the x'' axis
ψ	yaw displacement about the z'' axis
β	angular displacement from a nominal value of Ω^* about the y' axis

* Ω is the spin of the wheels. $\Omega = v/r_0$ with v being the traveling speed of the wheelset and r_0 the nominal radius of the wheels.

The wheelset has six degrees of freedom (see Table 2.2). The equations of motion of the wheelset were initially derived by Garg and Dukkipati [2.3]. They have been verified in the present study. Appendix A details the mathematical development of the model. Here only the resulting equations of motion are presented.

a) Longitudinal equation of motion

$$m\ddot{x} = F_{Lx} + F_{Rx} + N_{Lx} + N_{Rx} + F_{sx} \tag{2.1}$$

b) Lateral equation of motion

$$m\ddot{y} = F_{Ly} + F_{Ry} + N_{Ly} + N_{Ry} + F_{sy} \tag{2.2}$$

c) Vertical equation of motion

$$m\ddot{z} = F_{Lz} + F_{Rz} + N_{Lz} + N_{Rz} + F_{sz} - W_A \tag{2.3}$$

d) Roll equation of motion

$$\begin{aligned} I_{wx}\ddot{\phi} = {} & I_{wy}(v/r_0)\dot{\psi} + R_{Ry}(F_{Rz} + N_{Rz}) - R_{Rz}(F_{Ry} + N_{Ry}) \\ & + R_{Ly}(F_{Lz} + N_{Lz}) - R_{Lz}(F_{Ly} + N_{Ly}) + M_{Lx} + M_{Rx} + M_{sx} \end{aligned} \tag{2.4}$$

e) Spin equation of motion

$$\begin{aligned} I_{wy}\ddot{\beta} = {} & R_{Rz}F_{Rx} - R_{Rx}(F_{Rz} + N_{Rz}) + R_{Lz}F_{Lx} \\ & - R_{Lx}(F_{Lz} + N_{Lz}) + M_{Ly} + M_{Ry} + M_{sy} \end{aligned} \tag{2.5}$$

f) Yaw equation of motion

$$\begin{aligned} I_{wx}\ddot{\psi} = {} & -I_{wy}(v/r_0)\dot{\phi} + R_{Rx}(F_{Ry} + N_{Ry}) - R_{Ry}F_{Rx} \\ & + R_{Lx}(F_{Ly} + N_{Ly}) - R_{Ly}F_{Lx} + M_{Lz} + M_{Rz} + M_{sz} \end{aligned} \tag{2.6}$$

where m is the mass of the wheelset, I_{wx}, I_{wy} and I_{wz} are the mass moments of inertia of the wheelset about the x', y' and z' axes, respectively, or the so-called roll, pitch and yaw moments of inertia. Other variables are, v the traveling speed or forward speed of the

wheelset and r_0 the nominal wheel radius. The R-quantities are components of position vectors of contact points. The subscripts are, L for left wheel; R for right wheel; and x, y and z for the longitudinal, lateral and vertical axes, respectively. Over-dot indicates a first-order time derivative. Double over-dot means a second-order time derivative.

Of particular interest to the investigation of hunting instability are the lateral and yaw equations of motion. These two equations are obtained by solving N_L and N_R from Eqs. (2.3) and (2.4), taking their y-components N_{Ly} and N_{Ry}, and substituting N_{Ly} and N_{Ry} into Eqs. (2.3) and (2.6). The resulting lateral and yaw equations of motion are then

$$\begin{aligned} m\ddot{y} &= F_{Ly} + F_{Ry} + F_{sy} + N_R \sin(\delta_R - \phi) - N_L \sin(\delta_L + \phi) \\ I_{wx}\ddot{\psi} &= -I_{wy}(v/r_0)\dot{\phi} + (R_{Rx}F_{Ry} - R_{Ry}F_{Rx}) + (R_{Lx}F_{Ly} - R_{Ly}F_{Lx}) \\ &\quad + R_{Rx}N_R \sin(\delta_R - \phi) - R_{Lx}N_L \sin(\delta_L + \phi) + M_{Lz} + M_{Rz} + M_{sz} \end{aligned} \tag{2.7}$$

Simplified lateral and yaw equations of motion are, by assuming small roll and yaw angles φ and ψ, and small contact angles; neglecting the inertia forces due to the vertical and roll motions; and neglecting the vertical components of creep forces

$$\begin{aligned} m\ddot{y} + 2\frac{f_{11}}{v}\left[\dot{y} + \frac{r_L + r_R}{2}\dot{\phi} - v\psi\right] + 2f_{33}\left[1 - \frac{r_L + r_R}{2r_0}\right]\psi \\ + 2f_{12}\left[\frac{\dot{\psi}}{v} - \frac{\delta_L - \delta_R}{2r_0}\right] + W_A\left[\frac{\delta_L - \delta_R}{2} + \phi\right] = F_{sy} \end{aligned} \tag{2.8}$$

$$\begin{aligned} I_{wx}\ddot{\psi} + I_{wy}\frac{v}{r_0}\dot{\phi} + \frac{2a^2 f_{33}}{r_0}\left(\frac{r_L - r_R}{2a}\right) - \frac{2f_{12}}{v}\left[\dot{y} + \frac{r_L + r_R}{2}\dot{\phi} - v\psi\right] \\ + 2a^2 f_{33}\frac{\dot{\psi}}{v} - 2f_{22}\frac{\delta_L - \delta_R}{2r_0} - aW_A\frac{\delta_L + \delta_R}{2}\psi + 2f_{22}\frac{\dot{\psi}}{v} = M_{sz} \end{aligned} \tag{2.9}$$

where f_{11}, f_{12}, f_{22} and f_{33} are creep coefficients; r_L and r_R are the running radii of the left and right wheels, respectively. Contact angles δ_L and δ_R are defined in Figure 2.2b.

Finally, for conical wheels, with a conical angle λ, on knife-edged rails, it can be shown that

$$\begin{aligned} \frac{1}{2}(r_L - r_R) &= \lambda y, \quad \frac{1}{2}(r_L + r_R) = r_0 \\ \frac{1}{2}(\delta_L - \delta_R) &= 0, \quad \frac{1}{2}(\delta_L + \delta_R) = \lambda \end{aligned} \tag{2.10}$$

and

$$\phi = (\lambda / a) y \tag{2.11}$$

The equations of motion of the wheelset are then reduced to

$$\begin{aligned} m\ddot{y} + 2\frac{f_{11}}{v}\left[\dot{y} + r_0\frac{\lambda}{a}\dot{y} - v\psi\right] + \frac{2f_{12}}{v}\dot{\psi} + W_A\frac{\lambda}{a}y = F_{sy} \\ I_{wx}\ddot{\psi} + I_{wy}\frac{v}{r_0}\frac{\lambda}{a}\dot{y} + \frac{2af_{33}\lambda}{r_0}y - \frac{2f_{12}}{v}\left[\dot{y} + r_0\frac{\lambda}{a}\dot{y} - v\psi\right] \\ + 2a^2 f_{33}\frac{\dot{\psi}}{v} - aW_A\lambda\psi + 2f_{22}\frac{\dot{\psi}}{v} = M_{sz} \end{aligned} \tag{2.12}$$

2.3.2 Model II

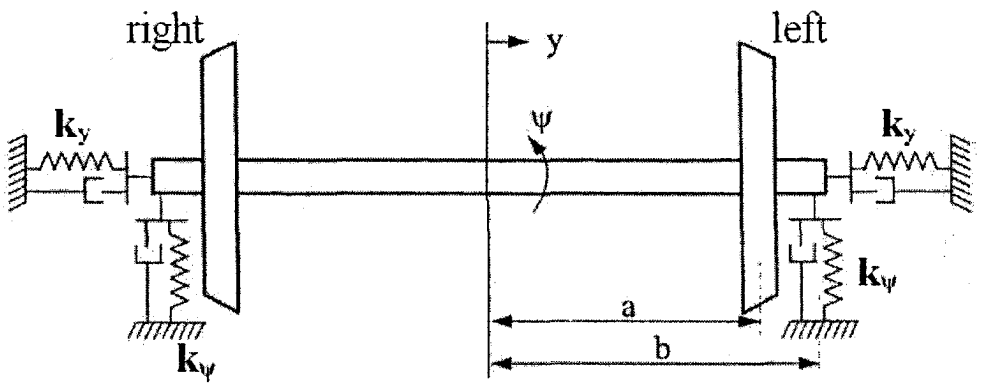

Figure 2.3 A single-axle wheelset – Viewed from z''' [2.4]

This model expands on the previous one. It considers a wheelset with flanges, connected to the truck frame by a set of springs and dampers, in both the longitudinal and lateral

directions (Figure 2.3). Variables used in this model and their parametric values were given in [2.4], and will be listed later in this chapter (see Table 2.6)

Neglecting viscous damping, the equations of motion for the wheelset are [2.4]

$$m\ddot{y} + \frac{2f_{11}}{v}\left[\left(1 + r_0\frac{\lambda}{a}\right)\dot{y} - v\psi\right] + \frac{2f_{12}}{v}\dot{\psi} + W_A\frac{\lambda}{a}y = F_{sy} - F_T(y) \tag{2.13}$$

$$\begin{aligned} I_{wx}\ddot{\psi} + I_{wy}\frac{v}{r_0}\frac{\lambda}{a}\dot{y} + \frac{2af_{33}\lambda}{r_0}y - \frac{2f_{12}}{v}\left[\left(1 + r_0\frac{\lambda}{a}\right)\dot{y} - v\psi\right] \\ + \frac{2a^2f_{33}}{v}\dot{\psi} - aW_A\lambda\psi + \frac{2f_{22}}{v}\dot{\psi} = M_{sz} - 2bF_d \end{aligned} \tag{2.14}$$

where the lateral suspension force and yaw moment are

$$F_{sy} = -2k_y y, \quad M_{sz} = -2k_\psi b^2\psi \tag{2.15}$$

and F_T is the flange force. It depends on lateral displacement y. $F_T(y)$ is given by

$$F_T(y) = \begin{cases} k_r(y - \delta) & y > \delta \\ 0 & -\delta \le y \le \delta \\ k_r(y + \delta) & y < -\delta \end{cases} \tag{2.16}$$

The nonlinear longitudinal yaw damping force F_d is described by

$$F_d = \begin{cases} C_1V_\psi + C_2V_\psi^2 + C_3V_\psi^3 + C_4V_\psi^4 & V_\psi \ge 0 \\ C_1V_\psi - C_2V_\psi^2 - C_3V_\psi^3 - C_4V_\psi^4 & V_\psi < 0 \end{cases}$$

where $V_\psi = b\dot{\psi}$. In the present study, the F_d force is set to zero for easy comparison with the other models.

It can be seen that, if F_d is removed from Eq. (2.14), and $-F_T(y)$ is added to the right side of Eq. (2.12), Models I and II become identical. In what follows, they are referred to, collectively, as Model II.

2.3.3 Model III

This model [2.5] is simpler than the two previous models. The wheelset has two degrees of freedom, the lateral displacement y and yaw motion ψ (Figure 2.4). The nonlinear creepage-creep force relation is that described by Vermeulen and Johnson [2.1], instead of the Kalker's linear creep theory used in Model II. This nonlinear creep force depends on y and ψ, and appears in both equations of motion. As a result, the two equations of motion are coupled. The equations of motion can be easily derived using the Langrange principle. Details of the derivation can be found in [2.5] and are not repeated here. A description of the variables used in the equations is given in Table 2.3. The resulting equations of motion are

$$\begin{aligned} m\ddot{y} + 2k_1 y + 2F_Y + F_T(y) &= 0 \\ I_{wz}\ddot{\psi} + 2k_2 d_1^2 \psi + 2aF_X &= 0 \end{aligned} \tag{2.17}$$

where the flange force $F_T(y)$ is given by Eq. (2.16) and the creep forces F_X and F_Y are

$$F_X = \frac{\xi_X}{\Phi}\frac{F_R}{\xi_R}, \quad F_Y = \frac{\xi_Y}{\Psi}\frac{F_R}{\xi_R} \tag{2.18}$$

with the resultant creep force being

$$F_R = \mu N \begin{cases} u - \frac{1}{3}u^2 + \frac{1}{27}u^3 & u < 3 \\ 1 & u \geq 3 \end{cases} \tag{2.19}$$

and $u = \dfrac{G\pi a_e b_e}{\mu N}\xi_R$. The creepages are

$$\xi_X = \frac{\lambda y}{r_0} + \frac{a\dot{\psi}}{v}, \quad \xi_Y = \frac{\dot{y}}{v} - \psi, \quad \xi_R = \sqrt{\left(\frac{\xi_X}{\Phi}\right)^2 + \left(\frac{\xi_Y}{\Psi}\right)^2} \tag{2.20}$$

The needed parametric values were given in [2.5] and will be listed later in the chapter (see part of Table 2.5).

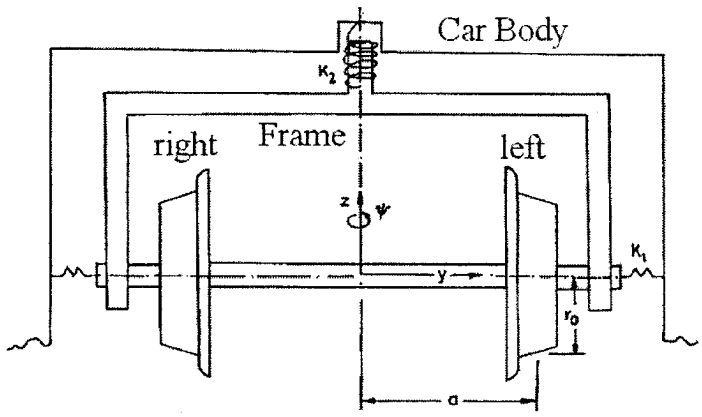

Figure 2.4 A single-axle wheelset – Viewed from x''' [2.5]

Table 2.3 Description of Variables

Variable	Description
F_R	resultant creep force
$\psi, \dot{\psi}$	yaw angle and angular velocity
ξ_Y	lateral creepage
ξ_X	longitudinal creepage
ξ_R	resultant creepage
F_X	longitudinal creep force
F_Y	lateral creep force
$y, \dot{y}$	lateral displacement and velocity
Φ, Ψ	coefficients of Johnson's theory
$F_T(y)$	flange contact force
k_1, k_2	lateral and yaw spring constants
v, t	velocity and time

2.4 Comparing the Models

A comparison of Models II and III is given in Table 2.4. The main difference lies in two aspects. The first one has to do with gravitational stiffnesses (the terms involving axle load W_A) and the gyroscopic couple or moment (the term associated with I_{wy}). Model III does not include such effects because it is derived without the inclusion of other degrees of freedom, namely the vertical displacement and roll motion. The second main difference lies in the contact theory for creep forces. Model II employed the Kalker linear theory to determine creep forces and moments. However Model III used the Vermeulen and Johnson nonlinear creep forces to evaluate creep forces and moments. Details of the Kalker linear theory can be found in Appendix A, see Eqs. (A.45) and (A.46) in particular. Details of the Vermeulen and Johnson nonlinear theory are presented in Eqs. (2.17) through (2.20), see Section 2.3.3. In addition, the two models have different parametric values. As a result, comparing the two models directly, that is, keeping the models at their present states and using the values given in [2.4] and [2.5] would make it difficult to interpret results and to draw conclusions. Worse, the conclusions could be inconclusive. Therefore, it is necessary to expand the two models so that issues can be isolated and investigated accordingly.

Table 2.4 Comparison of Models II and III

Considerations	Model II	Model III
Degrees of Freedom	y and ψ	y and ψ
Primary stiffness (lateral)	yes	yes
Primary damping (lateral)	yes	no
Yaw stiffness	yes	yes
Yaw damping	yes	no
Flange force	yes	yes
Lateral gravitational stiffness	yes	no
Yaw gravitational stiffness	yes	no
Gyroscopic couple	yes	no
Creep force theory	Kalker's linear	Vermeulen and Johnson's nonlinear
Longitudinal and lateral creep force	yes	yes
Spin creep moment	yes	no

2.5 Expanding Model III

Two expansions are considered.

The first expansion is to replace the creep forces by those of the Kalker's linear theory, or to linearize the creep forces. The steps involved are,

(1) Longitudinal and lateral creepages are determined by Eqs. (A.43) and (A.44). Spin creeps are set to zero, that is, $\xi'_{spL} = \xi'_{spR} = 0$. Longitudinal and lateral creep forces are then found by Eqs. (A.45), and transformed to the equilibrium axes by Eq. (A.4). The resulting creep forces are

$$
\begin{aligned}
F_{Lx} &= -(f_{33}/v)\left\{v[1-(r_L/r_0)]-a\dot{\psi}\right\}\cos\psi \\
&\quad +(f_{11}/v)[\dot{y}+r_L\dot{\phi}-v\psi]\cos(\delta_L+\phi)\sin\psi \\
F_{Ly} &= -(f_{33}/v)\left\{v[1-(r_L/r_0)]-a\dot{\psi}\right\}\sin\psi \\
&\quad -(f_{11}/v)[\dot{y}+r_L\dot{\phi}-v\psi]\cos(\delta_L+\phi)\cos\psi
\end{aligned}
\tag{2.21a}
$$

and

$$
\begin{aligned}
F_{Rx} &= -(f_{33}/v)\left\{v[1-(r_R/r_0)]+a\dot{\psi}\right\}\cos\psi \\
&\quad +(f_{11}/v)[\dot{y}+r_R\dot{\phi}-v\psi]\cos(\delta_R-\phi)\sin\psi \\
F_{Ry} &= -(f_{33}/v)\left\{v[1-(r_R/r_0)]+a\dot{\psi}\right\}\sin\psi \\
&\quad -(f_{11}/v)[\dot{y}+r_R\dot{\phi}-v\psi]\cos(\delta_R-\phi)\cos\psi
\end{aligned}
\tag{2.21b}
$$

(2) In Eq. (2.17), the creep force $2F_Y$ is replaced by $2F_Y = -\left(F_{Ly}+F_{Ry}\right)$. The moment about vertical axis due to F_X, that is, $2aF_X$, is replaced by $2aF_X = -a\left(F_{Rx}-F_{Lx}\right)$. On substitution from Eqs. (2.21a, b), these yield

$$
\begin{aligned}
2F_Y &= f_{33}[2-(r_L/r_0)-(r_R/r_0)]\sin\psi \\
&\quad +(f_{11}/v)\begin{Bmatrix}[\dot{y}+r_L\dot{\phi}-v\psi]\cos(\delta_L+\phi) \\ +[\dot{y}+r_R\dot{\phi}-v\psi]\cos(\delta_R-\phi)\end{Bmatrix}\cos\psi
\end{aligned}
\tag{2.22a}
$$

and

$$
\begin{aligned}
2aF_X &= a(f_{33}/v)\left\{v[(r_L/r_0)-(r_R/r_0)]-2a\dot{\psi}\right\}\cos\psi \\
&\quad -a(f_{11}/v)\begin{Bmatrix}[\dot{y}+r_R\dot{\phi}-v\psi]\cos(\delta_R-\phi) \\ -[\dot{y}+r_L\dot{\phi}-v\psi]\cos(\delta_L+\phi)\end{Bmatrix}\sin\psi
\end{aligned}
\tag{2.22b}
$$

(3) The assumption of small roll, pitch and contact angles, and Eqs. (A.60) and (A.61) simplify the above equations to

$$
2F_Y = 2\frac{f_{11}}{v}\left(\dot{y}+r_0\frac{\lambda}{a}\dot{y}-v\psi\right) \tag{2.23}
$$

$$
2aF_X = 2af_{33}\left(\frac{\lambda}{r_0}y+\frac{a}{v}\dot{\psi}\right)+\underline{\frac{2\lambda^2 f_{11}}{v}y\dot{y}\psi} \doteq 2af_{33}\left(\frac{\lambda}{r_0}y+\frac{a}{v}\dot{\psi}\right) \tag{2.24}
$$

The underlined term in Eq. (2.24) is a higher-order term that may be neglected. Finally,

(4) The equations of motion of the model are reduced to

$$\begin{aligned} m\ddot{y} + 2k_1 y + \frac{2f_{11}}{v}\left(\dot{y} + r_0\frac{\lambda}{a}\dot{y} - v\psi\right) + F_T(y) = 0 \\ I_{wz}\ddot{\psi} + 2k_2 d_1^2\psi + 2af_{33}\left(\frac{\lambda}{r_0}y + \frac{a}{v}\dot{\psi}\right) = 0 \end{aligned} \tag{2.25}$$

The second expansion differs from the first in that it includes the effect due to spin creep as well. The resulting creep forces and moment are given by Eqs. (A.49) and (A.50), which become, after applying the assumption of small roll, pitch and contact angles,

$$\begin{aligned} F_{Lx} &= -(f_{33}/v)\{v[1-(r_L/r_0)] - a\dot{\psi}\} \\ &\quad +(f_{11}\psi/v)[\dot{y} + r_L\dot{\phi} - v\psi] + (f_{12}\psi/v)[\dot{\psi} - \Omega\delta_L] \\ F_{Ly} &= -(f_{33}\psi/v)\{v[1-(r_L/r_0)] - a\dot{\psi}\} \\ &\quad -(f_{11}/v)[\dot{y} + r_L\dot{\phi} - v\psi] - (f_{12}/v)[\dot{\psi} - \Omega\delta_L] \\ M_{Lz} &= (f_{12}/v)[\dot{y} + r_L\dot{\phi} - v\psi] - (f_{22}/v)[\dot{\psi} - \Omega\delta_L] \end{aligned} \tag{2.26a}$$

$$\begin{aligned} F_{Rx} &= -(f_{33}/v)\{v[1-(r_R/r_0)] + a\dot{\psi}\} \\ &\quad +(f_{11}\psi/v)[\dot{y} + r_R\dot{\phi} - v\psi] + (f_{12}\psi/v)[\dot{\psi} + \Omega\delta_R] \\ F_{Ry} &= -(f_{33}\psi/v)\{v[1-(r_R/r_0)] + a\dot{\psi}\} \\ &\quad -(f_{11}/v)[\dot{y} + r_R\dot{\phi} - v\psi] - (f_{12}/v)[\dot{\psi} + \Omega\delta_R] \\ M_{Rz} &= (f_{12}/v)[\dot{y} + r_R\dot{\phi} - v\psi] - (f_{22}/v)[\dot{\psi} + \Omega\delta_R] \end{aligned} \tag{2.26b}$$

Next, $2F_Y$ and $2aF_X$ in Eq. (2.17) are replaced by $2F_Y = -(F_{Ly} + F_{Ry})$, and $2aF_X = -a(F_{Rx} - F_{Lx}) - M_{Rz} - M_{Lz}$, respectively. Eq. (2.17) then becomes

$$2F_Y = \frac{2f_{11}}{v}\left(\dot{y} + r_0\frac{\lambda}{a}\dot{y} - v\psi\right) + \frac{2f_{12}}{v}\dot{\psi} \tag{2.27a}$$

$$
\begin{aligned}
2aF_X &= \frac{2af_{33}}{v}\left(\frac{v\lambda}{r_0}y + a\dot{\psi}\right) + \frac{2f_{22}}{v}\dot{\psi} + \underline{\frac{2\lambda^2 f_{11}}{v}\psi y\dot{y}} - \frac{2f_{12}}{v}\left(\dot{y} + r_0\frac{\lambda}{a}\dot{y} - v\psi\right) \\
&\doteq \frac{2af_{33}}{v}\left(\frac{v\lambda}{r_0}y + a\dot{\psi}\right) + \frac{2f_{22}}{v}\dot{\psi} - \frac{2f_{12}}{v}\left(\dot{y} + r_0\frac{\lambda}{a}\dot{y} - v\psi\right)
\end{aligned}
\tag{2.27b}
$$

and the equations of motion reduce to

$$
\begin{aligned}
m\ddot{y} + 2k_1 y + \frac{2f_{11}}{v}\left(\dot{y} + r_0\frac{\lambda}{a}\dot{y} - v\psi\right) + \frac{2f_{12}}{v}\dot{\psi} + F_T(y) = 0 \\
I_{\omega z}\ddot{\psi} + 2k_2 d_1^2\psi + \frac{2af_{33}}{v}\left(\frac{v\lambda}{r_0}y + a\dot{\psi}\right) + \frac{2f_{22}}{v}\dot{\psi} - \frac{2f_{12}}{v}\left(\dot{y} + r_0\frac{\lambda}{a}\dot{y} - v\psi\right) = 0
\end{aligned}
\tag{2.28}
$$

For easy reference, the models represented by Eqs. (2.25) and (2.28), respectively, will be called Models IIIa and IIIb hereinafter. The parameters required by the models will be given in Table 2.5.

2.6 Concluding Remarks

So far four models have been presented. They are, Models II, III, IIIa and IIIb. These models can be used in certain combinations so that particular issues can be examined.

(1) **The first combination** is comprised of Models III, IIIa, and IIIb. This combination allows for the investigation into effects of ways of modeling creep forces and moments on the dynamic behaviors of a wheelset. The equations used in this combination, Eqs. (2.29) – (2.31), and the data table, Table 2.5, are given below. Data in Table 2.5 are taken mostly from [2.5]. The parameters f_{ij} are determined based on Eq. (A.46) and Table 4.2 of [2.3].

Model III

$$\begin{aligned} m\ddot{y} + 2k_1 y + 2F_Y + F_T(y) &= 0 \\ I_{wz}\ddot{\psi} + 2k_2 d_1^2 \psi + 2aF_X &= 0 \end{aligned} \tag{2.29}$$

Model IIIa

$$\begin{aligned} m\ddot{y} + 2k_1 y + \frac{2f_{11}}{v}\left(\dot{y} + r_0\frac{\lambda}{a}\dot{y} - v\psi\right) + F_T(y) &= 0 \\ I_{wz}\ddot{\psi} + 2k_2 d_1^2 \psi + 2af_{33}\left(\frac{\lambda}{r_0}y + \frac{a}{v}\dot{\psi}\right) &= 0 \end{aligned} \tag{2.30}$$

Model IIIb

$$\begin{aligned} m\ddot{y} + 2k_1 y + \frac{2f_{11}}{v}\left(\dot{y} + r_0\frac{\lambda}{a}\dot{y} - v\psi\right) + \frac{2f_{12}}{v}\dot{\psi} + F_T(y) &= 0 \\ I_{wz}\ddot{\psi} + 2k_2 d_1^2 \psi + \frac{2af_{33}}{v}\left(\frac{v\lambda}{r_0}y + a\dot{\psi}\right) + \frac{2f_{22}}{v}\dot{\psi} - \frac{2f_{12}}{v}\left(\dot{y} + r_0\frac{\lambda}{a}\dot{y} - v\psi\right) &= 0 \end{aligned} \tag{2.31}$$

(2) **The second combination** consists of Models II and IIa. Model IIa is obtained from Model II by removing the gravitational stiffness terms and the term associated with I_{wy}. The latter is the gyroscopic couple (or moment) due to the coupling of roll and spin motions. Therefore this combination makes it possible to examine the effect of gravitational stiffnesses and gyroscopic couple. The equations, Eqs. (2.32) and (2.33), and data table, Table 2.6, are listed below for easy reference. Table 2.6 is compiled from data given in [2.4].

Model II

$$
\begin{aligned}
&m\ddot{y} + 2k_y y + \frac{2f_{11}}{v}\left[\left(1 + r_0\frac{\lambda}{a}\right)\dot{y} - v\psi\right] + \frac{2f_{12}}{v}\dot{\psi} + W_A\frac{\lambda}{a}y + F_T(y) = 0 \\
&I_{wx}\ddot{\psi} + I_{wy}\frac{v}{r_0}\frac{\lambda}{a}\dot{y} + 2k_\psi b^2\psi + \frac{2af_{33}\lambda}{r_0}y - \frac{2f_{12}}{v}\left[\left(1 + r_0\frac{\lambda}{a}\right)\dot{y} - v\psi\right] \\
&\qquad + \frac{2a^2 f_{33}}{v}\dot{\psi} - aW_A\lambda\psi + \frac{2f_{22}}{v}\dot{\psi} = 0
\end{aligned}
\tag{2.32}
$$

where F_{sy} has been replaced by $F_{sy} = -2k_y y$, and M_{sz} by $M_{sz} = -2k_\psi b^2\psi$.

Model IIa

$$
\begin{aligned}
&m\ddot{y} + 2k_y y + \frac{2f_{11}}{v}\left[\left(1 + r_0\frac{\lambda}{a}\right)\dot{y} - v\psi\right] + \frac{2f_{12}}{v}\dot{\psi} + F_T(y) = 0 \\
&I_{wx}\ddot{\psi} + 2k_\psi b^2\psi + \frac{2af_{33}\lambda}{r_0}y - \frac{2f_{12}}{v}\left[\left(1 + r_0\frac{\lambda}{a}\right)\dot{y} - v\psi\right] \\
&\qquad + \frac{2a^2 f_{33}}{v}\dot{\psi} + \frac{2f_{22}}{v}\dot{\psi} = 0
\end{aligned}
\tag{2.33}
$$

(3) **The third combination** consists of Models IIb and III. Model IIb is Model II with its linear creep forces being replaced with the nonlinear counterparts by Vermeulen and Johnson, and the creep moment being neglected. The reason for choosing this combination will be seen in Section 4.4. The equations, Eqs. (2.34) and (2.35), and data table, Table 2.7, are listed below. Table 2.7 is compiled from data given in [2.5]. An estimated value is used for I_{wy}.

Model IIb

$$
\begin{aligned}
&m\ddot{y} + 2k_y y + 2F_Y + F_T(y) + W_A\frac{\lambda}{a}y = 0 \\
&I_{wx}\ddot{\psi} + I_{wy}\frac{v}{r_0}\frac{\lambda}{a}\dot{y} + 2k_\psi b^2\psi + 2aF_X - aW_A\lambda\psi = 0
\end{aligned}
\tag{2.34}
$$

Model III

$$\begin{aligned} m\ddot{y} + 2k_1 y + 2F_Y + F_T(y) &= 0 \\ I_{wz}\ddot{\psi} + 2k_2 d_1^2 \psi + 2aF_X &= 0 \end{aligned} \tag{2.35}$$

Table 2.5 Parametric Values for Models III, IIIa and IIIb

Constant	Value	Description
m	1022 kg	mass of wheelset
I_{wz}	678 $kg\ m^2$	moment of inertia
a	0.716 m	half of the track gauge
λ	0.05	slope of conical wheel
δ	9.1 mm	dead band
d_1	0.620 m	distance from center of gravity to k_2
k_r	14.60 MN/m	spring constant (flange)
k_1	18.23 kN/m	spring constant (lateral)
k_2	180 N/m	spring constant (yaw)
r_0	0.4572 m	centered wheel rolling radius
f_{11}	90.712 kN	lateral creep force coefficient
f_{22}	0.46739 $N\ m^2$	spin creep moment coefficient
f_{12}	258.88 $N\ m$	lateral-spin creep force coefficient
f_{33}	103.228 kN	longitudinal creep force coefficient
G	808 MN/m^2	shear modulus
Ψ	0.54192	constant
Φ	0.60252	constant
a_e	6.578 mm	major semiaxis of contact ellipse
b_e	3.934 mm	minor semiaxis of contact ellipse
μ	0.15	coefficient of friction
μN^*	10 kN	adhesive force

* N is the vertical force between wheel and rail.

Table 2.6 Parametric Values for Models II and IIa

Symbol	Value	Description
m	1800 kg	wheelset mass
$I_{wx} = I_{wz}$	625.7 $kg\ m^2$	roll/yaw moment of inertia of wheelset
I_{wy}	133.92 $kg\ m^2$	spin moment of inertia of wheelset
r_0	0.533 m	wheel radius
a	0.7176 m	half of the track gauge
λ	0.05	slope of conical wheel
W_A	18000 N	axle load
$k_y = k_1$	8.67×10^4 N/m	lateral stiffness of primary suspension
$k_\psi = k_2$	8.67×10^4 N/m	yaw spring stiffness of primary suspension
$b = d_1$	1.00 m	half of the primary yaw spring arm
f_{11}	6.728×10^6 N	lateral creep force coefficient
f_{22}	1000 $N\ m^2$	spin creep moment coefficient
f_{12}	1.2×10^3 $N\ m$	lateral-spin creep force coefficient
f_{33}	6.728×10^6 N	longitudinal creep force coefficient
k_r	1.617×10^7 N/m	lateral rail stiffness
δ	9.23 mm	flange clearance

Table 2.7 Parametric Values for Models IIb and III

Constant	Value	Description
m	1022 kg	mass of wheelset
I_{wz}	678 $kg\ m^2$	moment of inertia
I_{wy}	145 $kg\ m^2$	spin moment of inertia of wheelset (estimated)
a	0.716 m	half of the track gauge
λ	0.05	slope of conical wheel
δ	9.1 mm	dead band
d_1	0.620 m	distance from center of gravity to k_2
k_r	14.60 $MN\ m^{-1}$	spring constant (flange)
k_1	18.23 $kN\ m^{-1}$	spring constant (lateral)
k_2	180 $N\ m^{-1}$	spring constant (yaw)
r_0	0.4572 m	centered wheel rolling radius
G	808 $MN\ m^{-2}$	shear modulus
Ψ	0.54192	constant
Φ	0.60252	constant
a_e	6.578 mm	major semiaxis of contact ellipse
b_e	3.934 mm	minor semiaxis of contact ellipse
μ	0.15	coefficient of friction
μN^*	10 kN	adhesive force
W_A	133.33 kN	axle load

* N is the vertical force between wheel and rail.

Chapter 3

MONTE CARLO SIMULATION AND RANDOM NUMBER GENERATION

Monte Carlo simulation refers to solving mathematical problems by simulating random variables. It can perform simulation of any process influenced by random factors, being one of the most versatile and widely used numerical methods. One of the crucial elements in Monte Carlo simulation is the generation of random numbers of certain distribution such as the Gaussian or normal distribution for this thesis. In this chapter, some random number generating techniques are reviewed. Two major categories are examined, namely, the pseudo-random number generators and the true random number generators.

3.1 Pseudo-Random Number Generators

As the name suggests, pseudo-random numbers are not truly random. Rather, they are computed from a mathematical formula or simply taken from a pre-calculated list. A great deal of research has gone into the algorithms and techniques of generating pseudo-random numbers [3.1]. Pseudo-random numbers have the characteristic that they are predictable, or they have a period. Here period refers to the length of the random number sequence before it repeats itself.

Pseudo-random number generation algorithms fall into two categories, serial random number generators that are developed for use in single-processor computers, and parallel random number generators employed in multi-processor computers. Only serial random number generators are reviewed here.

An ideal serial random number generator should generate sequences that satisfy statistical tests for randomness, that are not correlated, that have a long period, that are reproducible, and that can be changed by adjusting the seed number. The generator should be fast and portable, and require limited memory. Some of the commonly used algorithms are,

(1) Linear Congruential Generators (LCGs)

LCGs represent one of the oldest and best-known pseudo-random number generator algorithms. The theory behind them is easy to understand, and they can be easily implemented and are fast. It is, however, well known that the properties of this class of generator are far from ideal.

LCGs are based on the following iterative scheme:

$$X_n = (a X_{n-1} + c) \pmod{m}$$

where m is the modulus, a the multiplier, and c the additive constant. And "mod" is the modulo operator. Note that a, c and m are all integers. The size of the modulus m constrains the period, and is usually a prime or a power of 2 number. When a, c and m are chosen appropriately, LCGs can generate a random number sequence with a maximum period equal to m.

(2) Lagged Fibonacci Generators (LFGs)

This class of pseudo-random number generator is aimed at being an improvement on the linear congruential generators. LFGs are based on generalized Fibonacci sequence, which can be described by the recursive relation: $S_n = S_{n-1} + S_{n-2}$, or the new term is the sum of the last two terms in the sequence. The lagged Fibonacci sequence is then:

$$S_n = (S_{n-j} * S_{n-k}) \pmod{m}, \quad 0 < j < k$$

Here the new term is some combination of any two previous terms. Modulus m is usually a power of 2 ($m = 2^M$), often 2^{32} or 2^{64}. The "*" operator denotes any binary operation. This may be addition, subtraction, multiplication, or the bitwise arithmetic exclusive-or operator (XOR). The choice of the "*" operation gives rise to a number of LFGs, for examples, Additive Lagged Fibonacci Generator or ALFG, Multiplicative Lagged Fibonacci Generator or MLFG, and Two-tap Generalized Feedback Shift Register or GFSR.

The LFGs tend to be very sensitive to the values of j and k. They should not be randomly chosen. With proper choices of j and k, and the first k values of S, the period is $(2^k - 1)\times 2^{(M-1)}$.

3.2 True Random Number Generators

True random numbers are those that exist in the physical world or created by hardware. Any random numbers generated by a deterministic algorithm are reproducible, therefore not truly random. However, it is possible to attain a random number series whose period is very large. Such a series is known as true random numbers. To obtain true random numbers, pseudo-random numbers need to be processed by randomization in the time domain. One such process is shown in Figure 3.1 [3.2]. It consists of delay, reverse, windowing, and lapping.

(1) Random delay and reverse

Let assume that there are 1,024 pseudo-random numbers, or sample data. A new random series is formed by randomly selecting any sample datum as the start datum while keeping the rest in the original and reversed orders, end to end. Since there are 1,024 choices of start datum, after random delay and reverse, the number of random series is

1,024 × 2 = 2,048. These 2,048 series of random numbers come from the same source, differing only in how the random numbers are sequenced. As a result, they possess the same characteristics in the frequency domain. Windowing is next applied so that the series will possess different spectra.

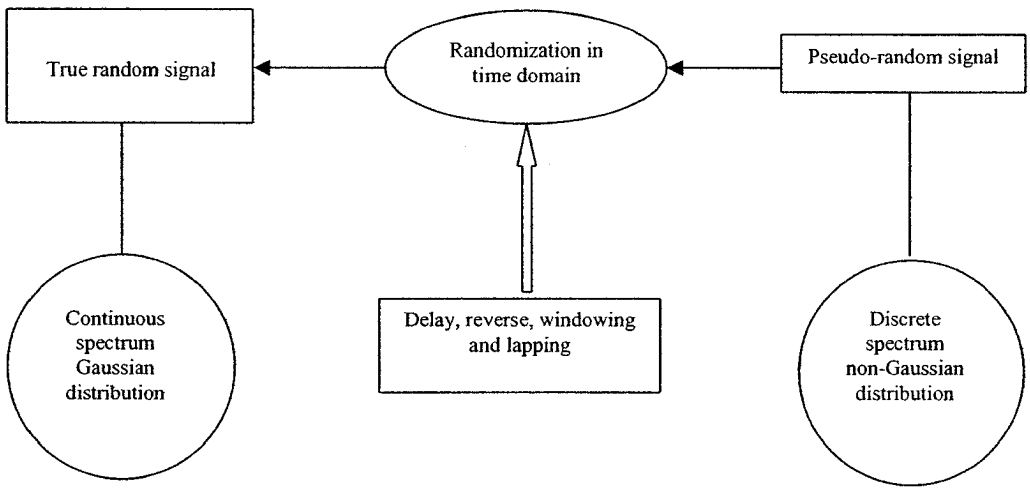

Figure 3.1 Process diagram of true random signal production

(2) Windowing and lapping

Windowing and lapping serve to obtain a continuous spectrum distribution. Usually the half sine wave window is used, as is illustrated in Figure 3.2.

Let $X_1(t)$, $X_2(t)$, ... , $X_N(t)$ (N = 1, ... , 2,048) denote the random number series obtained after delay and reversing. Window functions are $W_1(t)$, $W_2(t)$, ... , $W_N(t)$ (N = 1, ... , 2,048). Windowing means that a new random series is formed according to

$$X(t) = \sum_{i=1}^{N} W_i(t) X_i(t) \tag{3.1}$$

The variance of $X(t)$ is then

$$E[X^2(t)] = E[\sum_{i=1}^{N}(W_i(t)X_i(t))^2] = E[\sum_{i=1}^{N}W_i^2X_i^2 + \sum_{i=1}^{N}\sum_{j=i+1}^{N}2W_iW_jX_iX_j] \tag{3.2}$$

where $E[\cdot]$ denotes the expectation of a random variable. Terms such as $E[2W_iW_jX_iX_j]$ ($i \neq j$) are the correlation functions defined as $E[2W_iW_jX_iX_j] = \lim_{T\to\infty}\int_0^T (2W_iW_jX_iX_j)dt$ $= 2W_iW_j \lim_{T\to\infty}\int_0^T E[X_i(t)X_j(t)]dt$. Since $X_1(t), X_2(t), \cdots, X_N(t)$ are independent random processes, one has,

$$E[2W_iW_jX_iX_j] = 0, (i \neq j) \tag{3.3}$$

Substituting Eq. (3.3) into (3.2) yields

$$E[X^2(t)] = E[\sum_{i=1}^{N}W_i^2X_i^2] = \sum_{i=1}^{N}W_i^2E[X_i^2] = \sum_{i=1}^{N}W_i^2\sigma^2 = \sigma^2\sum_{i=1}^{N}W_i^2 \tag{3.4}$$

since the series $X_1(t), X_2(t), \cdots, X_N(t)$ have identical variance σ^2. Random signals in engineering applications are generally smoothly ergodic so that the characteristic of every sample is the same as the holistic average characteristic. That is,

$$E[X^2(t)] = E[X_1^2(t)] = E[X_2^2(t)] = E[X_3^2(t)] = \cdots = \sigma^2 \tag{3.5}$$

Substituting Eq. (3.5) into Eq. (3.4) gives rise to

$$\sum_{i=1}^{N}W_i^2(t) = 1 \tag{3.6}$$

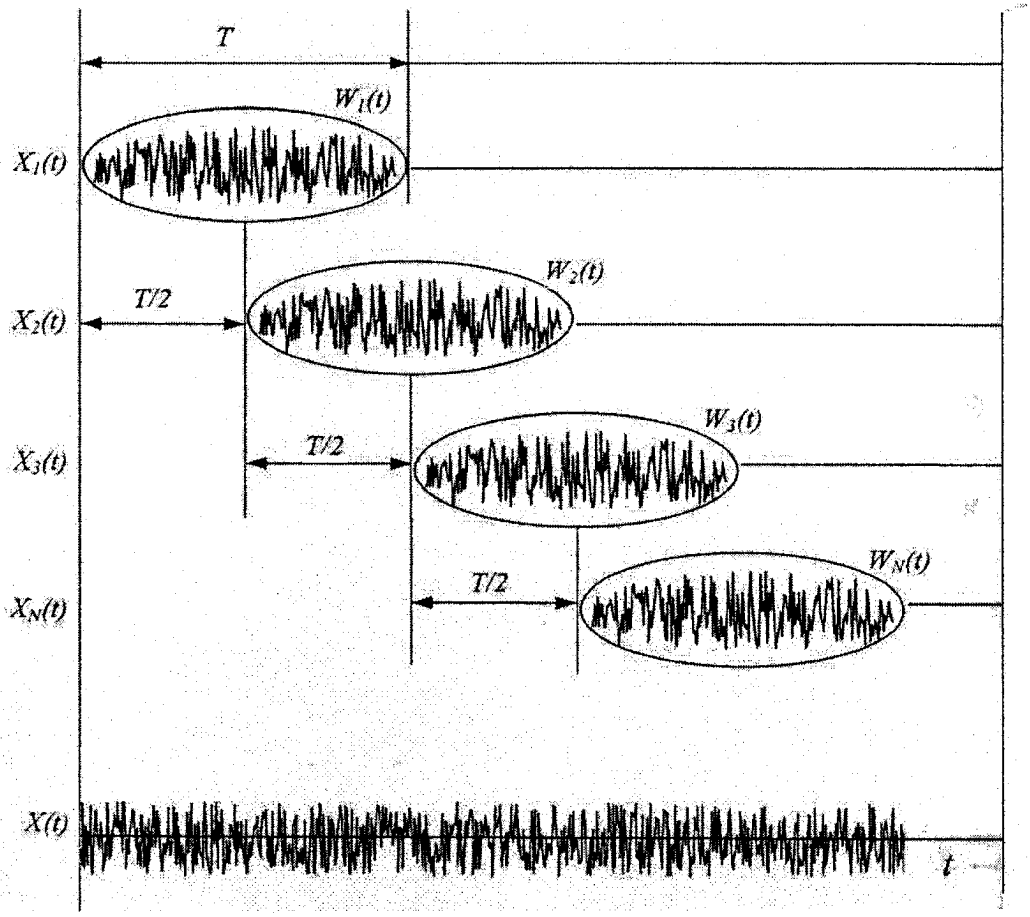

Figure 3.2 Windowing and lapping

This equation serves as the criterion of choosing window functions. In the present study, the windows are chosen as the half sine wave, or

$$W_1(t) = \begin{cases} \sin\frac{\pi}{T}t & 0 \le t \le T \\ 0 & t < 0, t > T \end{cases} \tag{3.7}$$

with $W_2(t), \cdots, W_N(t)$ each being delayed by $T/2$ from the one that precedes it.

Continuous spectrum Gaussian distribution is obtained after applying the half sine wave windows and the half-period lapping. Again, the series is still not truly random. But its period is large enough (about 17.5 years at a sampling interval of 0.25 second) to be considered a true random signal.

3.3 Generating Random Numbers for the Present Study

From the point of view of generating serial random numbers on a personal computer, one has, broadly speaking, two options. The first option is to rely on built-in random number generators provided by compilers (such as Fortran or C) or software packages (such as Maple, MatLab, etc.) The quality of these random numbers varies from good to fair. The second option is to use the so-called portable random number generators, pseudo or true. Here portable means that the generation of random numbers does not depend on using a specific brand of computers, or specific compilers or software. In the following discussions, two particular portable generators are discussed (although a few others have been examined).

Netlib, a website repository of mathematical software, has a Fortran code named zufall.f [3.3]. The code utilizes the lagged Fibonacci generator (LFG) to generate uniformly distributed random numbers which are then transformed to the standard Gaussian distribution. The random numbers generated by zufall.f are obviously not true random numbers. To make them true, they are fed into the process described in Section 3.2 to obtain true random numbers at the output. For easy reference, the algorithm of zufall.f is referred to as "Zufall", and the algorithm developed by the author (Reference [3.2]), is referred to as "True".

"Zufall" and "True" are then tested on their statistical goodness. "Zufall" proves to be of better quality, see Table 3.1. The tests involve generating a series of 25,600 random numbers of standard normal distribution. The mean, variance, skewness and kurtosis of the series are determined by the SPSS package [3.4]. The effectiveness of the two generators is measured by the CPU times taken to generate 256 sets of 25,600 random

numbers, or 6,553,600 random numbers. The CPU times are also listed in Table 3.1. "True" is found to take 24% more time than the "Zufall" counterpart. This is attributed to the extra time required for random delay, reverse, windowing and lapping. In the following chapters, zufall.f is chosen as the designated random number generator, since it is computationally effective, and the random numbers that it generates are of very good statistical goodness.

Table 3.1 Comparison of Pseudo-Random Number Generators

Algorithm	"True"		"Zufall"	
	Set 1	Set 2	Set 1	Set 2
Mean	-0.052	-0.044	-0.0037	0.011
Variance	0.988	0.887	1.004	1.000
Skewness	-0.055	-0.076	0.020	-0.013
Kurtosis	-0.18	-0.29	-0.016	-0.036
CPU time (seconds)	3.6152		2.9242	

3.4 Concluding Remarks

This chapter is concerned with generating random numbers for the purpose of Monte Carlo simulation. Algorithms for generating random numbers are reviewed. The pseudo nature of the random numbers is discussed, so is the process to make them true. The statistical goodness of two particular random number generators, "Zufall" and "True", is examined. "Zufall" is chosen for its good quality and computational efficiency.

Chapter 4

LYAPUNOV EXPONENTS AND INFORMATION DIMENSIONS OF SINGLE-AXLE WHEELSETS WITH RANDOMNESS

4.1 A Brief Introduction of the Theory of Chaos

Contrary to popular accounts, chaotic motion has nothing to do with whether the motion of a physical system is frenzied or wild in appearance. In fact, a chaotic system can actually evolve in a way that it appears smooth and ordered. So, what is chaos? At the core, chaos has to do with if it is possible to make accurate long-term predictions of the behaviour of the system.

Since the inception of chaos theory in the early 1960's, finding a definition of chaotic motion that was acceptable to all practitioners in the area had not been easy. For a few decades it was felt that it was easier to list the characteristics of chaotic motion than to define it. However, since the 1990's, the following definition by Devancy [4.1] has been seen to be most acceptable, by mathematicians at least:

> Let X be a metric space. A continuous map f: $X \rightarrow X$ is said to be chaotic on X if
> (1) f is topologically transitive.
> Transitive: for all non-empty open subsets U and V of X, there exists a natural number k such that $f^k(U) \cap V$ is non-empty.
> (2) The periodic points of f are dense in X.
> The point x in X is a periodic point of period n if $f^n(x) = x$. The least positive n for which $f^n(x) = x$ is called the prime period of x.
> If for any two points a and b in X, $a \neq b$, $a < b$, and there exists a periodic point p that $a < p < b$, then the periodic points of f are dense in X.

(3) f has sensitive dependence on initial conditions.
If there is a positive real number δ (a sensitivity constant) such that for every point x in X and every neighbourhood N of x there exists a point y in N and a non-negative integer n such that the n^{th} iterates $f^n(x)$ and $f^n(y)$ of x and y respectively, are more than distance δ apart.

This definition tells us that the three characteristics of chaotic motion are:

(a) It is topologically transitive.

Topological transitivity means that the system will evolve over time in a way that any given region or open set of its phase space will eventually overlap with any other given region. Or in a lay person's language, a starting state, if observed for long enough time, will eventually pass through any little piece of the state space.

(b) Its periodic orbits are dense

Periodic motion refers to that which repeats itself again and again. Dense periodic orbit means, loosely speaking, that an orbit in phase space exists next to any other orbits in the same phase space, or a periodic orbit may be found everywhere in the accessible phase space. Dense orbits or chaotic motions are found around a strange attractor, which is a set toward which a dynamical system evolves after a long enough period of time, or a set with fractal structures, geometrically speaking (Figure 4.1). A strange attractor can be identified if the trajectories in the phase space appear to skip around randomly so that there are gaps or holes in the phase space (Figure 4.1).

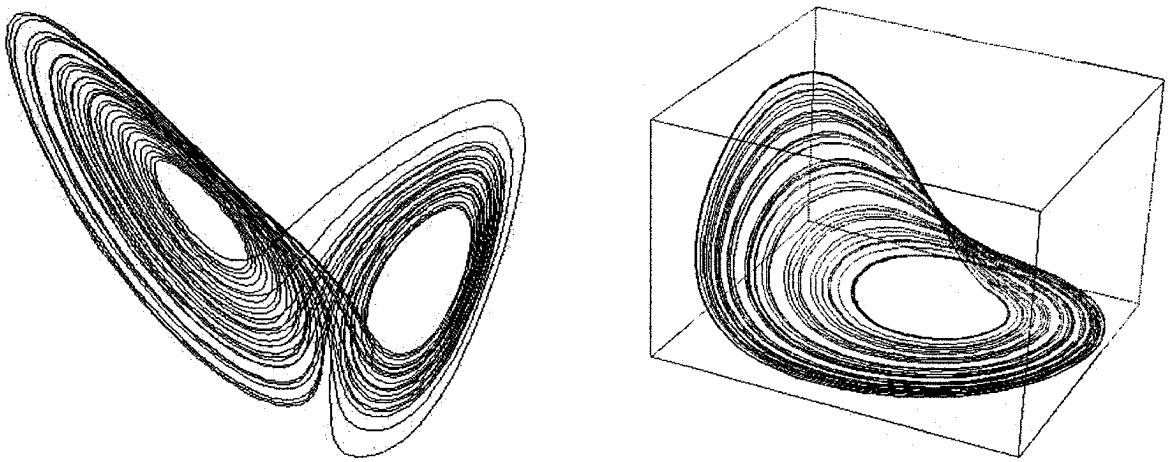

(a) (b)

Figure 4.1 Strange attractors (a) Lorenz strange attractor; (b) Rossler strange attractor

(c) It is sensitive to initial conditions

Sensitivity to initial conditions, also known as the "Butterfly effect", means that a slight quantitative difference in starting state can lead to major qualitative differences in long term behaviour (Figure 4.2).

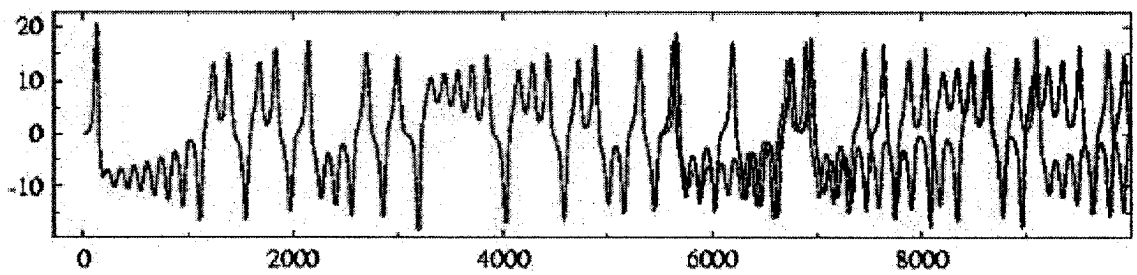

Figure 4.2 Sensitivity to initial conditions

There are a number of ways to quantify and to identify chaos. They are, for example, time history, phase portraits, return maps or recurrence plots, Poincaré maps, power spectrum, Lyapunov exponents, and fractal dimensions, to name just a few. It is important

to note that, on its own, none of the measures is sufficient to ascertain the presence of chaos.

One of the effective indicators of chaotic behaviour in a system is believed to be its set of Lyapunov exponents. The exponents measure the average rate of convergence (if negative exponent) or divergence (if positive exponent) of nearby trajectories in the phase space. A positive Lyapunov exponent indicates exponential divergence of trajectories in that particular direction, and the system has sensitive dependence on initial conditions, a defining signature of chaotic behaviour. In this chapter, the single-axle wheelset models previously presented in Chapter 2 will be investigated by the means of time history, phase portrait, Lyapunov exponents and Lyapunov dimension. The time history and phase portrait are used to examine the models for similarities and differences. The focus, however, is to employ Lyapunov exponents and Lyapunov dimension to study the effect of randomness on the dynamic behaviour of the single-axle wheelset.

4.2 Lyapunov Exponents and Information Dimensions

4.2.1 Determination of Lyapunov Exponents

The determination of Lyapunov exponents and spectrum follows that by Wolf *et al.* [4.2]. Consider two trajectories starting close to one another in the phase space. They will move exponentially away from or toward each other for small times on average. Let d_0 be a measure of the initial distance between the two starting points, at a small but later time, the distance will be

$$d(t) = d_0 2^{\lambda t} \tag{4.1}$$

where the constant λ is called the Lyapunov exponent.

Similarly, areas, spheres and super-spheres of the phase space may stretch or contract under the dynamic process. Accordingly, there are respective Lyapunov exponents to measure the extent to which the principal axes of the initially small areas, spheres or super-spheres are stretched or contracted. The Lyapunov spectrum is then defined as the set of Lyapunov exponents $\{\lambda_i\}$ ($i = 1, 2, \cdots, n$ and $\lambda_1 \geq \lambda_2 \geq \cdots \geq \lambda_n$). As stated earlier, a positive Lyapunov exponent is an indictor of the system having sensitive dependence on initial conditions. The Lyapunov spectrum tells how nearby points move together or away from each other along different axes. The sum of all the exponents says if the phase space as a whole will expand (if positive sum) or contract (if negative sum) or is invariant (if zero sum).

For an autonomous dynamic system, its equations of motion of the system can be written as:

$$\dot{Y} = f(Y, c) \tag{4.2}$$

where f is a vector of n functions and c a vector of parameters. The solution to Eq. (4.2), $Y^*(t, c)$, is termed the reference trajectory and can be sought by methods such as the 4th order Runge-Kutta (RK4) method.

As the next step, one considers variations from the reference trajectory. If η is the variation vector, $Y^* + \eta$ is a point near Y^*. Substituting $Y^* + \eta$ into Eq. (4.2) yields

$$\begin{aligned} \frac{d}{dt}(Y^* + \eta) &= f(Y^* + \eta, c) \\ \frac{dY^*}{dt} + \dot{\eta} &= f(Y^* + \eta, c) \\ f(Y^*, c) + \dot{\eta} &= f(Y^* + \eta, c) \\ \dot{\eta} &= f(Y^* + \eta, c) - f(Y^*, c) \end{aligned} \tag{4.3}$$

Taking the Taylor expansion of $f(Y^* + \eta, c)$ and keeping only the first-order term gives,

$$\dot{\eta} \doteq A(Y^*, c)\eta \tag{4.4}$$

where $A = \nabla f$ is the Jacobian matrix of f, that is:

$$A_{ij} = \left.\frac{\partial f_i}{\partial Y_j}\right|_{Y=Y^*} \tag{4.5}$$

Eq. (4.4) can also be solved by RK4 and the solution is called the second trajectory or tangent space.

Measuring the i-th variation η_i at different time instants t_0, t_1, t_2, $\cdots$, t_M (M being a large integer), the i-th Lyapunov exponent λ_i can be determined by:

$$\lambda_i = \frac{1}{t_M - t_0} \sum_{k=0}^{M-1} \log_2 \frac{|\eta_i(t_{K+1})|}{|\eta_i(t_K)|} \tag{4.6}$$

where $|\eta_i(t)|$ denotes the norm of $\eta_i(t)$. The definition of λ_i by Eq. (4.6) is known as the evolution of λ_i since λ_i is function of time. When t_M is large enough, $\lambda_i(t)$ converges to certain values and become steady. Such steady values are needed for the accurate evaluation of the Lyapunov exponents.

4.2.2 Determination of Lyapunov Spectrum

To find the Lyapunov spectrum, a set of n orthonormal variation vectors η_i ($i = 1, 2, \cdots, n$) is set up to span over the entire phase space. The evolutionary process of the λ_i's is

then observed, i.e., at each time step, RK4 is employed to numerically integrate $Y^*(t,c)$ from Eq. (4.2) as well as the n η_i's from Eq. (4.4), then the n λ_i's as defined by Eq. (4.6) are calculated. As time goes on, each η_i will eventually fall into the principal axes of the super-sphere and the λ_i's become steady.

Attention is especially paid to the two following aspects:

(1) Since the η_i's grow exponentially with time, to avoid overflow in the computation, they are normalized to unity at the beginning of each time step; and

(2) Due to the fact that $A = \nabla f$ and gradients are the local directions of the most rapid growth, the η_i's will become indistinguishable during the course of evolution. Therefore the Gram-Schmidt renormalization procedure (see Reference [4.2]) is adopted to ensure that the η_i's will always span over the entire phase space.

The Lyapunov exponent is a quantitative measure of sensitivity of a dynamic system to change in initial conditions, or a quantitative measure of loss of information during its motion. As informational loss is associated with strange attractors, another quantitative measure, information dimension, is commonly utilized. The information dimension measures the extent to which orbits of the dynamical process fill a certain subspace. A non-integer dimension is a hallmark of a strange attractor and implies the existence of chaos [4.3].

4.2.3 Determination of Lyapunov and Information Dimensions

When a dynamic system possesses a strange attractor, regions of the phase space are stretched, contracted, folded and remapped onto the original space, which can be

mathematically described by the Smale horseshoe transformation (Figure 4.3). This remapping leaves gaps in the phase space. This means that orbits tend to fill up a subspace whose dimension is less than an integer. Information dimension, like other fractal dimensions, measures the extent to which orbits fill a certain subspace.

There are a few useful definitions of a fractal dimension [4.3]. These include, the capacity dimension (commonly known as the box counting dimension), the Hausdorff dimension which is an improved version of the capacity dimension, the information dimension and the correlation dimension. It can be proved that information dimension is in fact the weighted capacity dimension since each box size is weighted with the frequency with which the trajectory visits the box. It is believed that information dimension is one of the most direct measures of an attractor [4.1, 4.3].

Kaplan and Yorke proposed a dimension that is based on the Lyapunov exponents. This dimension, D_L, termed the Lyapunov dimension, is determined by the following equation [4.4]:

$$D_L = J + \frac{1}{|\lambda_{J+1}|}\sum_{i=1}^{J}\lambda_i \tag{4.7}$$

where J is the largest integer that satisfies $\sum_{i=1}^{J}\lambda_i > 0$ and $\sum_{i=1}^{J+1}\lambda_i < 0$. As can be seen in Figure 4.4, D_L is an estimate of the dimension of the phase space that neither grows nor decays. Kaplan and Yorke conjectured that D_L might be equal to the information dimension D_I. In what follows, Eq. (4.7) will be used to determine the wheelsets' information dimension.

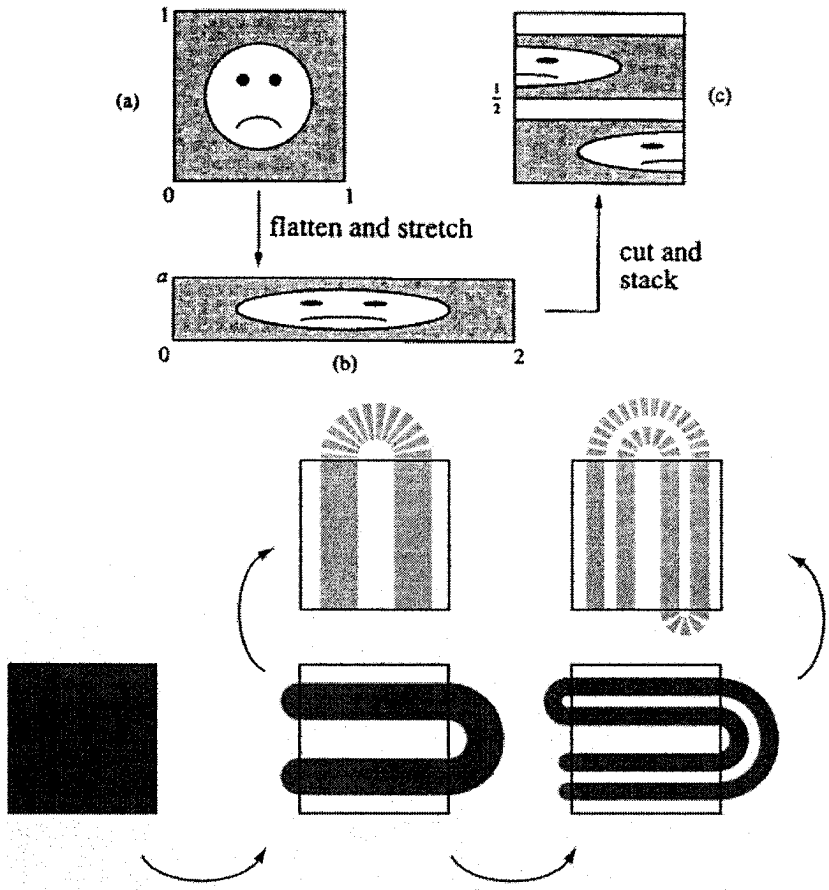

Figure 4.3 (Top) The Smale horseshoe map; (Bottom) Horseshoe transformation of phase space

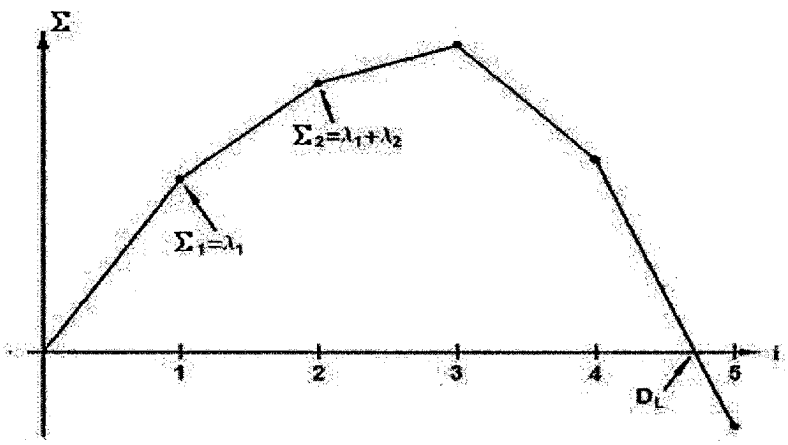

Figure 4.4 Lyapunov dimension as determined by Eq. (4.7)

In passing, a direct quote from [4.3] may be warranted: "While both quantitative tests can be automated using computer control, experience and judgment are still required to

provide a conclusive assessment as to whether the motion is chaotic or strange attractor. Finally, almost all physical examples of strange attractors have been found to be chaotic, that is non-integer d implies $\lambda > 0$. However, a few mathematical models have been studied where one does not imply the other." Here "both quantitative tests" refer to the Lyapunov exponents and fractal dimensions; d refers to a fractal dimension, and λ to a Lyapunov exponent. In other words, for the investigation of chaotic behavior in a dynamic system, it is only prudent to not rely on one single measure to identify chaos.

4.3 Incorporating Randomness into Chaotic Motion

The publications on random chaotic motion are very limited in the open literature. The several publications found were intensely mathematical [4.5-4.10], even though the systems investigated were rather simple, such as the logistic map used in [4.7]. The random chaotic map proposed by [4.5] was composed of maps of trigonometric and elliptic types, and the invariant measure was the eigenfunction of the Perron-Frobenius operator. Reference [4.6], with particular attention to short noisy systems, discussed the statistical analysis of a dynamical system based on estimating the leading (i.e., the largest) Lyapunov exponent. Reference [4.7] found that "dynamic noise can dramatically change the dynamics of low-dimensional chaotic systems". Here dynamic noise refers to noise that "acts as a driving term in the equations of motion". The authors of [4.7] found that the statistical tests for chaos proposed by Shintani and Linton [4.8, 4.9] and by Whang and Linton [4.10] may fail to characterize chaos by producing negative Lyapunov exponents.

The present investigation chooses to incorporate the randomness numerically. The approach is expanded from that of [4.11]. The approach is a combination of Monte Carlo simulation (see Chapter 3) and determination of Lyapunov exponents (see Section 4.2). Specifically, 256 random series are generated. Each series consists of 25,600 normally distributed random numbers. These random numbers are then added to the parameters that are considered random. Next, the Lyapunov exponents of the wheelset are determined. Once the exponents of all 256 realizations are computed, ensemble averages of the Lyapunov exponents are computed. Finally, the information dimension is evaluated based on the ensemble averages of the exponents.

4.4 Preliminary Results and Discussions

In this section, the wheelset models and combinations previously discussed in Chapter 2 are to be investigated, with the aim of comparing the models and combinations for further examination. The means used for the preliminary investigation are: time history, phase portrait, Lyapunov exponents and information dimension.

4.4.1 Combination 1

This combination is comprised of Models III, IIIa, and IIIb. The parametric values are listed in Table 2.5. This combination aims to examine the effects of employing different theories of creep forces and moments.

(a) Deterministic Time History and Phase Portrait

The RK4 method is used to numerically integrate Eqs. (2.29), (2.30) and (2.31). Initial condition is set to $y(0) = \delta$, $\dot{y}(0) = \psi(0) = \dot{\psi}(0) = 0$, where δ is the dead band. Time step size is $\Delta t = 0.001$ s, and forward speed (traveling speed) is $v = 15$ m/s. The total steps are 150,000, covering a 150-second time interval. The plots of lateral displacement versus time are given in Figures 4.5 through 4.7 for Models III, IIIa and IIIb, respectively, where only typical snapshots of time history between $t = 140$ s and $t = 150$ s are shown.

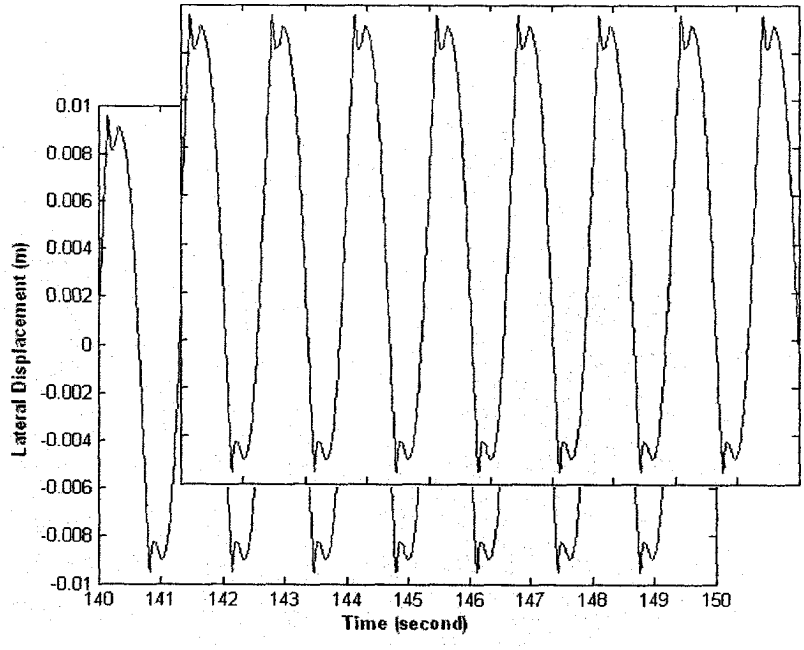

Figure 4.5 Lateral response of wheelset at $v = 15$ m/s, Model III

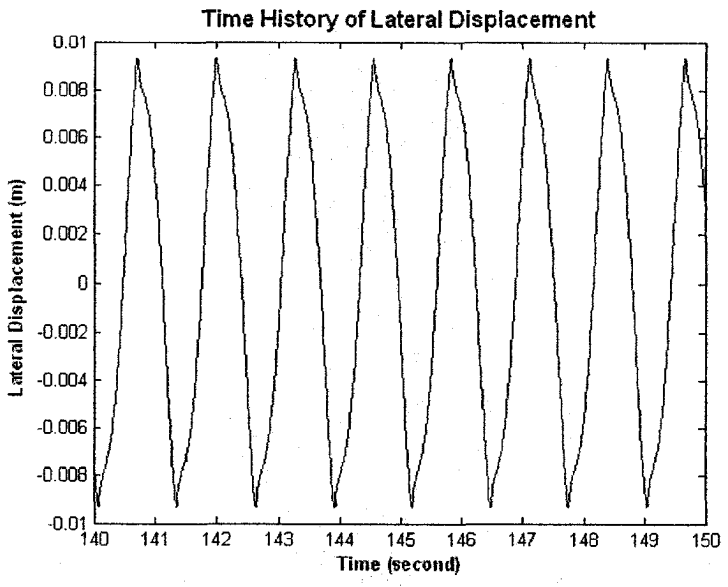

Figure 4.6 Lateral response of wheelset at v = 15 m/s, Model IIIa

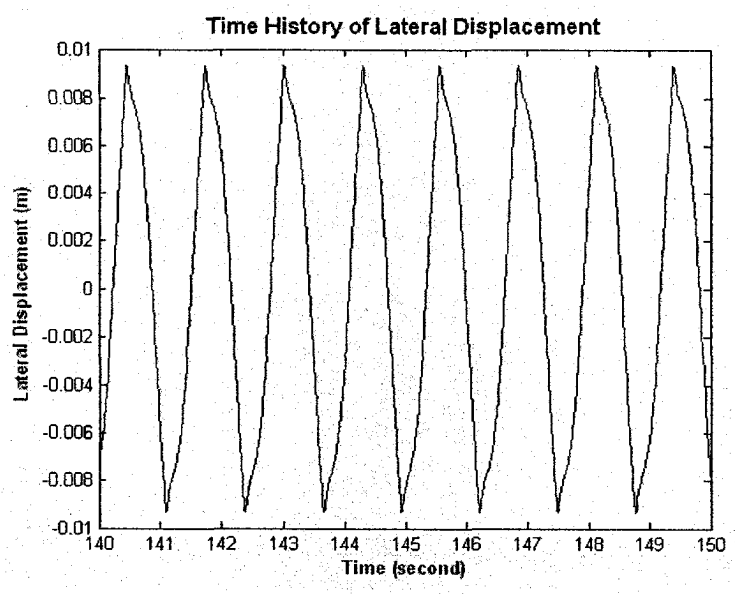

Figure 4.7 Lateral response of wheelset at v = 15 m/s, Model IIIb

Figures 4.5 through 4.7 show that the periods of the models are almost identical, being approximately 1.25 seconds. The difference between Models IIIa and IIIb is indiscernible. The difference between Model III and the other two models lies in the small oscillations near the maximum and minimum displacements. The effect of these small oscillations can

be seen more clearly by comparing the respective phase portraits, see Figures 4.8 through 4.10, where the small oscillations are seen as the small inner loops in Figure 4.8. It seems that Model III is able to capture better the details of the dynamic behaviour.

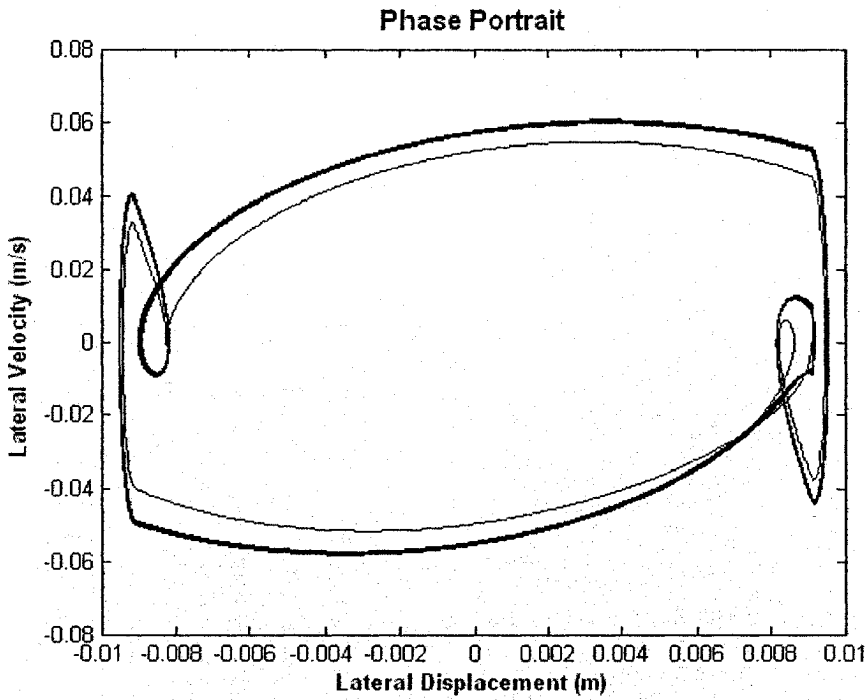

Figure 4.8 Phase portrait of lateral displacement at v = 15 m/s, Model III

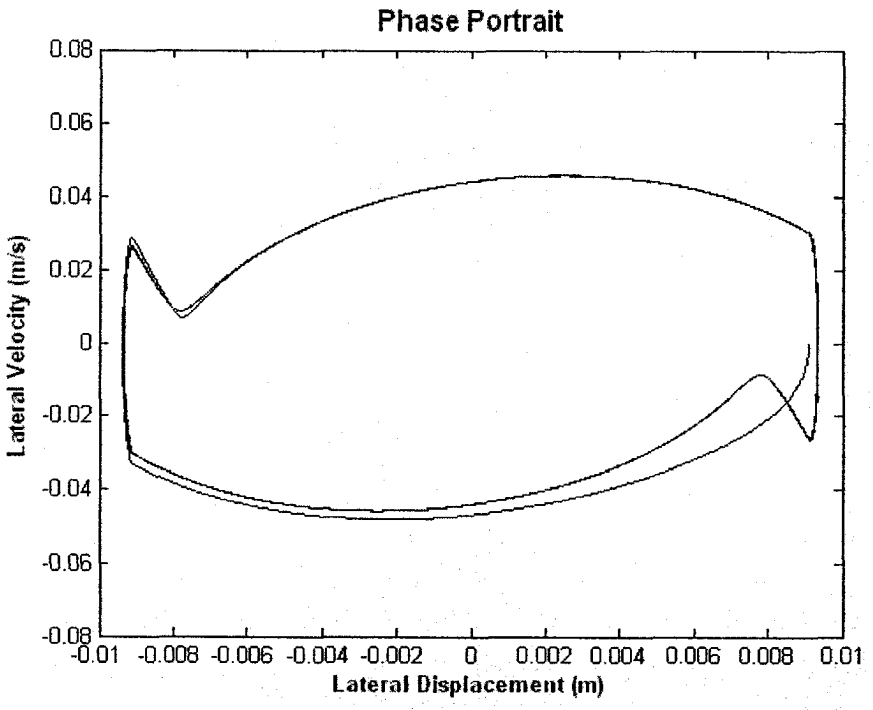

Figure 4.9 Phase portrait of lateral displacement at $v = 15$ m/s, Model IIIa

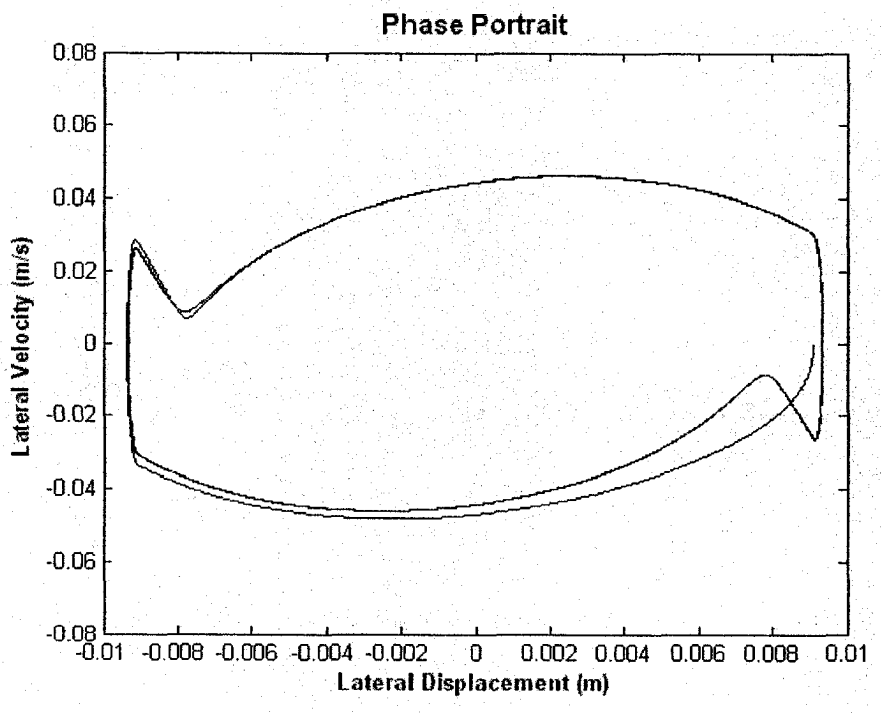

Figure 4.10 Phase portrait of lateral displacement at $v = 15$ m/s, Model IIIb

(b) Lyapunov Exponents and Information Dimensions

In the computation of the Lyapunov exponents and information dimensions, RK4 is again used to numerically integrate the response $Y(t_k)$ and variations $\eta_i(t_k)$. The forward velocity v varies between 10 m/s and 20 m/s with an increment of 0.1 m/s. Initial condition is kept the same as that for time history. Spectral intensity S_0 is set to several values between 0 and 100. Note that the variance of a random series is related to the spectral intensity of the series by $\sigma^2 = 2\pi S_0$. Therefore, $S_0 = 0$ is indicative of a deterministic case.

The range of forward speed is so chosen because the critical speed (the speed at which hunting occurs) can be found by the following formula [4.12] for conically shaped wheels,

$$v_c^2 = \frac{r_0 a\left(W_A \lambda a + 2k_1 a^2 + 2k_2 d_1^2\right)}{\lambda\left(I_{wz} + ma^2\right)} \tag{4.8}$$

The critical speed for Models III, IIIa and IIIb is determined to be v_c = 11.008 m/s, using the data from Table 2.5. This value is rather close to that predicted by [4.13] which found that the first super-critical Hopf bifurcation would take place at 10.16 m/s. Reference [4.13] also found that the wheelset would experience, within the speed range of 10 m/s to 20 m/s, a variety of complex dynamical behaviours such as flange hitting rails, chaos explosions and reverse period doubling, in addition to super-critical Hopf bifurcation.

The numerical integration is performed over a total of 15000 steps with a time step size of 0.001s, or to cover 15 seconds in the time domain. The large integer M in Eq. (4.6)

is set to 7500. The (temporal) average of these 7500 values of λ_i is then considered the λ_i of a sample, or a realization. Finally, the ensemble averages of λ_i over 256 samples are used to determine the information dimension by means of Eq. (4.7). It is observed that each computer run requires about 8 hours of computing time. On the other hand, a deterministic case requires only about 25 seconds of computing time.

Due to space limitation, only the mean (or averaged) values of representative leading Lyapunov exponents and the corresponding information dimensions are presented, as plots, in this section and the remainder of the thesis. It should be pointed out that the mean square and variance values are also examined and are found to be within reasonable range. Appendix B contains the plots of root mean squares and variances of a typical case with randomness of $S_0 = 1$ in forward speed and incorporated into Model III. Sample results of the four computed Lyapunov exponents and information dimensions are presented in Appendix C.

Figures 4.11, 4.13 and 4.14 illustrate how information dimensions for Models III, IIIa and IIIb vary with respect to the averaged forward speed when the forward speed is assumed random with spectral intensity of 0.0025, 0.01, 1, 25 and 100, respectively. The leading Lyapunov exponent, λ_1, of Model III with the same randomness levels in forward speed is shown in Figure 4.12. In all four plots, the information dimensions and leading Lyapunov exponent for the deterministic case have been included for comparison.

The figures show that,

(1) Model III is the only model for which the information dimensions of the wheelset do not exceed the value of 4, the dimension of the phase space. With reference to Figure 4.12, it can be seen that the motion of the wheelset is very similar when S_0 = 0, 0.0025 and 0.01, with the exception that, in the deterministic cases, there are two small windows (around v = 18 m/s) of non-chaotic motion. For the case of S_0 = 1, two windows of non-chaotic motion are also observed, one being at 12 m/s, the other being 12.4 – 13.5 m/s. On the other hand, the information dimensions shown in Figure 4.11 are, for $S_0 < 1$, either 0 or close to 2. For higher randomness, chaotic motion is seen over the entire speed range, as indicated by the non-integral information dimensions in Figure 4.11 and the large positive leading Lyapunov exponents in Figure 4.12. In the present investigation, the spectral intensity is restricted to values of up to 100 only. Reference [4.14] has shown that the values of the model's information dimensions are still within 4 even when S_0 is as high as 10,000.

(2) As indicated in Figures 4.13 and 4.14, when randomness is small ($S_0 \leq 1$), Models IIIa and IIIb predict information dimensions with values between 0 and 2. However, with increased spectral intensity, the two models give rise to information dimensions that are in the tens, and that do not seem to show any general trend. Different computer runs have confirmed the high information dimension values, and the lack of a general trend;

(3) Models IIIa and IIIb do not yield the same information dimensions, regardless of the values of the spectral intensity S_0. Therefore, indiscernible time histories do not lead to same or close information dimensions;

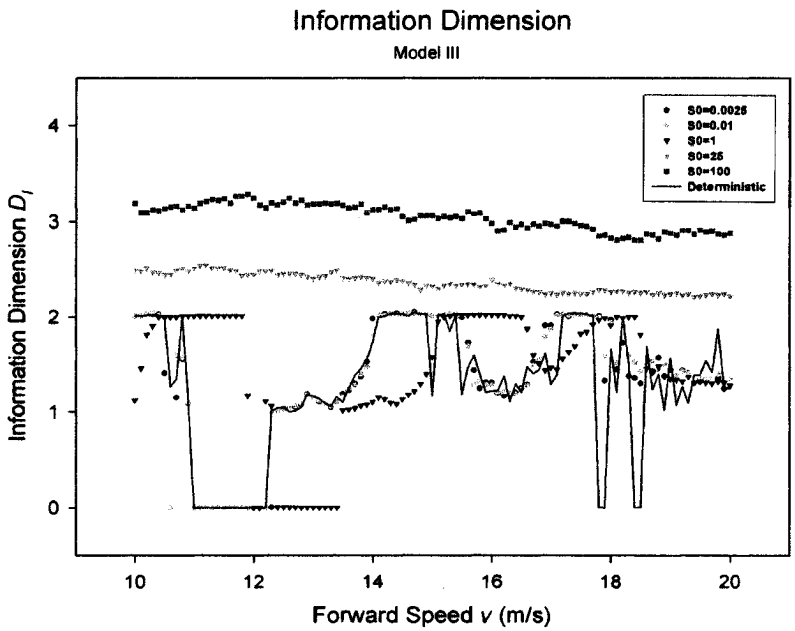

Figure 4.11 Information dimensions with randomness in speed, Model III

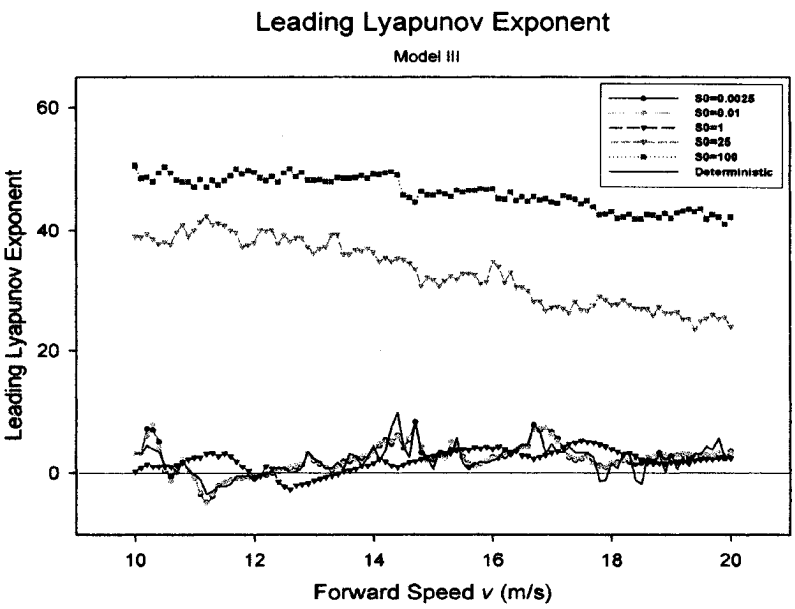

Figure 4.12 Leading Lyapunov exponents with randomness in speed, Model III

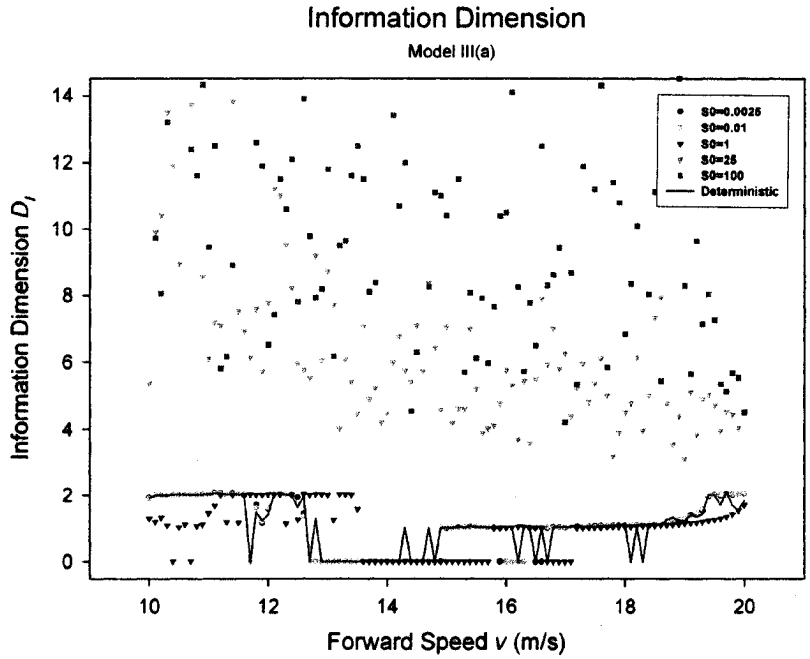

Figure 4.13 Information dimensions with randomness in speed, Model IIIa

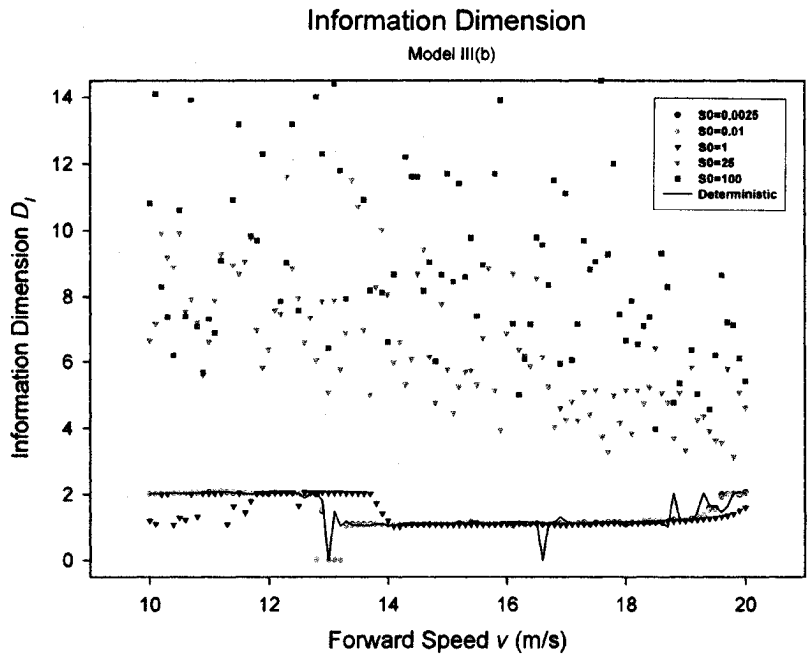

Figure 4.14 Information dimensions with randomness in speed, Model IIIb

(4) Considering small randomness ($S_0 \leq 1$), the information dimension plots of Models IIIa and IIIb do not resemble that of Model III;

(5) Recalling that Model III employs the nonlinear Vermeulen and Johnson theory to evaluate creep forces, it may be concluded that linearization of creep forces may be inappropriate. Figure 4.15 compares the two creep force theories, where the normalized creepages are $\xi_X \frac{G\pi a_e b_e}{\mu N}$ (longitudinal), $\xi_Y \frac{G\pi a_e b_e}{\mu N}$ (lateral) and $\xi_R \frac{G\pi a_e b_e}{\mu N}$ (resultant), respectively, and the normalized creep forces are F_X/N, F_Y/N and F_R/N, respectively. The comparison uses data in Table 2.5. Significant differences are observed, affirming that linearizing the creep forces may not be desirable.

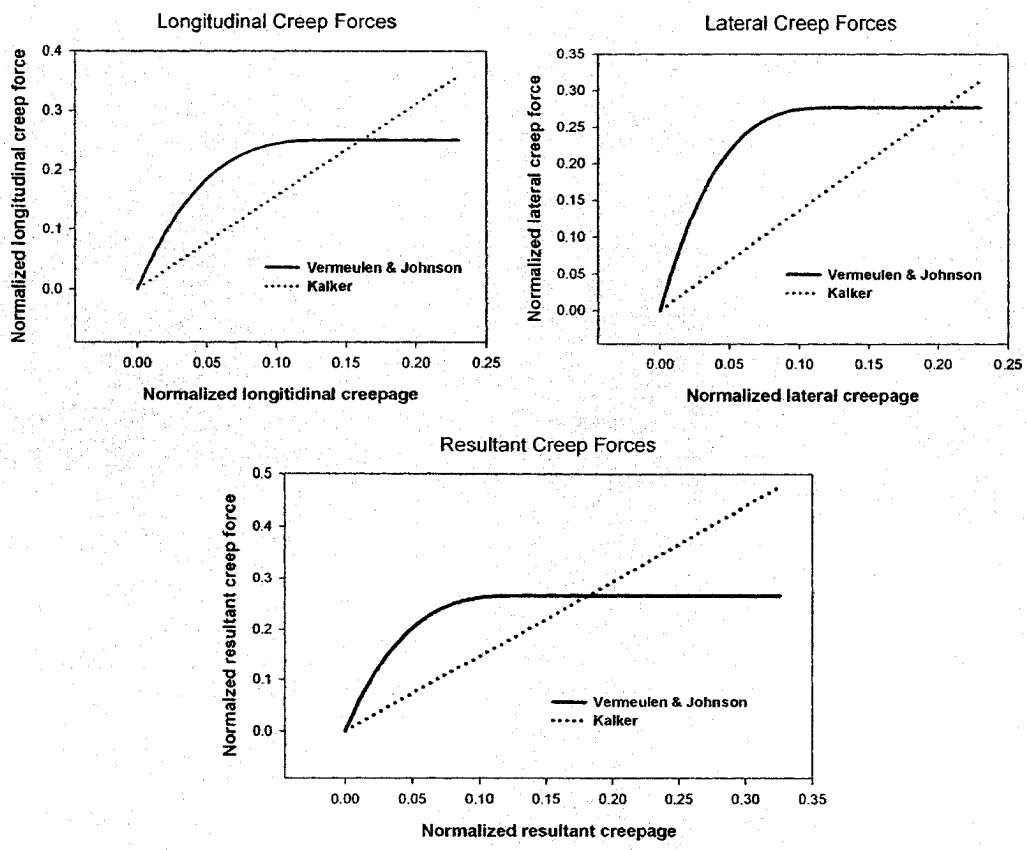

Figure 4.15 Normalized creep forces

4.4.2 Combination 2

Combination 2 consists of Models II and IIa. The parametric values are given in Table 2.6. This combination is devised to investigate the effects due to gravitational stiffnesses and the gyroscopic couple. The critical hunting speed is found to be $v_c = 36.020$ m/s, using Eq. (4.8) which is rewritten in terms of symbols used for Models II and IIa,

$$v_c^2 = \frac{r_0 a\left(W_A \lambda a + 2k_y a^2 + 2k_\psi b^2\right)}{\lambda\left(I_{wz} + ma^2\right)} \tag{4.9}$$

(a) Deterministic Time History

Time histories are computed using RK4, for a forward velocity of v = 35 m/s. Initial conditions are $y(0) = \delta,\ \dot{y}(0) = \psi(0) = \dot{\psi}(0) = 0$ where δ is the dead band. Time step size is 0.001 second. The two responses shown in Figure 4.16 illustrate the lateral displacement $y(t)$ for a 150-second period of time.

It is seen that the models' lateral displacement with v = 35 m/s are rather similar. One visible difference is the time taken for the oscillation to be damped to technical zero. Model IIa needs about 80 seconds while Model II takes approximately 50 seconds. The other difference seems to be the envelope formed by oscillating amplitudes. Model II has an envelope that "slims" down faster and encloses a smaller "area".

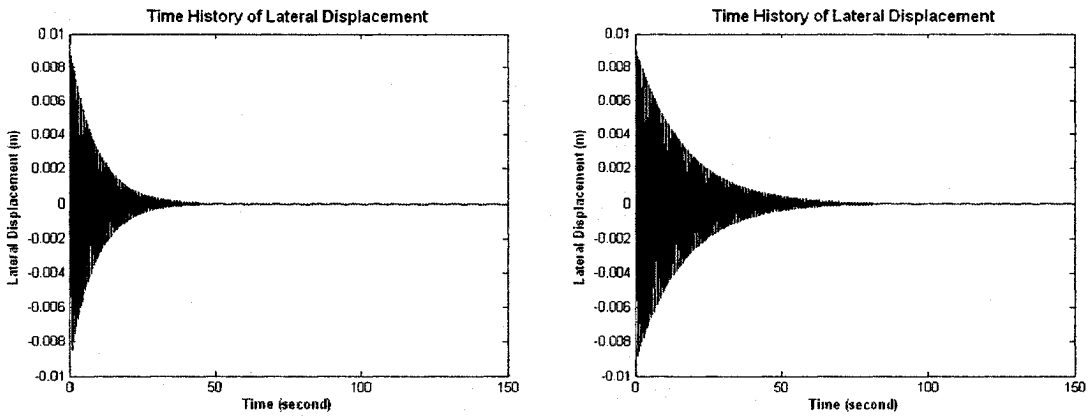

Figure 4.16 Lateral responses of wheelset at v = 35 m/s (Left) Model II ; (Right) Model IIa

(b) Lyapunov Exponents and Information Dimensions

For the Lyapunov exponents and information dimensions, the forward velocity v is varied between 30 m/s and 40 m/s, and the spectral intensity S_0 between 0 and 1 for both models. Other settings are the same as for Combination 1. Values of S_0 greater than unity are found to cause numerical overflow. The reason for this is not yet completely clear. But the following may be stipulated. As will be seen later in Section 4.4.3 where Model IIb will be used in Combination 3, no numerical overflow is encountered. Since Model IIb differs from Model II in the modeling of creep forces and moments, and in the parametric values of the model data, one may conclude, from the modeling perspective, that linear creep forces and moments are not suitable for cases with S_0 values greater than unity. This in fact is one of the findings of Section 4.4.1. From the point of view of parametric values for the model, it is noted that Model IIb is computed based on, mainly, data for Model III. Although this may lead to the conclusion that model data are also the cause of numerical

overflow, it is more likely that it is modeling (linear vs. nonlinear creep forces and moments) that plays a more dominating role.

Information dimension plots are shown in Figure 4.17 for S_0 = 0, 0.0025, 0.01 and 1, respectively. It is seen that,

(1) For Model II, the information dimension changes from being close to 2 to being 0 at approximately 38.6 m/s. This remains unchanged for the other three S_0 values computed; and

(2) Model IIa, on the other hand, obtains zero information dimension at lower speed (v < 36.8 m/s approximately). At higher speed and with the introduction of randomness in speed, the information dimension drops to values between 1 and 0.

The Lyapunov exponents and information dimensions computation is repeated for the speed range of 10 m/s to 20 m/s. The resulting plots are given in Figures 4.18 through 4.21 for leading Lyapunov exponents and Figures 4.22 through 4.25 for information dimensions, respectively. Here it is very interesting to observe that the leading Lyapunov exponent and information dimension both "oscillate". The wheelset seems to go into chaotic motion then come out of it, and so on and so forth, over a rather wide range of speed (v > 14 m/s for S_0 = 0, 0.0025 and 0.01; and v > 13-14 m/s for S_0 =1). The plots of the leading Lyapunov exponents (Figures 4.18 through 4.21) suggest that the two models possess acceptable difference, especially when S_0 < 1. However, the difference in information dimensions is more considerable. This difference in information dimensions is partly attributed to the fact that a small negative λ_1 gives rise to a zero information

dimension; however a small positive λ_1 leads to generally a non-integer information dimension.

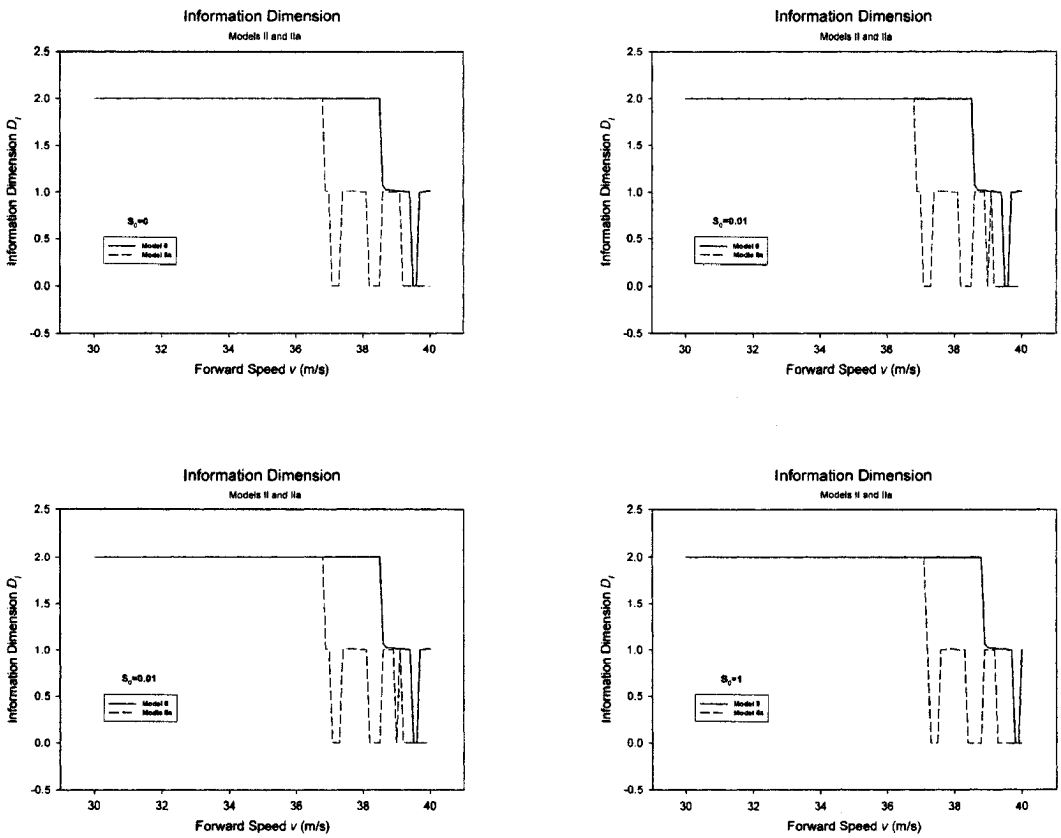

Figure 4.17 Information dimensions with randomness in speed, v = 30 to 40 m/s

Therefore, the effects of gravitational stiffnesses and gyroscopic couple are in general not to be disregarded. Model II, which includes the gravitational stiffnesses and gyroscopic couple, employs the Kalker's linear theory for its creep forces and moments. From the discussions in Section 4.4.1, it would be ideal to have the creep forces formulated by the Vermeulen and Johnson's nonlinear theory.

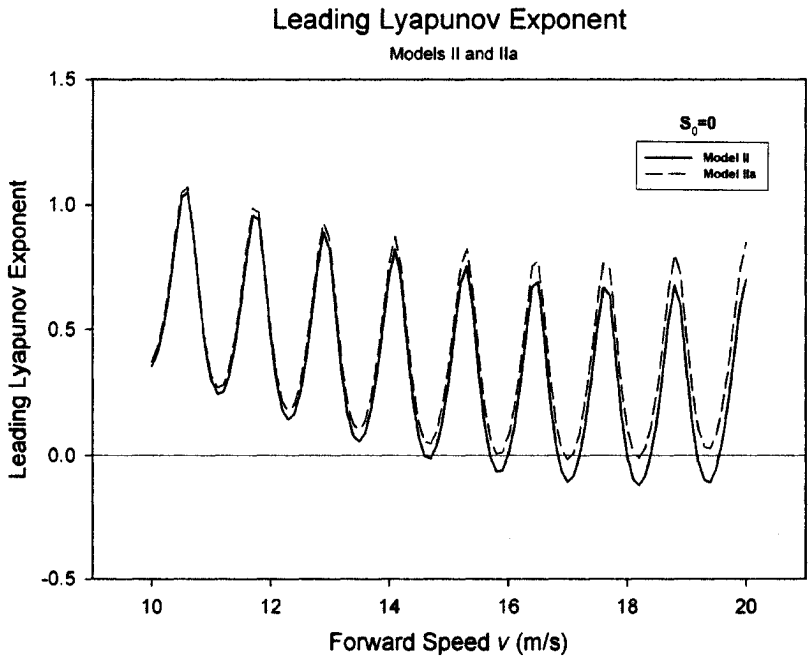

Figure 4.18 Leading Lyapunov exponents, randomness in speed, $S_0 = 0$

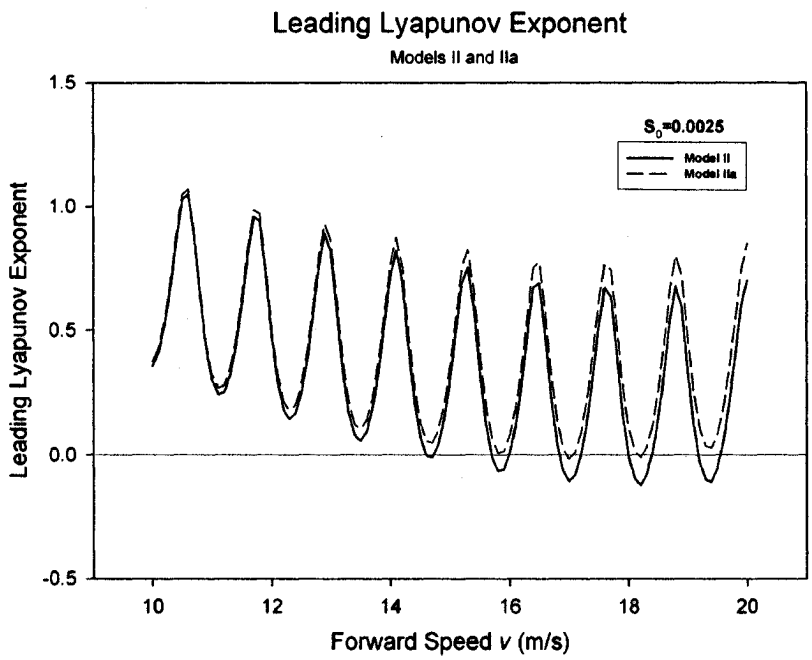

Figure 4.19 Leading Lyapunov exponents, randomness in speed, $S_0 = 0.0025$

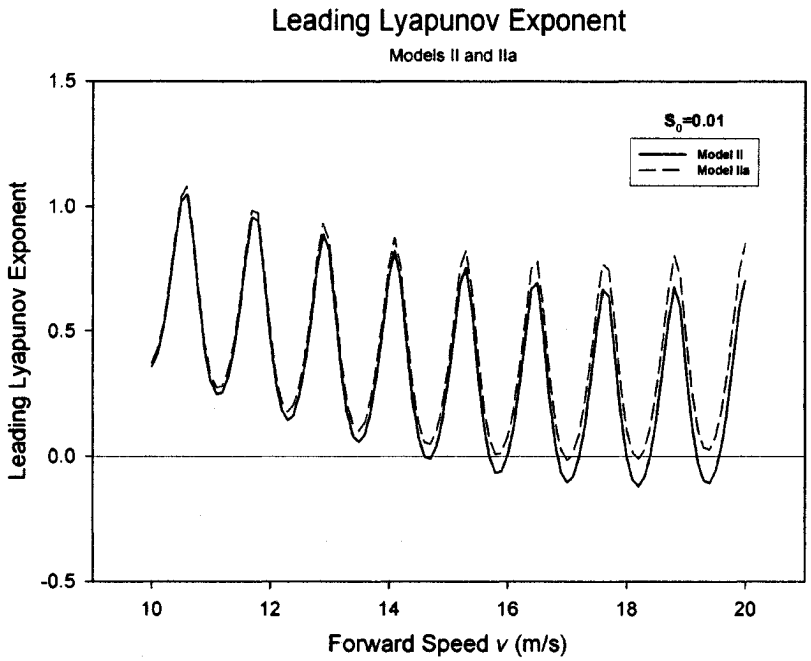

Figure 4.20 Leading Lyapunov exponents, randomness in speed, $S_0 = 0.01$

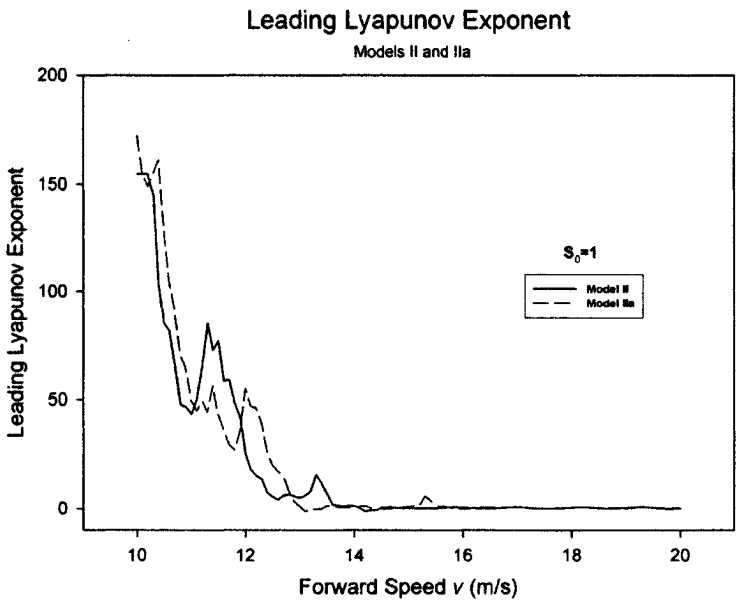

Figure 4.21 Leading Lyapunov exponents, randomness in speed, $S_0 = 1$

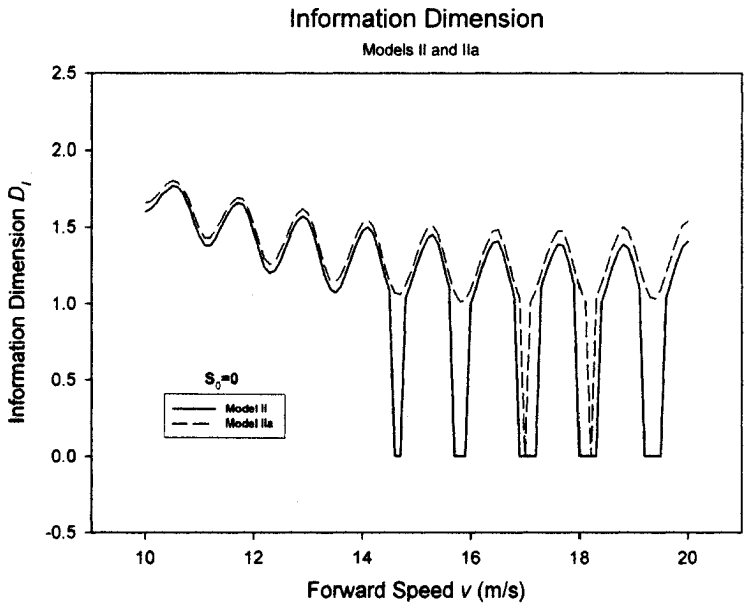

Figure 4.22 Information dimensions with randomness in speed, $S_0 = 0$

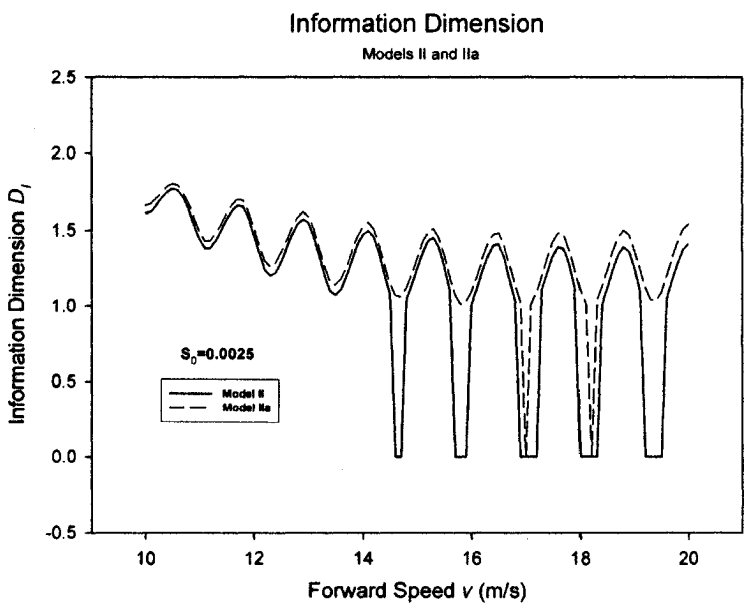

Figure 4.23 Information dimensions with randomness in speed, $S_0 = 0.0025$

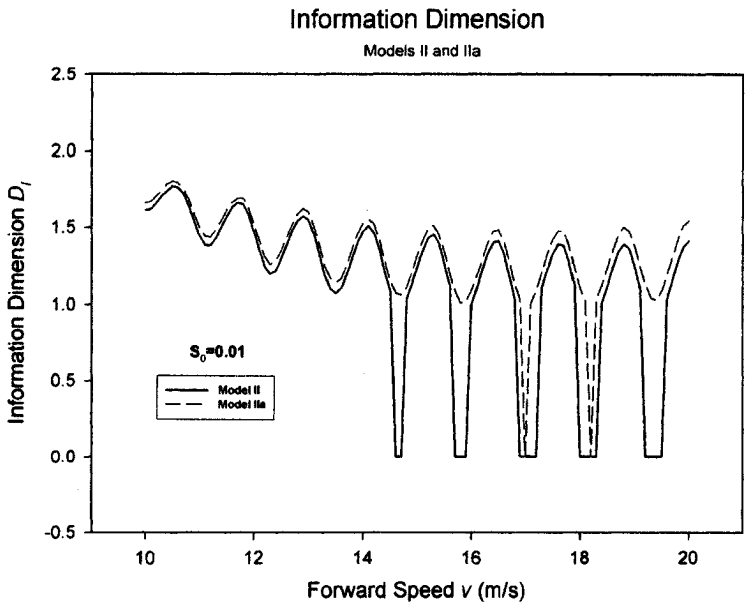

Figure 4.24 Information dimensions with randomness in speed, $S_0 = 0.01$

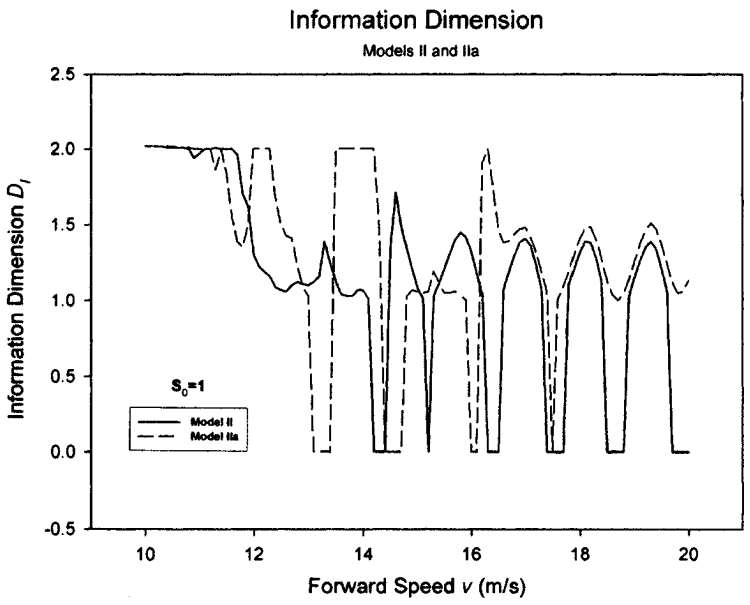

Figure 4.25 Information dimensions with randomness in speed, $S_0 = 1$

4.4.3 Combination 3

The results from Combinations 1 and 2 can be chiefly and briefly summarized as follows: First of all, using Kalker's linear theory to determine creep forces and moments is not recommended, especially for cases where $S_0 > 1.0$; Second, the gravitational stiffnesses and gyroscopic couple are in general not to be omitted. Therefore, it is suggested to construct a model that employs the Vermeulen and Johnson's nonlinear creep theory and that includes the gravitational stiffnesses and the gyroscopic term. Mathematically, this is straight forward, as has been shown in Chapter 2. Numerically, the challenge lies in what set of data to use and how to determine 'missing' data. Attempt was first made, without much success, to start with data for Model II, and then determine constants such as a_e, b_e, Ψ and Φ that are needed for creep forces. Another option would be to use existing data from Model III, and assume a value for I_{wy}. In the end, the second option is adopted. Due to the lack of wheelset data, it is decided to estimate the value of I_{wy} by proportionality with I_{wz}. Obviously, it would be ideal if an estimated value of I_{wy} can be avoided.

As with Combinations 1 and 2, time histories are computed using RK4, with initial conditions of $y(0) = \delta,\ \dot{y}(0) = \psi(0) = \dot{\psi}(0) = 0$, time step size of 0.001 s for a total of 150,000 steps, and a forward velocity at v = 15 m/s. Figures 4.26 and 4.27 show the responses of lateral displacement for the time interval of 140 s to 150 s. Note that Figure 4.27 is a repeat of Figure 4.5. It is interesting to note that Model IIb which adopts the nonlinear theory of creep is not associated with the small oscillations. From results of Section 4.4.1, Model IIb would be expected to experience those small oscillations. Further

investigation reveals that, when the nonlinear theory of creep is used, the small oscillations are due to the exclusion of gyroscopic effect, see Figure 4.28 where the spin moment of the wheelset has been neglected by setting $I_{wy} = 0$.

The Lyapunov exponents and information dimensions are shown in Figure 4.29 for the cases of $S_0 = 25$ and 100, and in Figures 4.30 through 4.33 for cases of $S_0 = 0$, 0.0025, 0.01 and 1, respectively. It is noted that, with higher spectral intensity, Models IIb and III do not show much difference, including or excluding the gyroscopic effect (Figure 4.29). This is understandable since higher level of randomness will very likely push the wheelset to the chaotic motion regime from the non-chaotic one. As a result, difference in modeling (this is, whether to include gravitational stiffnesses and gyroscopic couple) is masked. Differences, sometimes not negligible, are however observed when small to moderate amount of randomness is present (Figures 4.30-4.33). In particular, when setting $I_{wy} = 0$, the information dimension from Models IIb and III are closer or more similar to each other, compared with the case of $I_{wy} \neq 0$. Note that setting W_A and I_{wy} to zero in Model IIb will yield Model III.

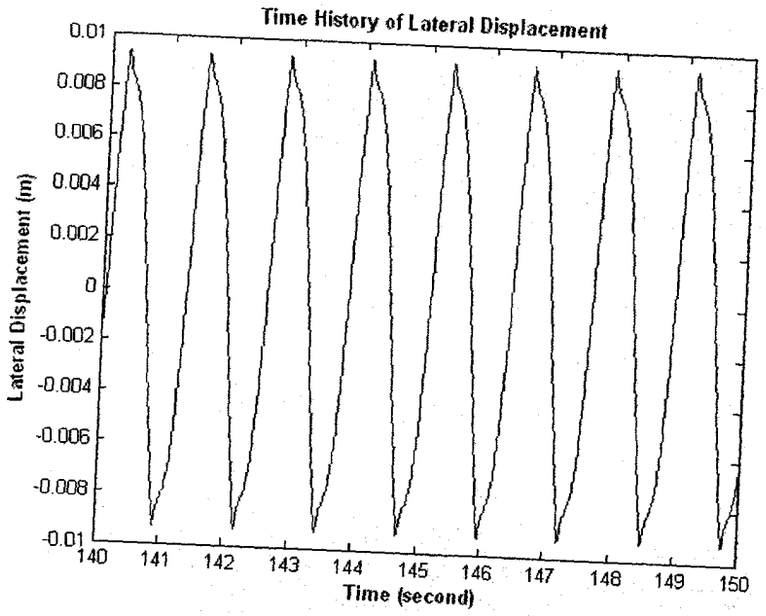

Figure 4.26 Lateral response of wheelset at $v = 15$ m/s, Model IIb

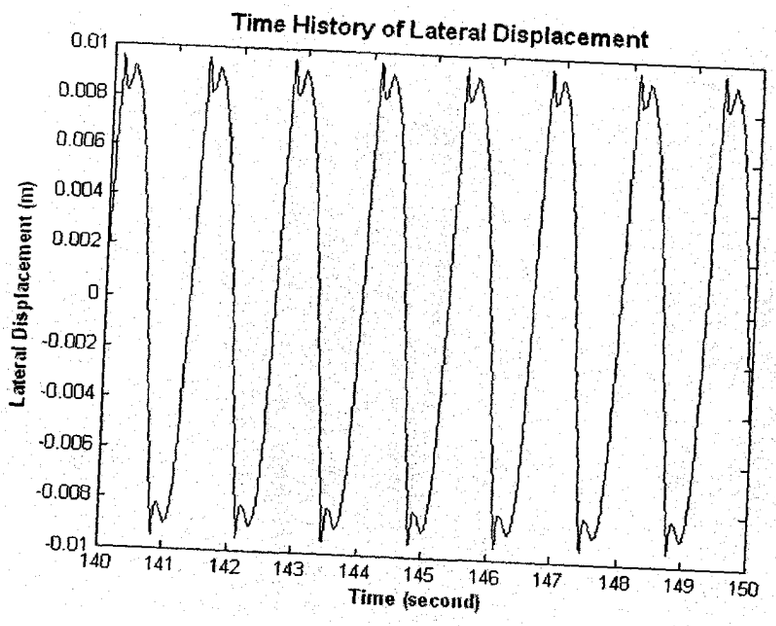

Figure 4.27 Lateral response of wheelset at $v = 15$ m/s, Model III

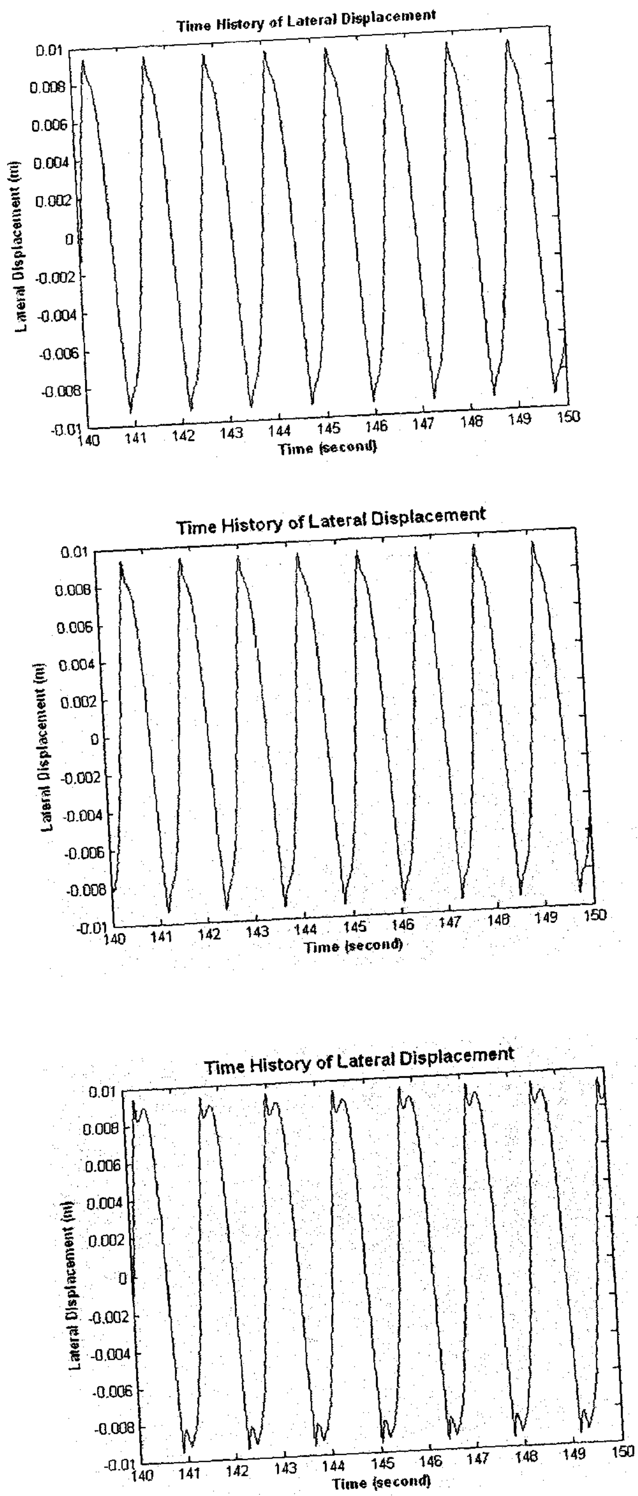

Figure 4.28 Time histories of Model IIb (Top) $W_A \neq 0, I_{wy} \neq 0$; (Middle) $W_A = 0, I_{wy} \neq 0$; (Bottom) $W_A \neq 0, I_{wy} = 0$

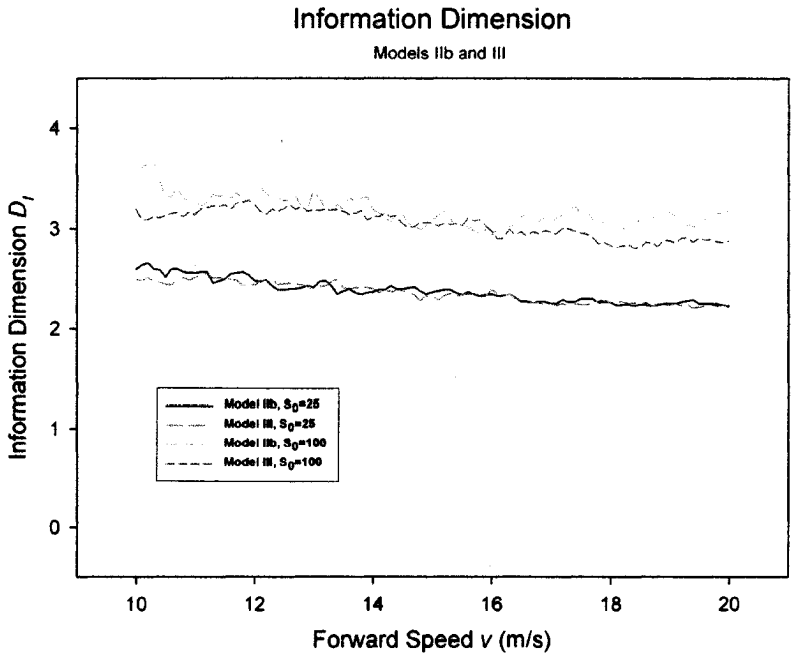

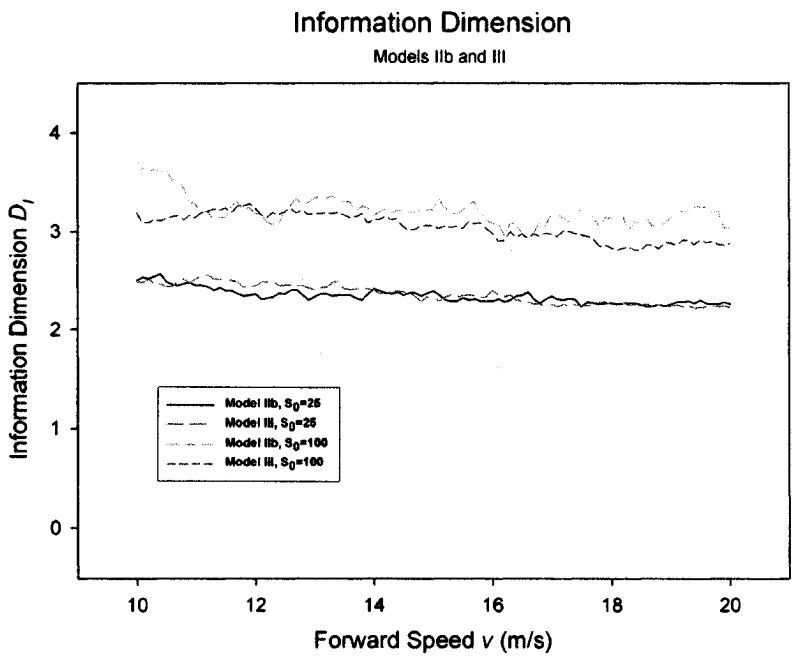

Figure 4.29 Information dimensions with randomness in speed, $S_0 > 1$ (Top) $I_{wy} \neq 0$; (Bottom) $I_{wy} = 0$

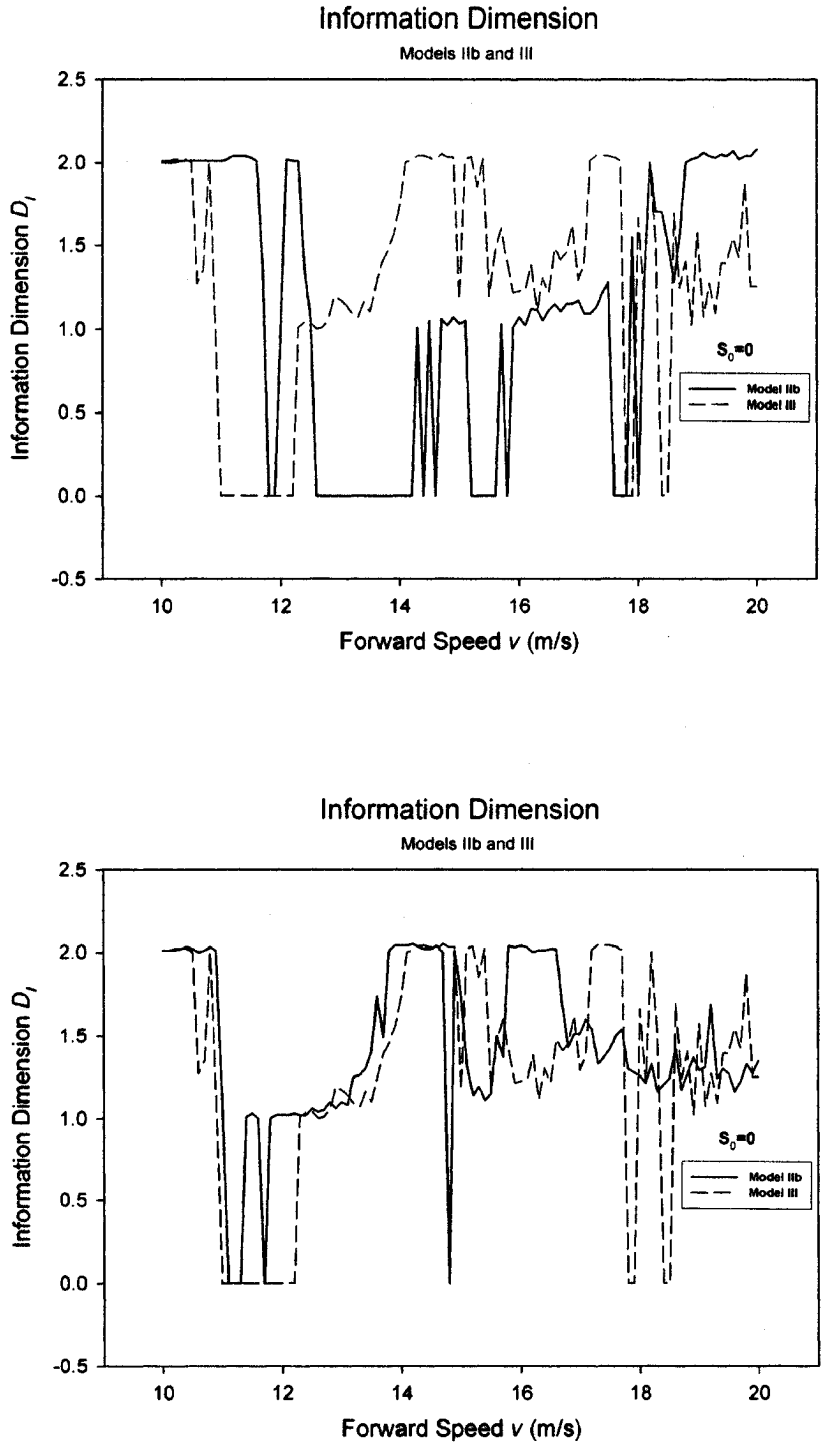

Figure 4.30 Information dimensions with randomness in speed, $S_0 = 0$ (Top) $I_{wy} \neq 0$; (Bottom) $I_{wy} = 0$

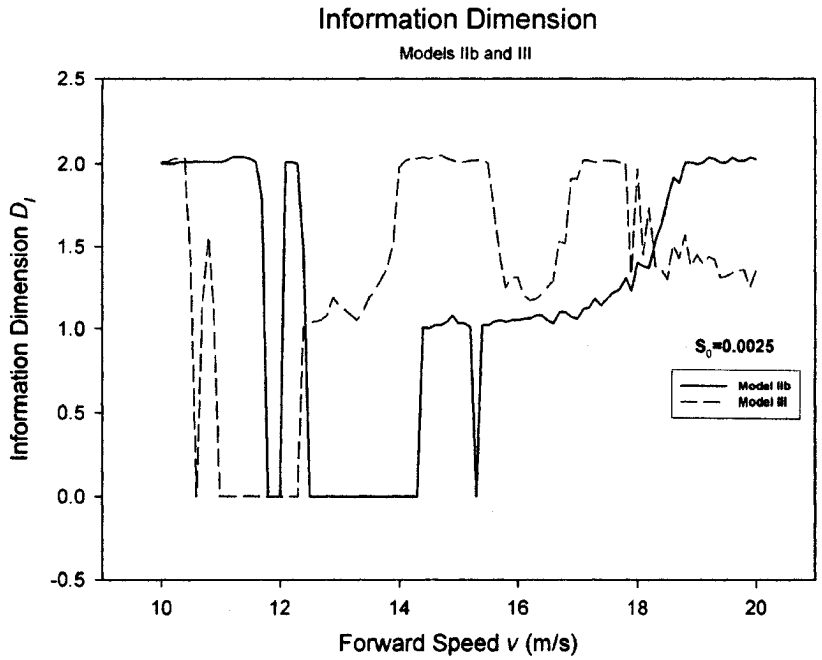

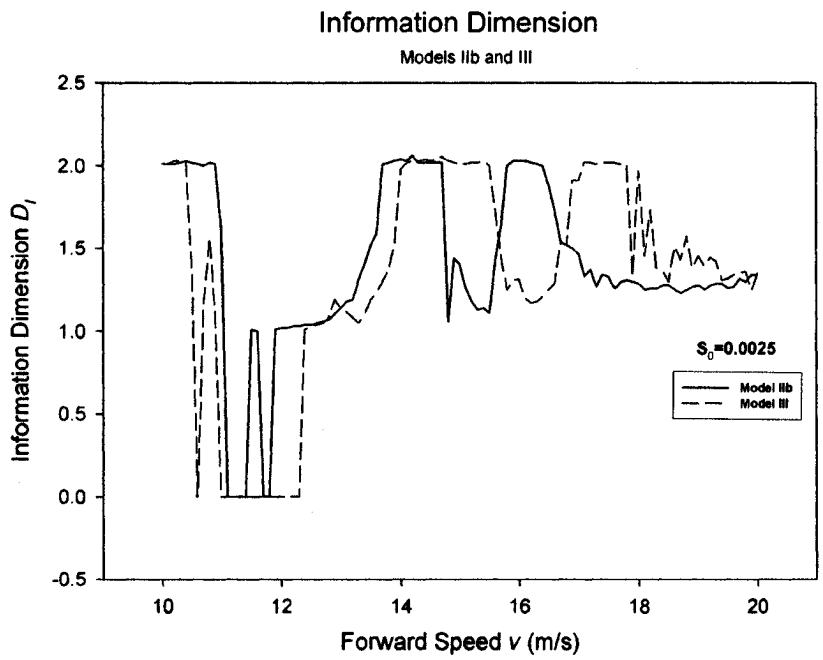

Figure 4.31 Information dimensions with randomness in speed, $S_0 = 0.0025$ (Top) $I_{wy} \neq 0$; (Bottom) $I_{wy} = 0$

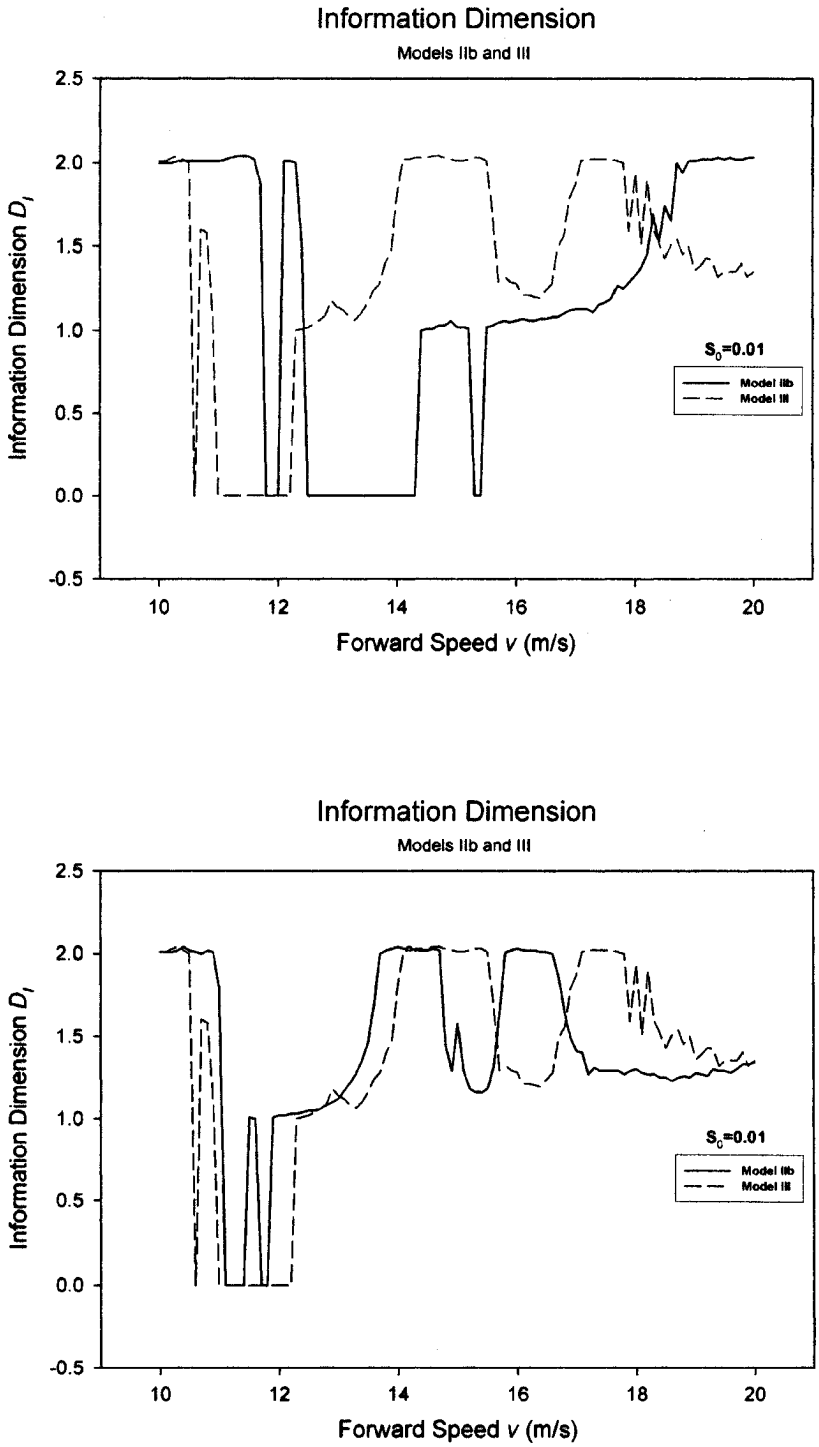

Figure 4.32 Information dimensions with randomness in speed, $S_0 = 0.01$ (Top) $I_{wy} \neq 0$; (Bottom) $I_{wy} = 0$

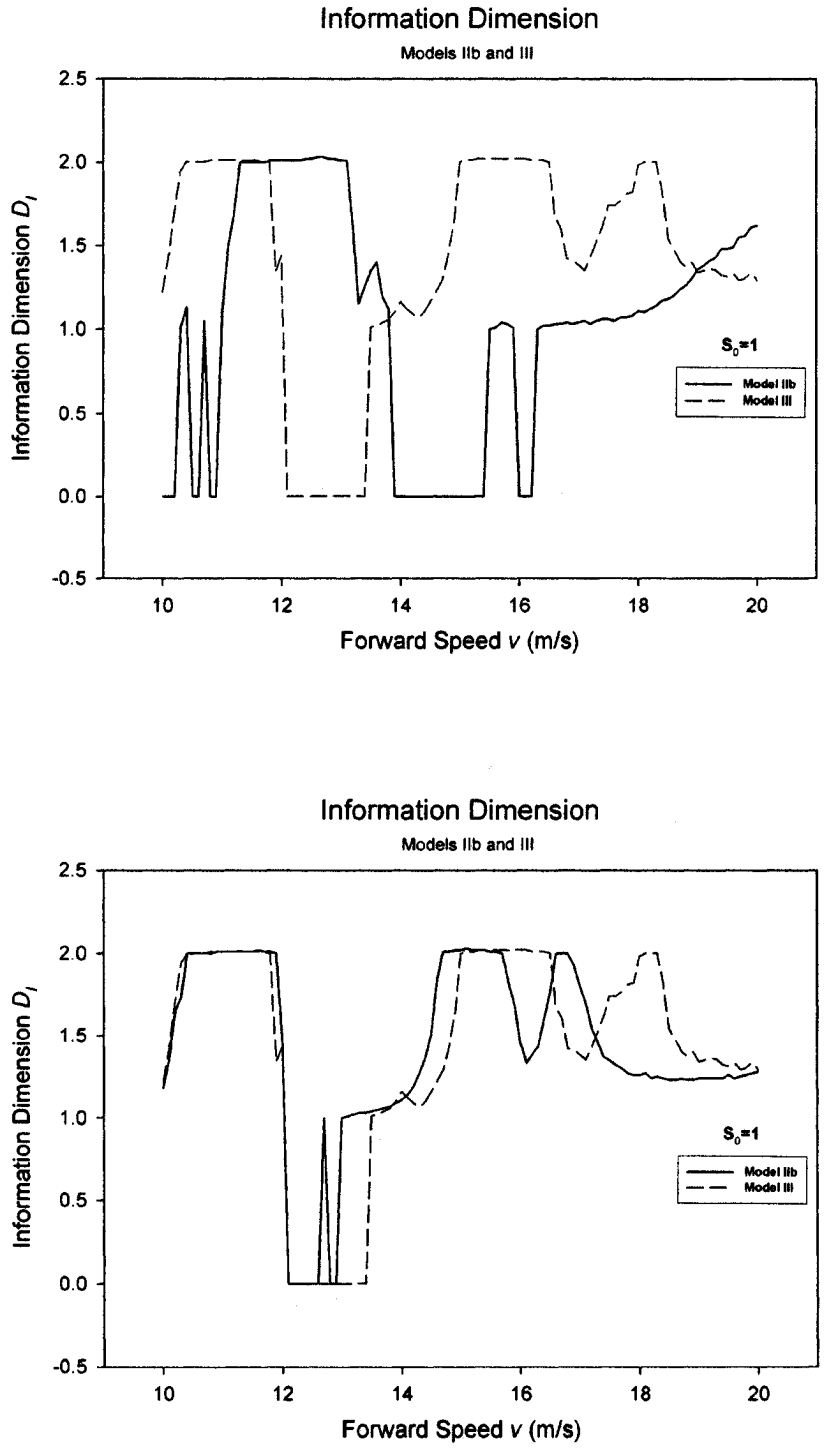

Figure 4.33 Information dimensions with randomness in speed, $S_0 = 1$ (Top) $I_{wy} \neq 0$; (Bottom) $I_{wy} = 0$

4.5 Further Discussions

In this section, Models IIb and III are further investigated for the following cases:

(1) Deterministic forward speed and dead band;

(2) Random forward speed but deterministic dead band;

(3) Random dead band but deterministic forward speed; and

(4) Randomness in both forward speed and dead band.

Here forward speed and dead band are chosen to be associated with randomness because under any practical operating conditions, a wheelset will travel with varying speed. The lateral clearance is seldom constant due to uneven wear in wheel flanges and in rails. It should be noted that for case (4) above, the randomness in forward speed and in dead band are considered independent. For simplicity, the same spectral intensity will be applied to both random series.

Computed information dimensions are given in Figures 4.34 through 4.36. The speed range is 10 to 15 m/s with an increment of 0.1 m/s. The following remarks are in order.

(1) With the presence of large randomness ($S_0 \geq 100$) in forward speed, information dimensions have rather limited variation, compared with the cases of low to moderate randomness in speed. This is true for both models;

(2) When dead band, or dead band together with forward speed, is associated with any amount of randomness ($S_0 \neq 0$), information dimensions are almost constant, regardless of forward speed. Again this is true for both models;

(3) Both models show that randomness in dead band dominates. This means, making sure dead band is as even as possible is more effective in controlling the wheelset's behavior than attempting to travel with constant, or almost constant, forward speed;

(4) The presence of small randomness ($S_0 \leq 0.01$) in forward speed seems not to change the nature of the wheelset's motion. That is, the motion does not switch from non-chaotic to chaotic, or vice versa. In fact, the information dimensions are basically indiscernible between the two models when $S_0 = 0$, 0.0025 and 0.01; and

(5) The case of $S_0 = 1$ with forward speed is the most interesting to examine. The wheelset's dynamic behavior is seen altered over certain speed range. In particular, chaotic motion may be suppressed. As shown in Figure 4.34, the information dimension of Model IIb when $S_0 = 1$ is zero for some speeds between 10-11 m/s and between 14-15 m/s. Similarly, for Model III, such speeds are 11.8-13.5 m/s.

4.6 Conclusions

Discussions in Section 4.4 show that Model IIb is a model that takes into considerations essential aspects of mathematical modeling of a single-axle wheelset, namely, creep forces are nonlinear as by the Vermeulen and Johnson theory, and gravitational stiffnesses and gyroscopic effect are included. Computationally speaking, the model does not lead to problems such as overflow and information dimensions greater than the dimension of the phase space. From the point of view of modeling, Model III is the second best choice. It employs the Vermeulen and Johnson theory so that creep forces are not linearized. It is

computationally reliable in that it will not cause numerical overflow and will not yield information dimensions that are beyond the dimension of the phase space. It has the advantage of being simple (that is, it contains less parameters). Therefore it is applicable to cases where parametric values for I_{wy} and W_A are not available and where S_0 is high ($S_0 > 1$).

Other conclusions are,

(1) Linearization of creep forces and moments should be exercised very cautiously. This is especially true when dealing with higher level of randomness ($S_0 > 1$).

(2) When randomness is small to moderate ($S_0 \leq 1$), the effects of gravitational stiffnesses and gyroscopic couple need to be included.

(3) Small randomness ($S_0 < 1$) in forward speed seems not to alter dynamic behaviour of the wheelset. That is, the motion does not change from non-chaotic to chaotic, or vice versa.

(4) Randomness in dead band dominates over randomness in forward speed. Reducing the unevenness in dead band is more effective in controlling the wheelset's behavior than attempting to travel with constant, or almost constant, forward speed.

(5) Large randomness ($S_0 \geq 100$) in forward speed, or dead band, or both, seems to keep the information dimensions constant over the range of velocity considered. It also seems to universally push the wheelset's response into the chaotic realm.

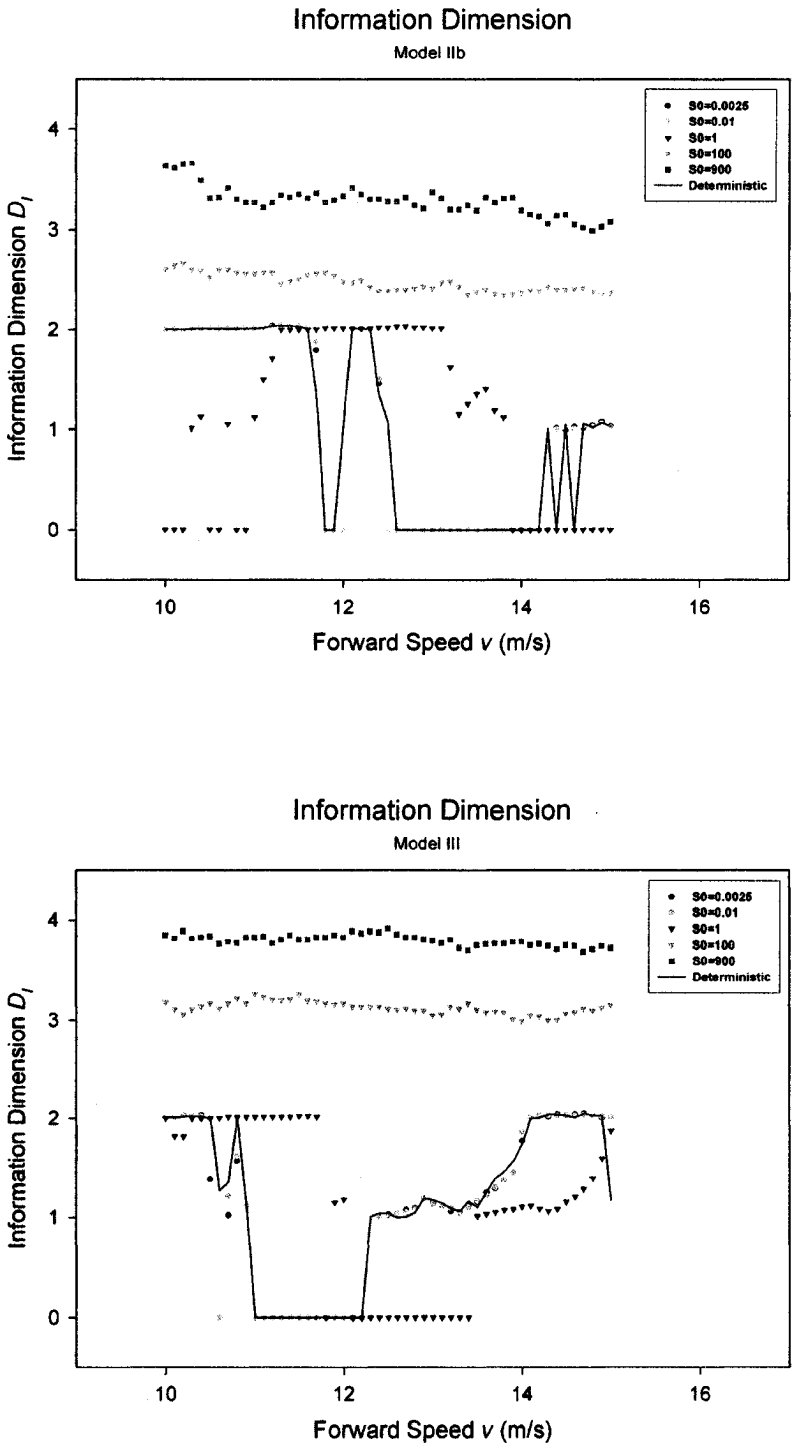

Figure 4.34 Information dimensions versus forward speed with randomness in speed (Top) Model IIb; (Bottom) Model III

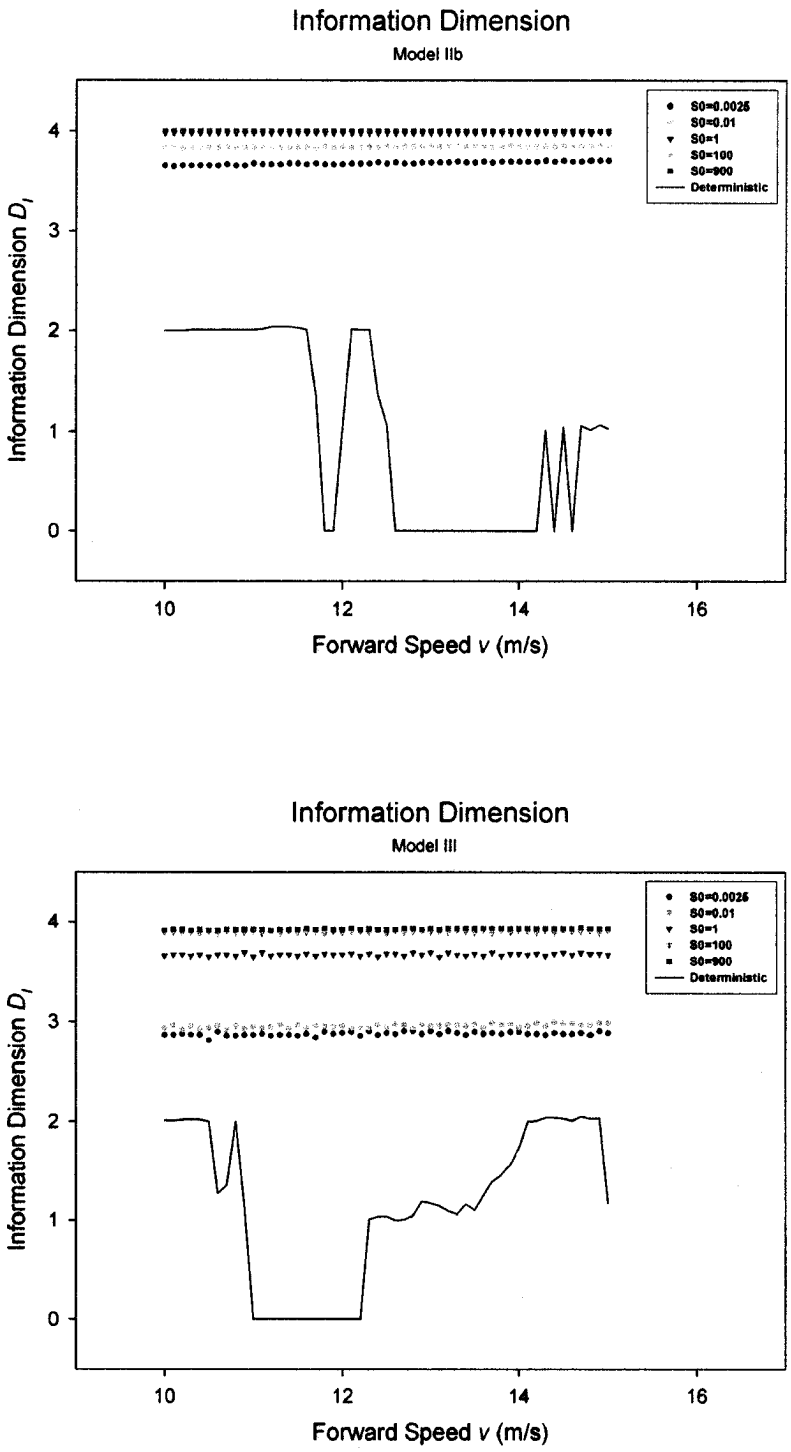

Figure 4.35 Information dimensions versus forward speed with randomness in dead band (Top) Model IIb; (Bottom) Model III

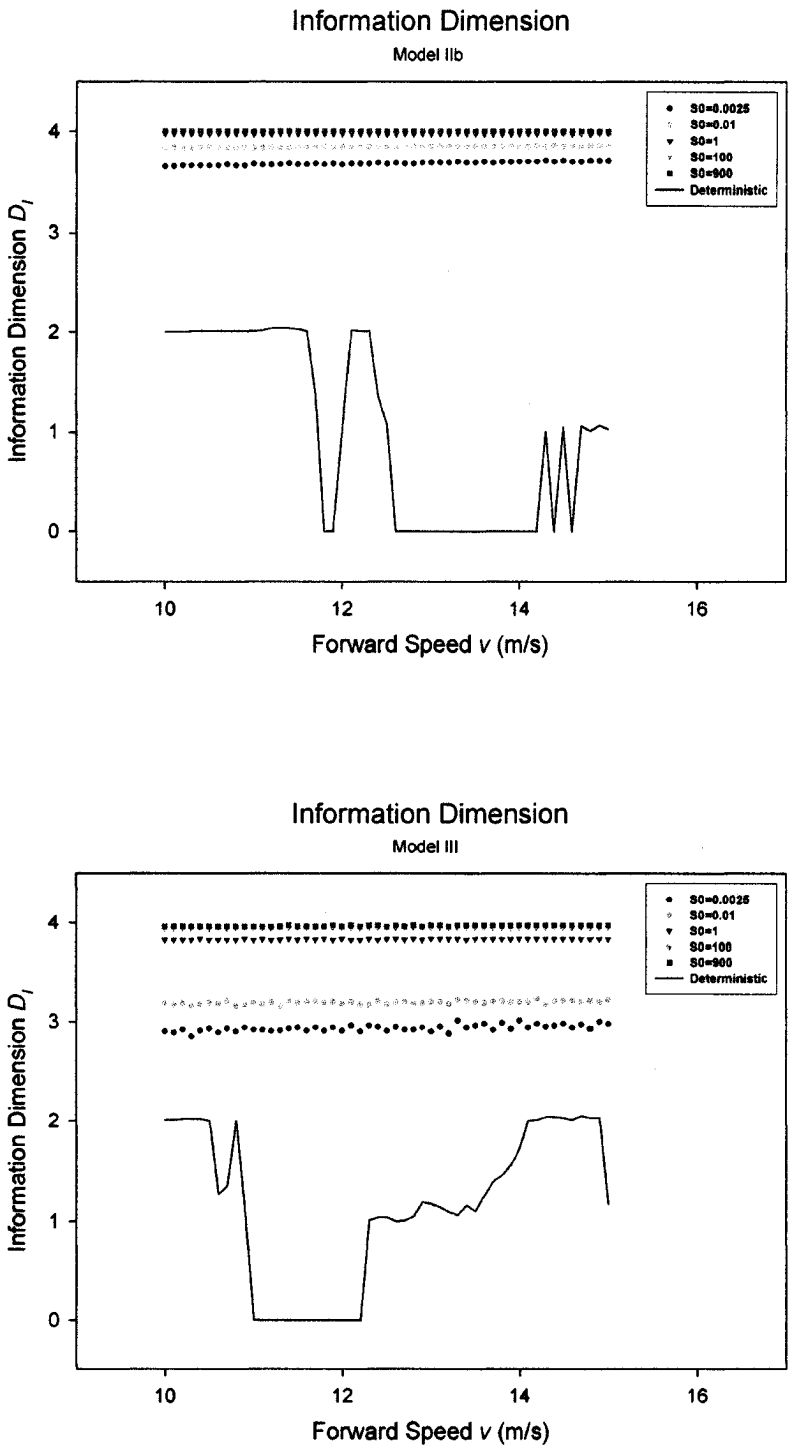

Figure 4.36 Information dimensions versus forward speed with randomness in forward speed and dead band (Top) Model IIb; (Bottom) Model III

Chapter 5

CONTROL OF SINGLE-AXLE WHEELSETS INCORPORATING RANDOMNESS

5.1 Control Strategies of Dynamical Systems with Chaos

In direct contrast to the control of dynamical systems, there is no obvious way to define the "control of chaos". This is because, to a large extent, chaos is a rich and global dynamic behaviour, and its "stabilization" can have vastly differing interpretations. For example, some authors [5.1-5.2] employed a small amplitude control law in a restricted region of the state space, thereby stabilizing a pre-existing equilibrium or periodic orbit. Since the control vanishes in most of the state space, closed-loop system trajectories follow erratic paths for some time, until they enter part of the neighborhood in which the control is effective, after which they are attracted to the equilibrium or periodic orbit of interest. Other authors applied non-local linear or nonlinear feedback to stabilize nominal equilibrium points [5.3-5.4]. The control systems approach used in [5.5-5.7] may prove to be useful in the control of chaos. Chaos and bifurcation control can be achieved by nonlinear controllers or by control strategies. In this thesis, two control strategies are used: semi-active control and active control [5.8].

These control strategies are aimed at the nonlinear dynamics of the wheelset. It is realized that higher values of the primary longitudinal stiffness k_2 yield higher critical velocities, see Eqs. (4.8) and (4.9). However, high values of k_2 are largely undesirable,

since they make the wheelset suspension very rigid. Any disturbance to the wheels will result in a forcing function in the equations of motion, thereby facilitating the transfer of the wheelset oscillations to the car body, leading to a poorer ride quality. As an alternative to using sustained high values of k_2 throughout the ride, the semi-active and active control approaches are attempted.

5.1.1 Semi-Active Control

The semi-active approach assumes a nominal value of k_2 for a portion of the simulation time. On a need basis, this value is made to increase for limited portions of the oscillatory cycle. In this approach, k_2 is considered a function of the yaw displacement of the wheelset. Two levels of k_2 will be used, one below a certain yaw angle threshold and the other beyond that threshold. In the present study, below the threshold, the stiffness k_2 is taken at the moderate value of 180 N/m which is also the value used in Chapter 4. As the speed of the vehicle is increased, so is the yaw displacement. Once the yaw threshold is reached, the value of k_2 is increased to 1.2387×10^5 N/m. It should be noted that this increased k_2 value is chosen to achieve a critical hunting speed of 25.23 m/s.

Therefore the semi-active longitudinal suspension control condition can be written as follows (see also Figure 5.1)

$$k_2 = \begin{cases} 180 \quad (\mathrm{N/m}) & |\psi| \le \psi_{threshold} \\ 1.2387 \times 10^5 \quad (\mathrm{N/m}) & |\psi| > \psi_{threshold} \end{cases} \tag{5.1}$$

where $|\psi|$ is the absolute value of the wheelset's yaw displacement, and $\psi_{threshold}$ the threshold value on yaw displacement.

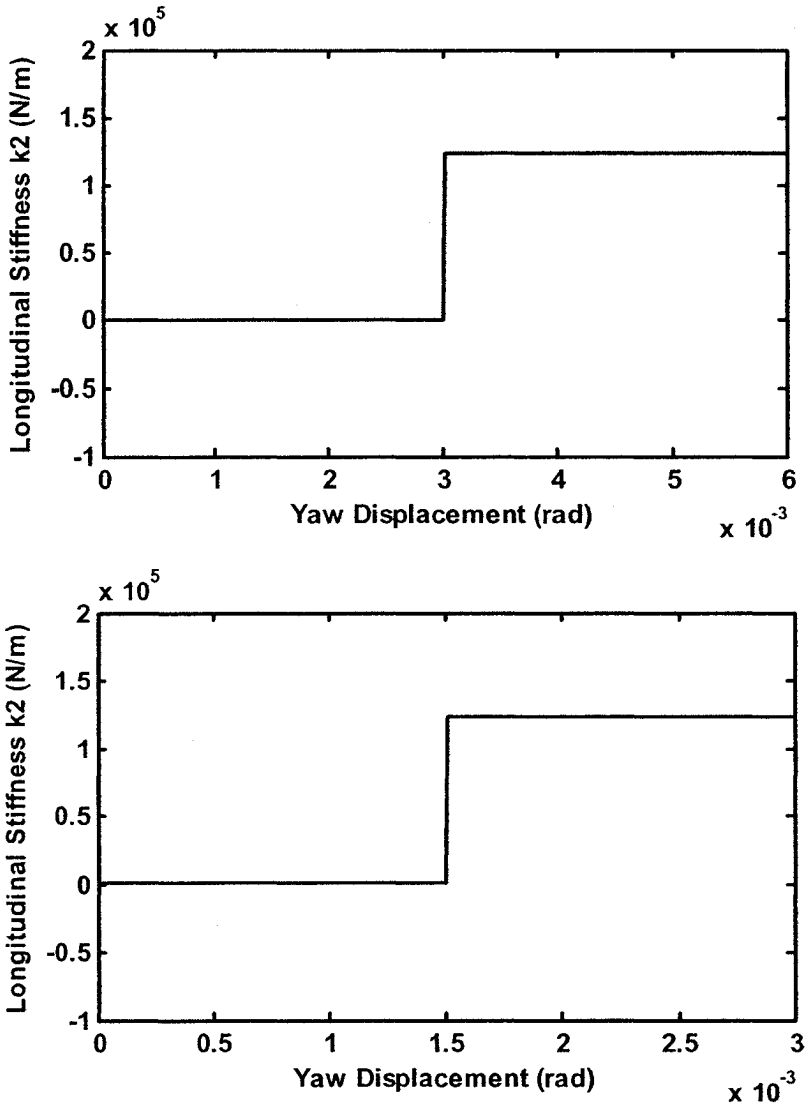

Figure 5.1 Semi-active primary longitudinal suspension control (Top) yaw threshold = 0.003 rad; (Bottom) yaw threshold = 0.0015 rad

The resulting critical velocity has a low and a high value, depending on the value of the yaw threshold chosen. If the threshold is low, the high value of k_2 will be in effect for a longer duration, so a higher critical velocity is obtained. If the threshold is high, the high value of k_2 is in effect for a short duration, resulting in a low critical velocity. In the

present study, three different values are tested, 0.0015, 0.003 and 0.006 rad. The last value is found too large for the semi-active control to take effect. In the remainder of the thesis, the yaw displacement threshold will be 0.0015 rad or 0.003 rad.

The drawback of semi-active control is the abrupt change of k_2 value at the threshold value of yaw displacement. This in turn leads to abrupt change in displacements (see Figure 5.4). One way to eliminate this abruptness is to implement an active control.

5.1.2 Active Control

This strategy considers the primary longitudinal stiffness a linear function of the absolute value of the yaw displacement (Figure 5.2). That is, the longitudinal suspension control condition can be written as:

$$k_2 = 2.0\times10^7|\psi|+180 \ (N/m) \tag{5.2}$$

The relative effectiveness of the two strategies will be compared in the next section.

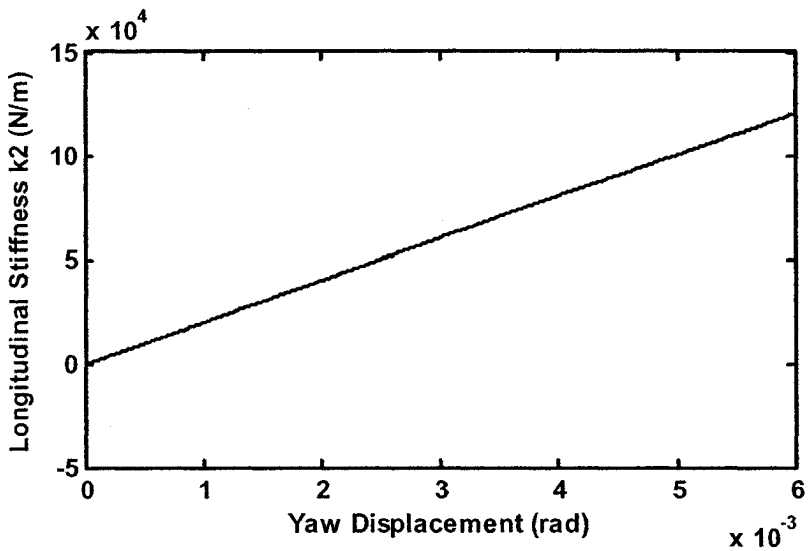

Figure 5.2 Active primary longitudinal suspension control

5.2 Phase Portraits and Information Dimensions

In this section, the first part of numerical study involving the semi-active and active control strategies is presented. Model III is chosen to be the model to be investigated. The first part of the numerical study focuses on phase portraits and information dimensions. The second part is comprised of bifurcation diagrams, which is to be presented in Section 5.3.

5.2.1 Phase Portraits of Yaw Displacement

The computation of phase portraits is performed using the same setting as in Section 4.4. The plots of yaw displacement versus yaw velocity are given in Figures 5.3 through 5.5 for no control, semi-active control and active control, respectively.

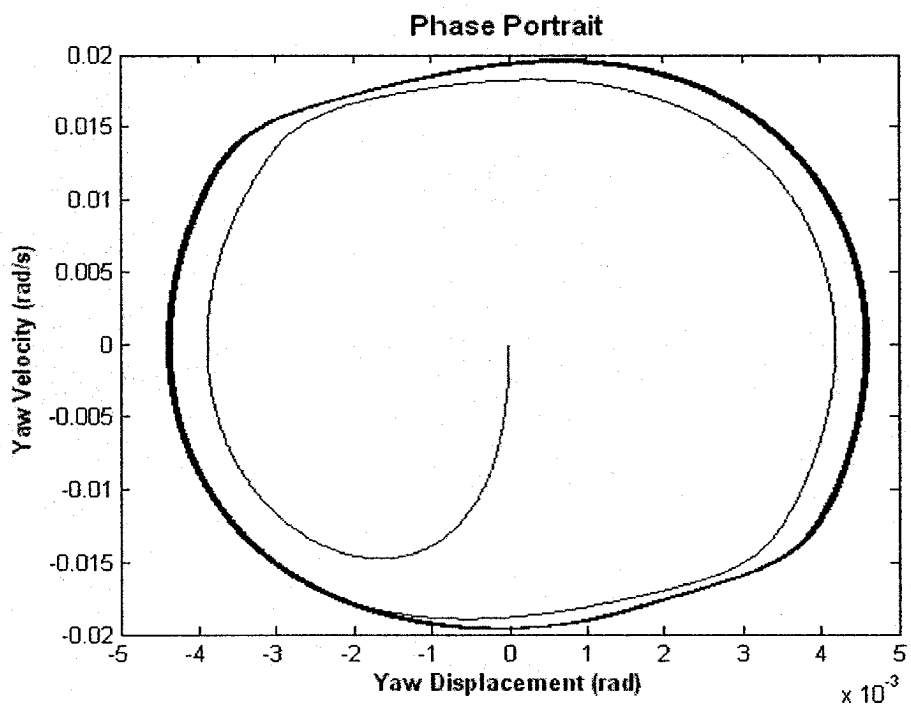

Figure 5.3 Phase portrait of yaw displacement at v = 15 m/s, no control

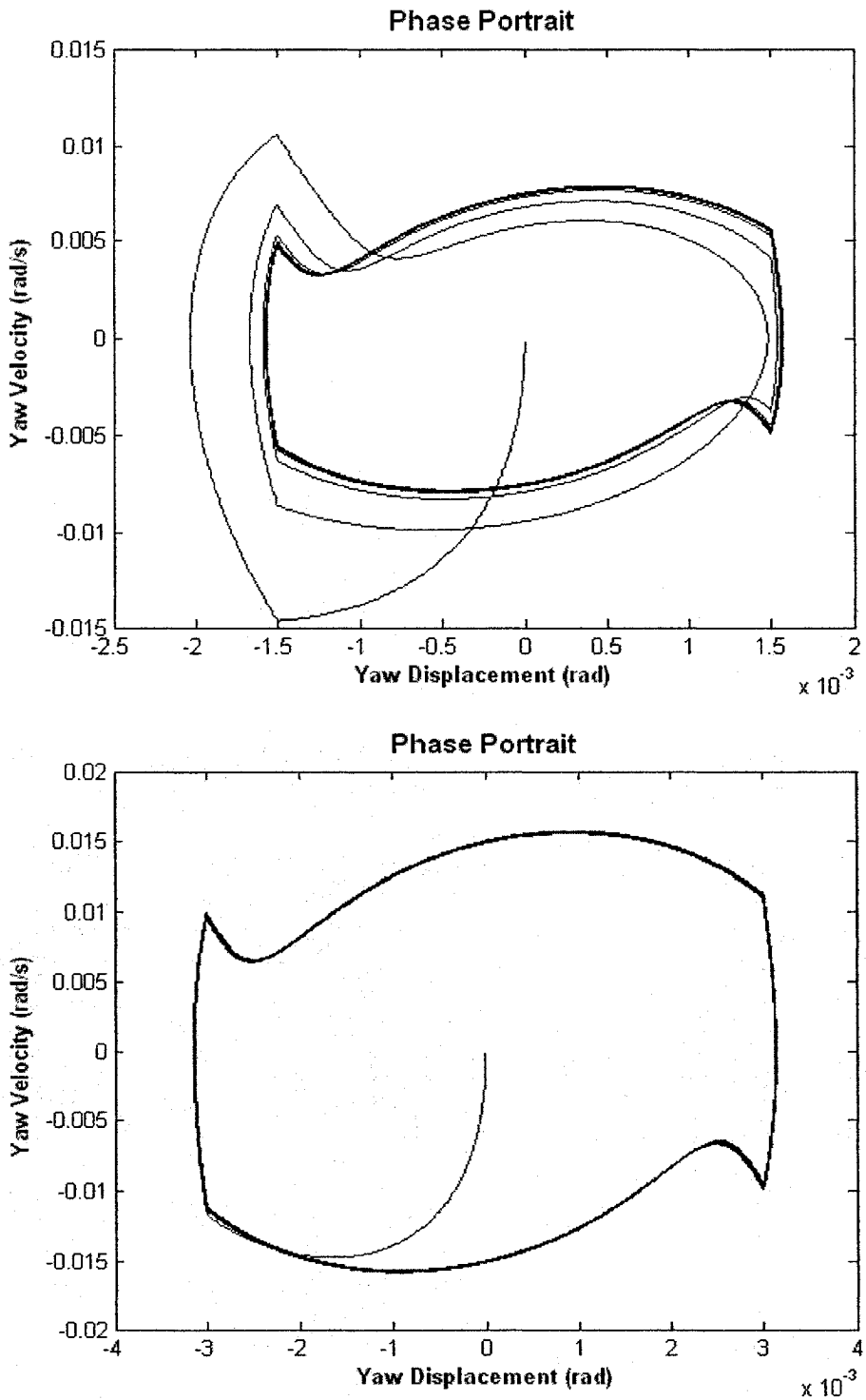

Figure 5.4 Phase portrait of yaw displacement at v = 15 m/s, semi-active control (Top) threshold = 0.0015 rad; (Bottom) threshold = 0.003 rad

Figure 5.4 shows that the yaw phase portrait has sharp "corners" at or near the value of yaw threshold. These sharp corners are indicative of abrupt changes in displacements due to the abrupt changes in stiffness k_2. Comparing the phase portraits in Figure 5.4, one can see that yaw displacements are indeed limited by the respective threshold values. In addition, a lower threshold value gives rise to a smaller range of yaw velocity, hence a lower value for the extreme yaw velocity.

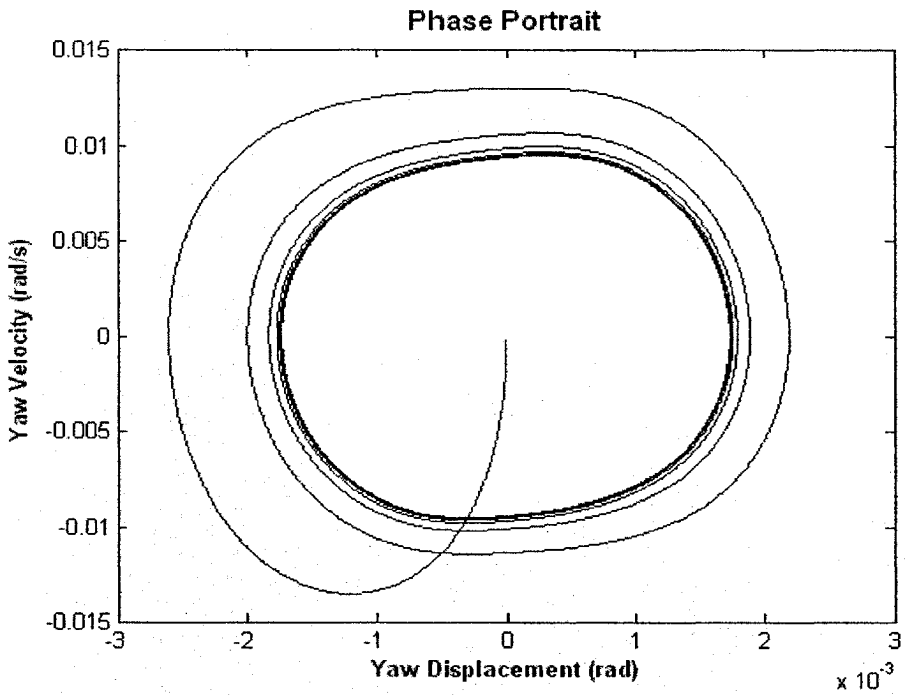

Figure 5.5 Phase portrait of yaw displacement at v = 15 m/s, active control

The phase portrait of active control in Figure 5.5 shows smooth egg-shaped loops. In terms of limits of yaw displacement and yaw velocity, the active control falls between semi-active control with a threshold of 0.0015 rad and semi-active control with a threshold of 0.003 rad. However, unlike the critical speed of the semi-active control which has a low and a high value, the critical speed of the active control is continuous (see Figure 5.6).

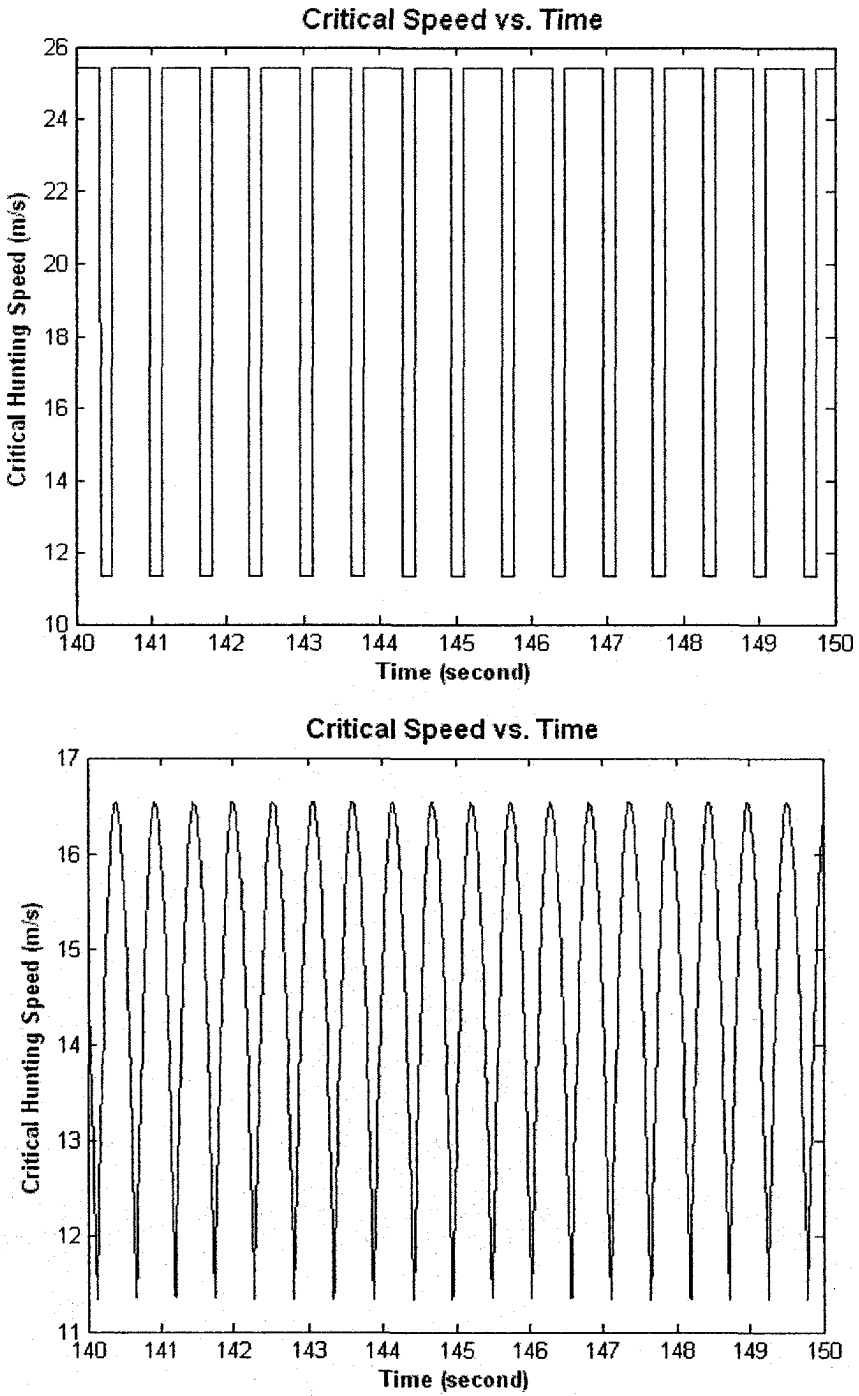

Figure 5.6 Critical speed versus time
(Top) semi-active, threshold 0.0015 rad; (Bottom) active control

5.2.2 Information Dimensions

Information dimensions are calculated with the forward velocity v varying between 10 m/s

and 20 m/s by an increment of 0.1 m/s. Spectral intensity S_0 is set to 0, 0.0025, 0.01, 0.25, and 1, respectively. Other settings remain the same as in Chapter 4. For brevity, only the 0.0015-rad threshold is considered for semi-active control.

Figures 5.7 through 5.9 illustrate how information dimensions vary with respect to the averaged forward speed, when randomness is considered to be associated with the forward speed, the dead band, and both the forward speed and dead band. Figures 5.7 through 5.9 show that,

(1) Compared with the no control case, the application of control strategies alters the information dimension plots substantially.

(2) Semi-active and active controls do not give rise to the same or close information dimensions, regardless of the spectral intensity S_0. For example, when the randomness is with forward speed, the information dimensions are above 2 for the semi-active control case (with the exception of when $v = 10 - 11$ m/s and $S_0 = 1$). However, information dimensions vary between 0 and slightly above 1 when active control is employed.

(3) Considering the case of randomness in forward speed, the motion of the wheelset is chaotic when semi-active control is implemented, for all speed and spectral intensity considered. On the other hand, with active control and low forward speed ($v < 14.5$ m/s), the motion of the wheelset is non-chaotic for all spectral intensities considered.

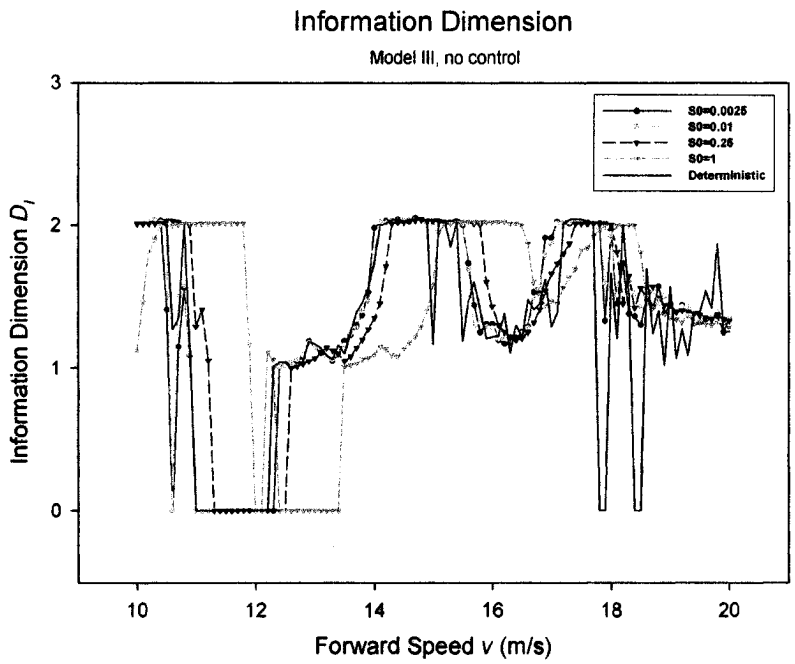

Figure 5.7(a) Information dimension with randomness in speed, no control

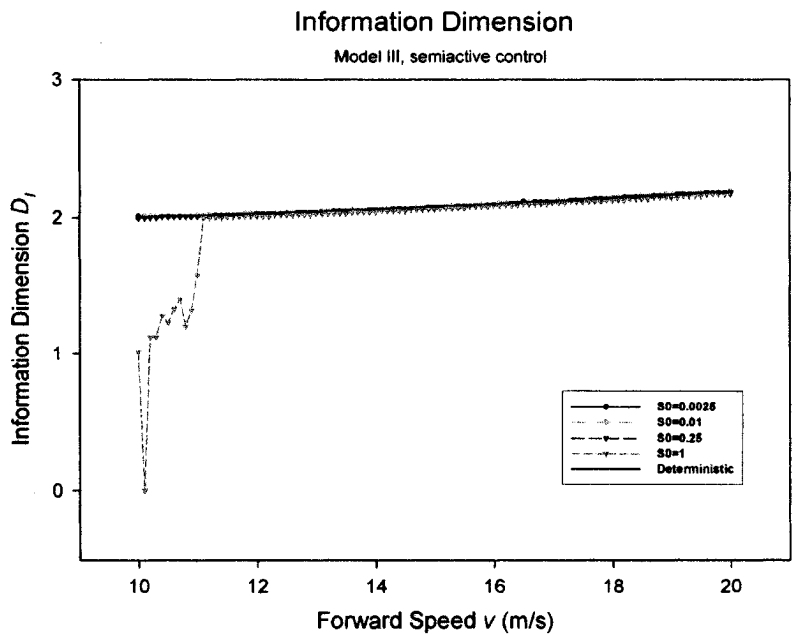

Figure 5.7(b) Information dimension with randomness in speed, semi-active control

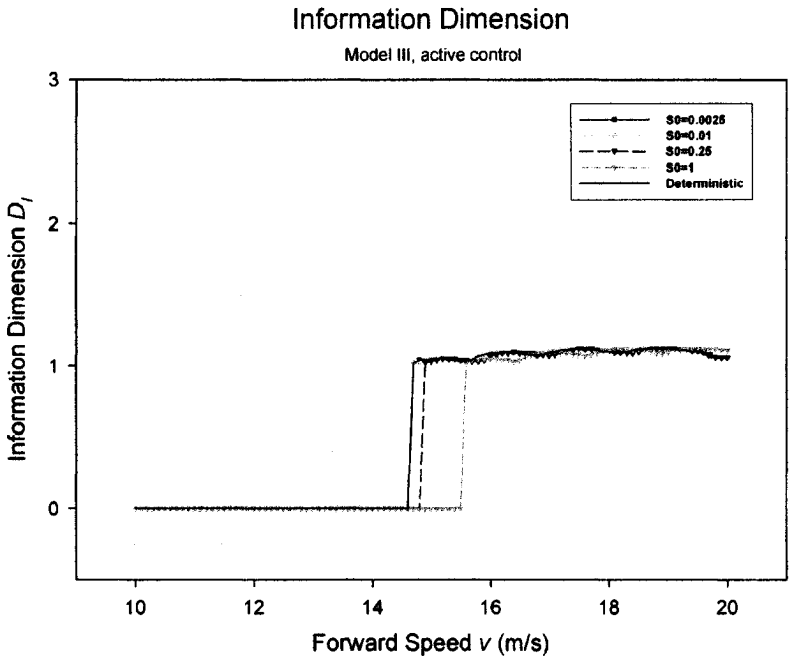

Figure 5.7(c) Information dimension with randomness in speed, active control

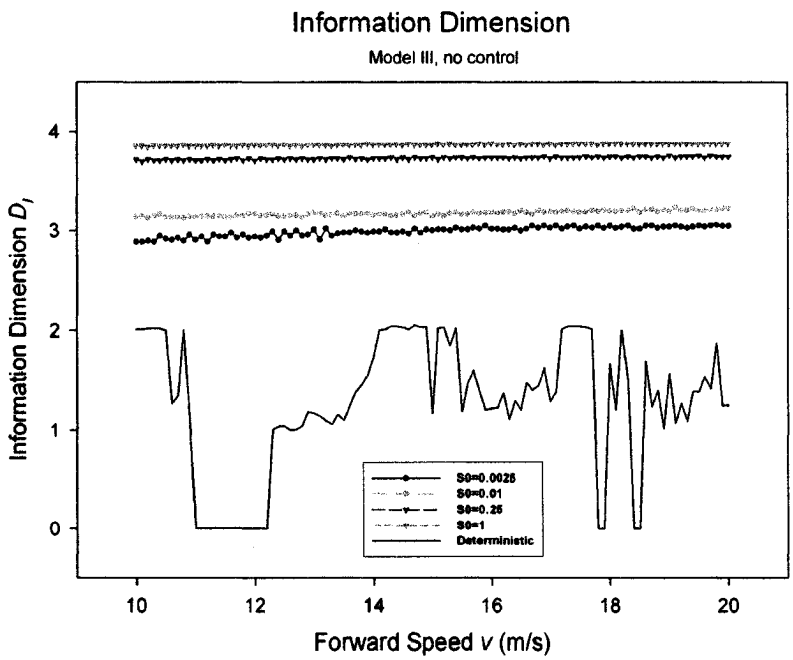

Figure 5.8(a) Information dimension with randomness in dead band, no control

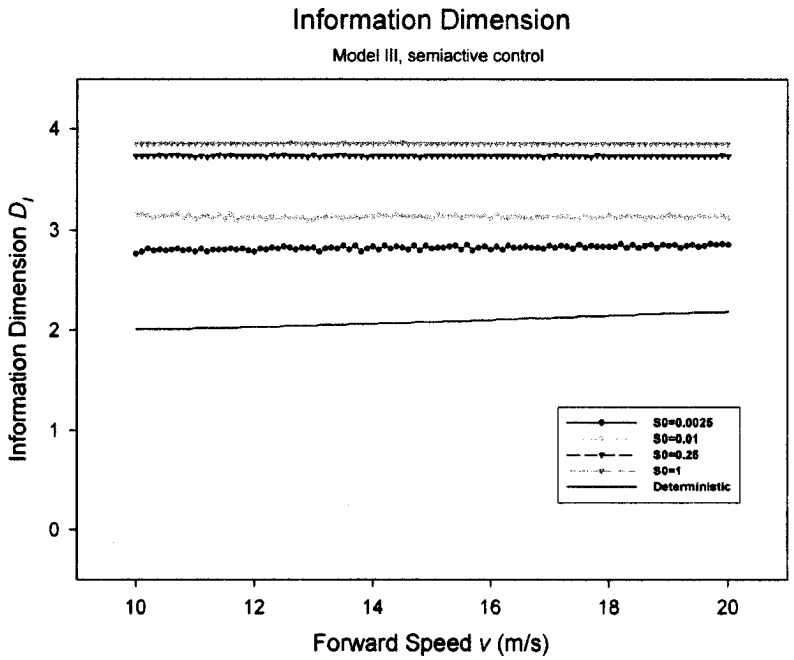

Figure 5.8(b) Information dimension with randomness in dead band, semi-active control

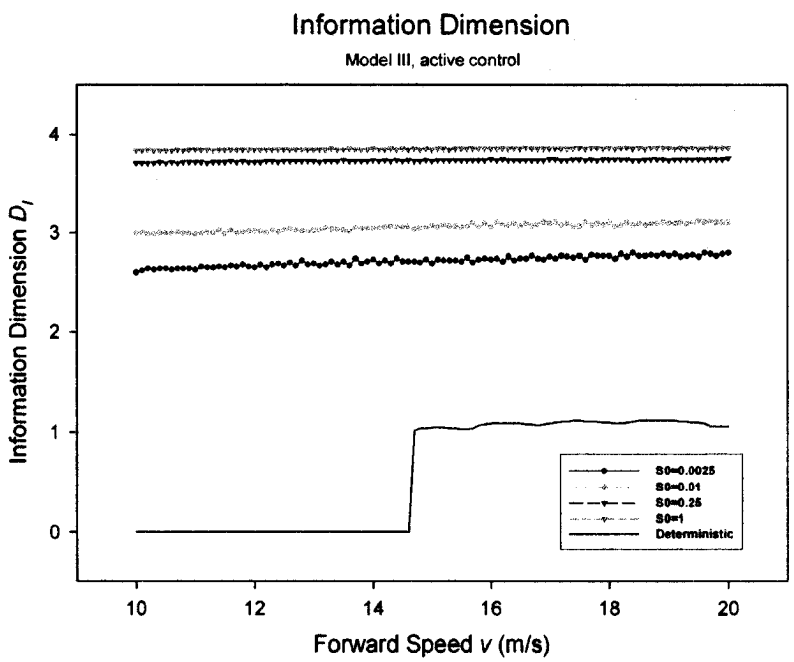

Figure 5.8(c) Information dimension with randomness in dead band, active control

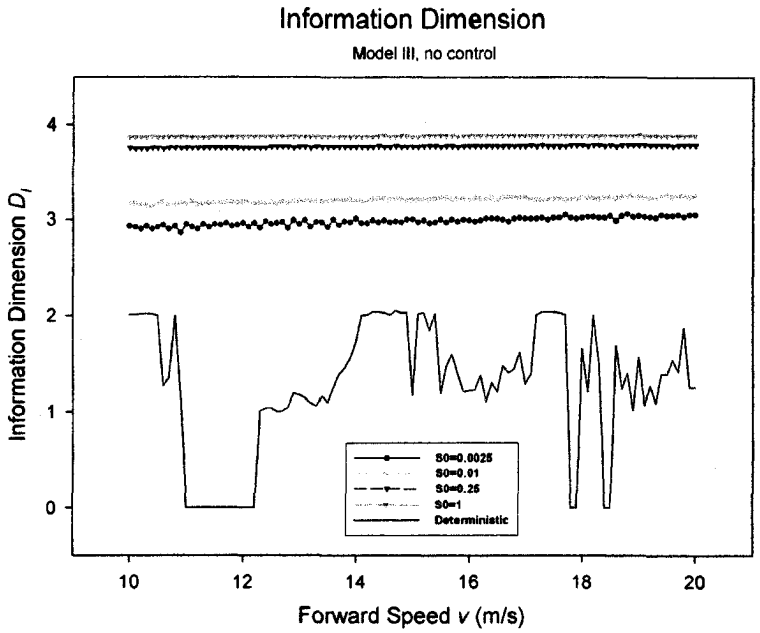

Figure 5.9(a) Information dimension with randomness in speed and dead band, no control

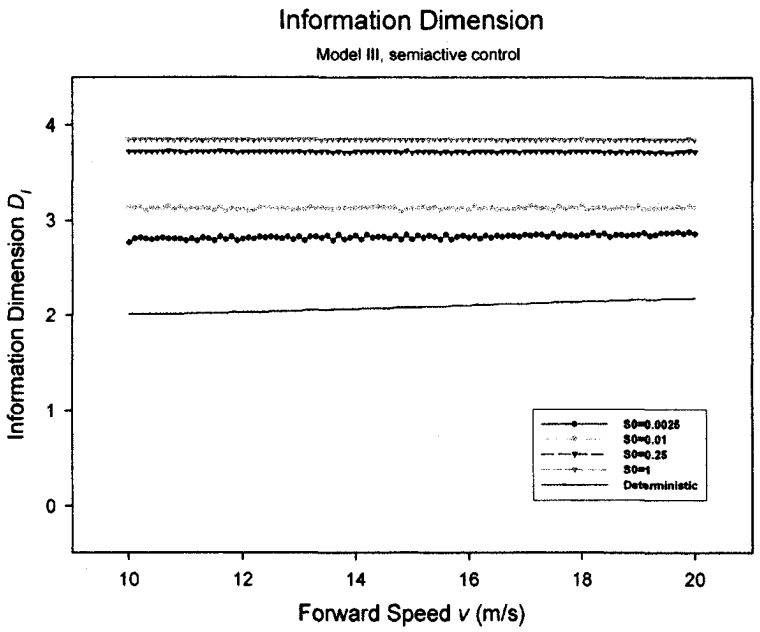

Figure 5.9(b) Information dimension with randomness in speed and dead band, semi-active control

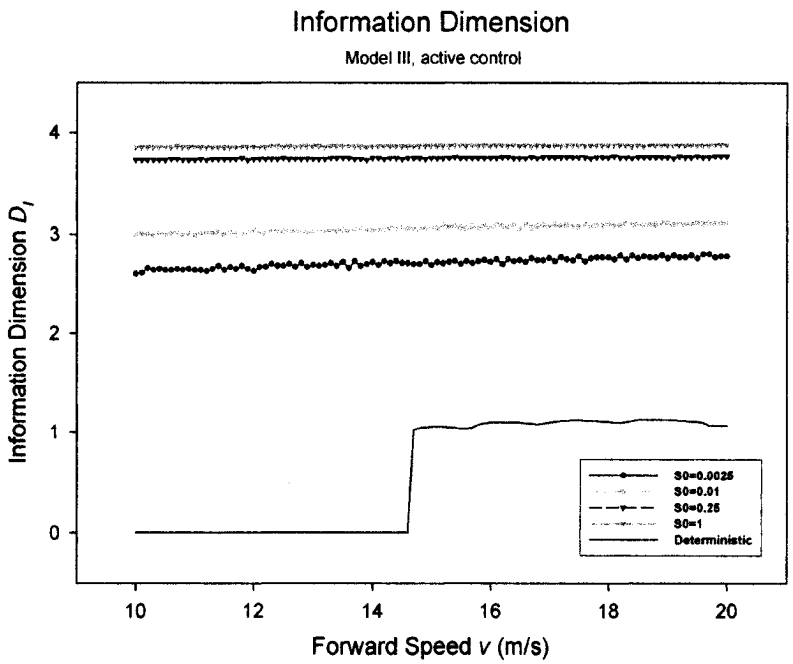

Figure 5.9(c) Information dimension with randomness in speed and dead band, active control

(4) When randomness is associated with the dead band, or with both speed and dead band, the wheelset will experience chaotic motion, regardless of whether and what control strategy is applied. The information dimensions are seen either varying over a small range, or being almost constant.

5.3 Bifurcation Diagrams

Before computed bifurcation diagrams are presented, a brief introduction to bifurcation and bifurcation diagram is in order.

5.3.1 Bifurcation

As the parameters of a dynamic system are changed, the stability of the equilibrium points will also change as well as the number of equilibrium points. How the changes in system parameters affect the stability of the equilibrium points are the subject of bifurcation theory. Values of these parameters that correspond to changes in the qualitative or topological nature of motion are known as the critical or bifurcation values. A bifurcation occurs when a small smooth change made to the parameter values causes a sudden qualitative or topological change in the system's long-term dynamical behavior. Bifurcations can be divided into two principal classes: local bifurcations and global bifurcations. The former refers to changes in the local stability properties of equilibria, periodic orbits or other invariant sets as parameters cross through critical thresholds. The latter often occurs when larger invariant sets of the system 'collide' with each other, or with the equilibria of the system. In the remainder of the section, focus will be placed on local bifurcations.

A local bifurcation occurs when a parameter change causes the stability of an equilibrium to change. For continuous dynamical systems, this corresponds to the real part of an eigenvalue of an equilibrium passing through zero. There are six types of local bifurcation. They will be seen after the introduction of bifurcation diagrams.

5.3.2 Bifurcation Diagram

Bifurcation diagram provides a useful means to show how a system's behaviour changes according to the value of a control parameter. It is widely used for examining the pre-chaotic or post-chaotic changes in a dynamical system under parameter variations.

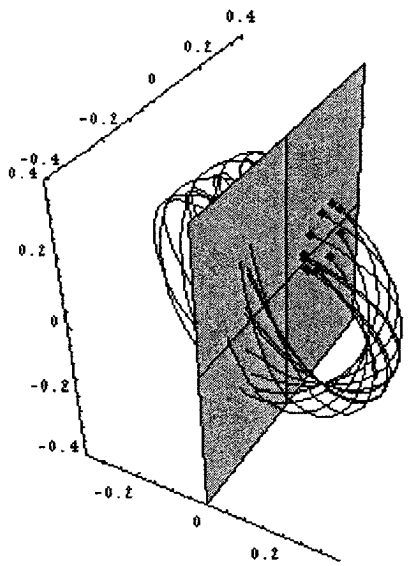

Figure 5.10 Poincaré section

One of the easiest ways to visualize the change in the dynamics of a system is to introduce a Poincaré section Σ and plot a point every time the trajectory crosses the section as the control parameter changes. Poincaré section Σ is in fact a sub-domain of the phase space (Figure 5.10). For example, if the phase space is four dimensional with the following states y, $\dot{y}$, ψ, $\dot{\psi}$, the hyper-plane satisfying $\dot{y} = 0$ is then a Poincaré section.

5.3.3 Local Bifurcations and Bifurcation Diagrams

The six types of local bifurcation and the corresponding bifurcation diagrams are as follows. It should be mentioned that only descriptive classification is presented here, instead of the more rigorous eigen-analysis based classification.

(a) Saddle-node bifurcation. This occurs when two fixed points of a dynamical system collide and annihilate each other, see Figure 5.11a.

(b) Trans-critical bifurcation. A trans-critical bifurcation refers to the stability of two equilibrium points being exchanged when the points collide. For example, before the bifurcation, there is one unstable and one stable fixed point. After bifurcation, the unstable fixed point becomes stable and vice versa (Figure 5.11b).

(c) Pitchfork bifurcation. Pitchfork bifurcation is a symmetric bifurcation. If a fixed point bifurcates into three points, with two being stable and one unstable, the bifurcation is called a super-critical pitchfork bifurcation (Figure 5.11c); A sub-critical pitchfork bifurcation, on the other hand, will have a unstable fixed point bifurcate into one stable and two unstable fixed points (Figure 5.11d).

(d) Period-doubling bifurcation. The system switches to a new behaviour with twice the period of the original system before the bifurcation (see the right half of Figure 5.11e). A series of period-halving bifurcations leads the system from order to chaos.

(e) Period-halving bifurcation. The system switches to a new behavior with half the period before bifurcation. A series of period-halving bifurcations leads the system from chaos to order (see the left half of Figure 5.11e).

(f) Hopf bifurcation. It refers to, either a fixed point losing stability and bifurcating into a stable limit cycle (the super-critical Hopf bifurcation), or a unstable limit cycle shrinking into a fixed point (the sub-critical Hopf bifurcation), see Figure 5.11f.

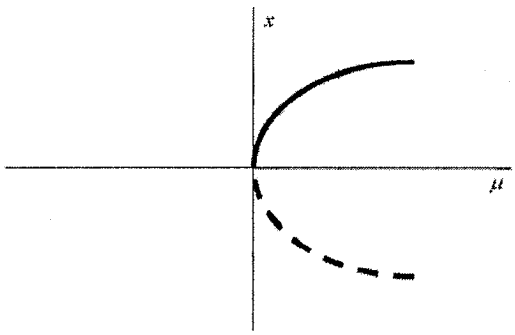

Figure 5.11a Saddle-node bifurcation

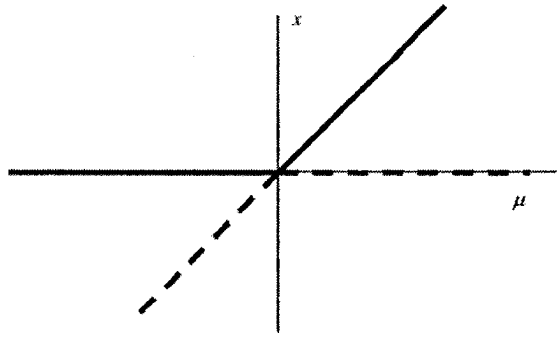

Figure 5.11b Trans-critical bifurcation

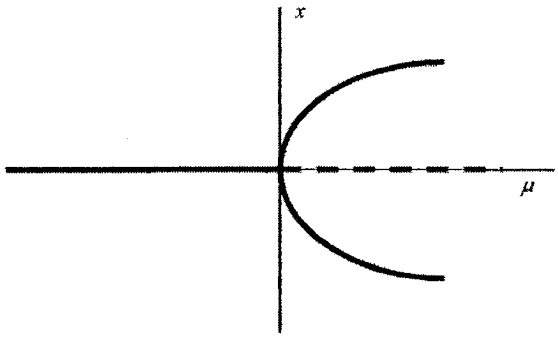

Figure 5.11c Super-critical Pitchfork bifurcation

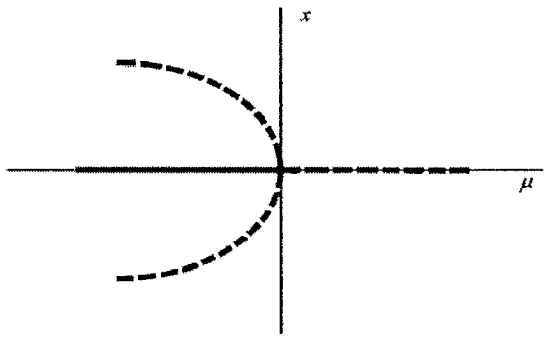

Figure 5.11d Sub-critical Pitchfork bifurcation

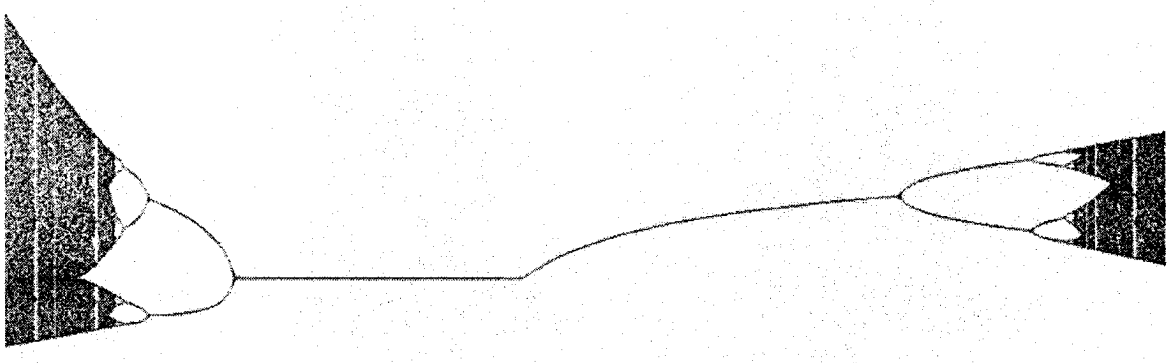

Figure 5.11e (Left) period-halving bifurcation; (Right) period-doubling bifurcation

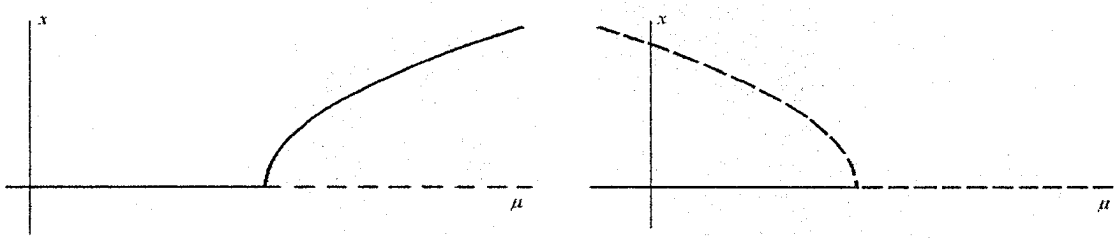

Figure 5.11f Hopf bifurcation diagram (Left) super-critical; (Right) sub-critical

5.3.4 Computed Railroad Wheelset Bifurcation Diagrams

The computation of the railroad wheelset bifurcation diagrams covers forward velocities between 1 and 50 m/s by an increment of 0.025 m/s, with the forward speed being the chosen bifurcation parameter. Randomness is considered to be associated with forward speed. Spectral intensity S_0 is set to values of 0, 0.01 and 1 only. The computing time is about 3.5 hours each (the deterministic cases require 4 to 5 minutes each). Other settings are kept the same as in information dimension computation.

a. Selecting a Poincaré section:

Four different ways of selecting a Poincaré section are examined. They are, $y = 0, \dot{y} = 0$, $\psi = 0$ and $\dot{\psi} = 0$. Bifurcation diagrams are then constructed by plotting yaw displacement versus forward speed for Poincaré section $y = 0$, and lateral displacement versus speed for the other three sections. The plots are shown in Figure 5.12. It is seen that the choice of $\dot{y} = 0$ gives the richest bifurcation information. For example, it is the only Poincaré section that shows period-three oscillation when v = 13-33 m/s. The overall construct of this diagram is also seen in relevant references ([5.9-5.11], for example). Therefore, the Poincaré section $\dot{y} = 0$ will be the default choice in the remainder of the section.

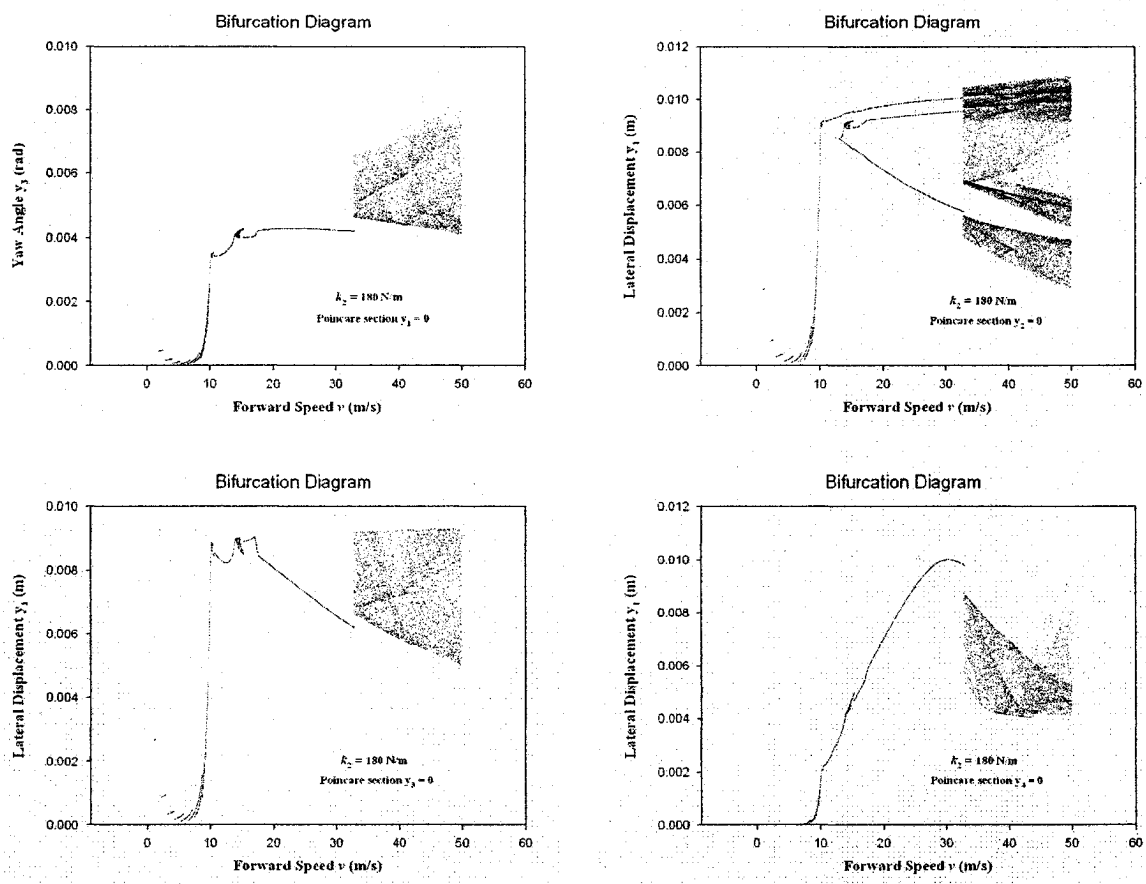

Figure 5.12 Bifurcation diagrams ($y_1 = y, y_2 = \dot{y}, y_3 = \psi, y_4 = \dot{\psi}$)

b. Bifurcation diagrams

They are seen in Figures 5.13 through 5.15 for the deterministic cases, Figure 5.16 though 5.18 for the case of S_0 = 0.01, and Figure 5.19 through 5.21 for S_0 = 1. The diagrams for cases with randomness in forward speed (Figures 5.16 through 5.21) cover averaged speed from 10 m/s to 50 m/s only, though computations are performed over the speed range of 1-50 m/s. Bifurcation diagrams that contain the entire computed speed range are presented in Appendix D. From Appendix D it can be seen that large lateral displacements exist in the range of v = 1-10 m/s, usually very clustered and without any apparent trend. Upon

further investigation, it is realized that the large clustered lateral displacements are non-physical. Such displacements can be circumvented by using smaller time step size or by increasing the time duration during which response is considered transient. From the practical perspective, wheelsets travel usually faster than 10 m/s or 36 km/h. Therefore it is reasonable and logical that the focus of the study be on the range of v = 10-50 m/s. The following remarks are in order.

(1) Figure 5.13 shows the bifurcation scenario for varying speed from 1 to 50 m/s without any randomness in speed and any control. It reveals the transition from stability to chaos. It is seen that a super-critical Hopf bifurcation occurs around v = 10 m/s and the lateral displacement is equal to the dead band (y = 0.0091 m). A period tripling takes place shortly after v = 10 m/s. A chaotic attractor develops and explodes around v = 33 m/s into a few bands. This behavior exists up to v = 50 m/s. It is evident that increasing speed leads to chaos in the system.

(2) In Figure 5.14 it is shown that, with the implementation of semi-active control, the super-critical Hopf bifurcation still occurs around v = 10 m/s but the lateral displacement is much less, at only 0.004 m. There is a bridging curve between v = 10 m/s and v = 31 m/s. The former speed is associated with super-critical Hopf bifurcation, while the latter is when the lateral displacement y reaches 0.0091 m, the dead band. Then the lateral displacement increases slowly with further increase in speed. However, there is no evidence of chaos.

(3) For the case of active control (Figure 5.15), again there is no evidence of the wheelset experiencing chaos. Compared with the semi-active cases, active control seems to give rise to no apparent bifurcation. Between v = 10 and 20 m/s there is a continuous increase in lateral displacement. Lateral displacement is nearly constant after v =20 m/s.

(4) Applying the semi-active and active control strategies has a profound impact on the wheelset's behavior. It is observed from Figures 5.14 and 5.15 that the bifurcation scenario is changed and the chaotic regime disappears. Therefore the chaotic oscillations can be suppressed with increasing yaw stiffness.

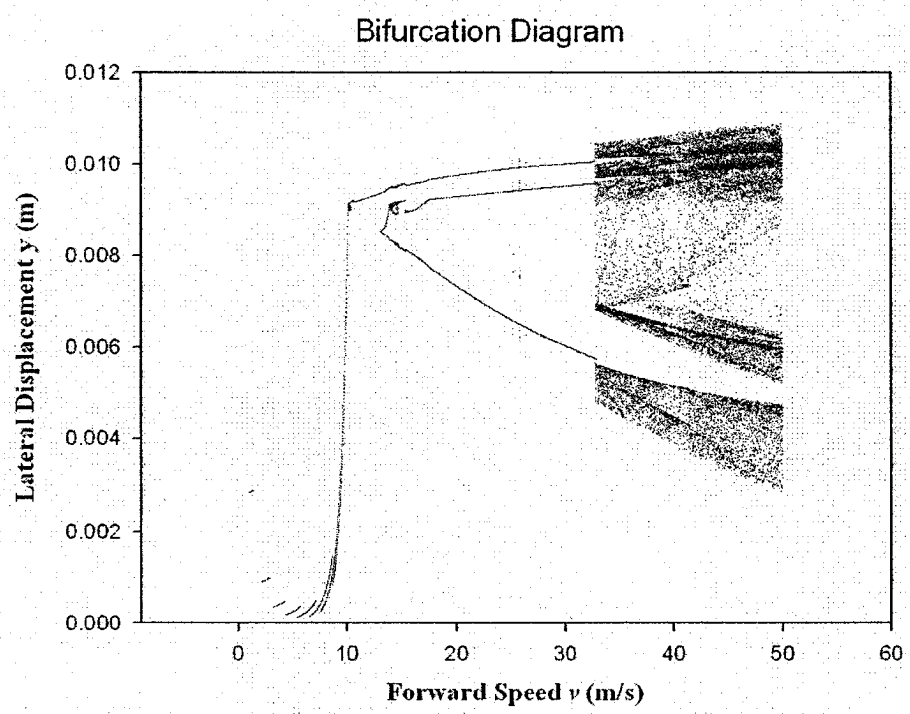

Figure 5.13 Bifurcation diagram, no control, $S_0 = 0$

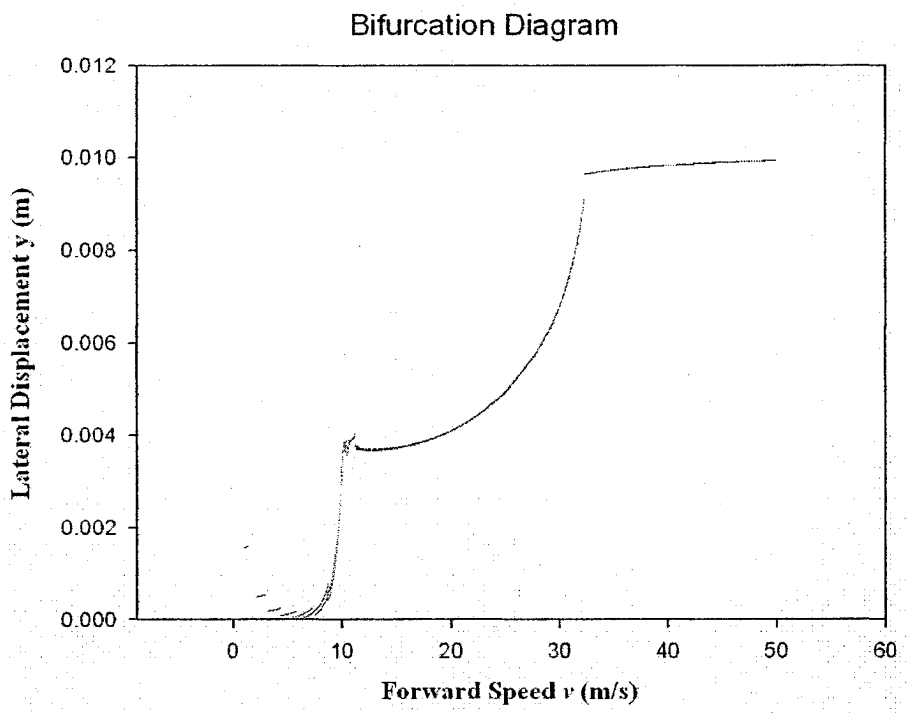

Figure 5.14 Bifurcation diagram, semi-active control, $S_0 = 0$

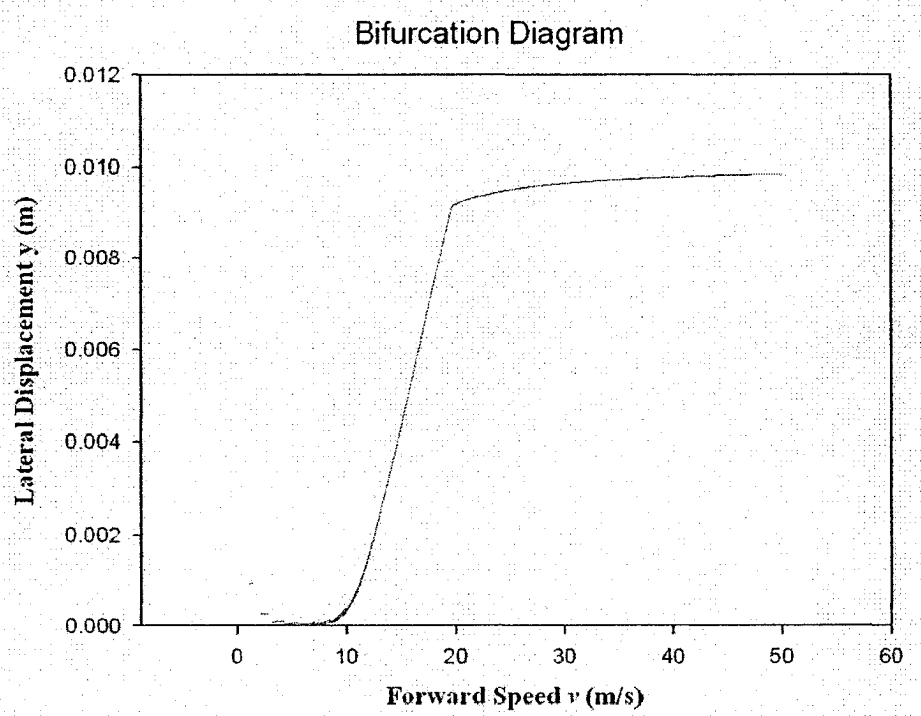

Figure 5.15 Bifurcation diagram, active control, $S_0 = 0$

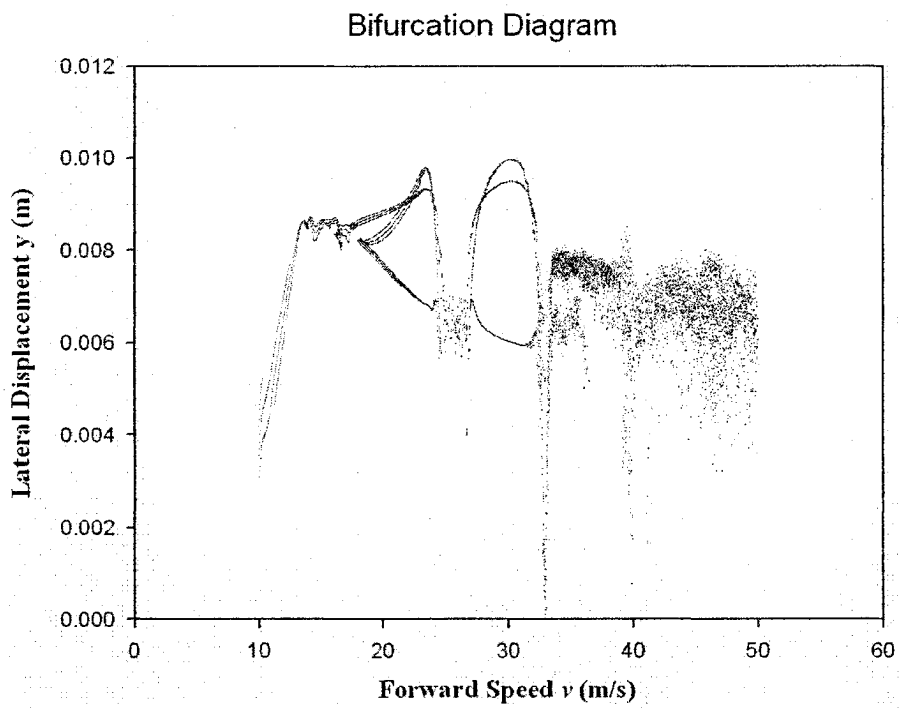

Figure 5.16 Bifurcation diagram, no control, $S_0 = 0.01$

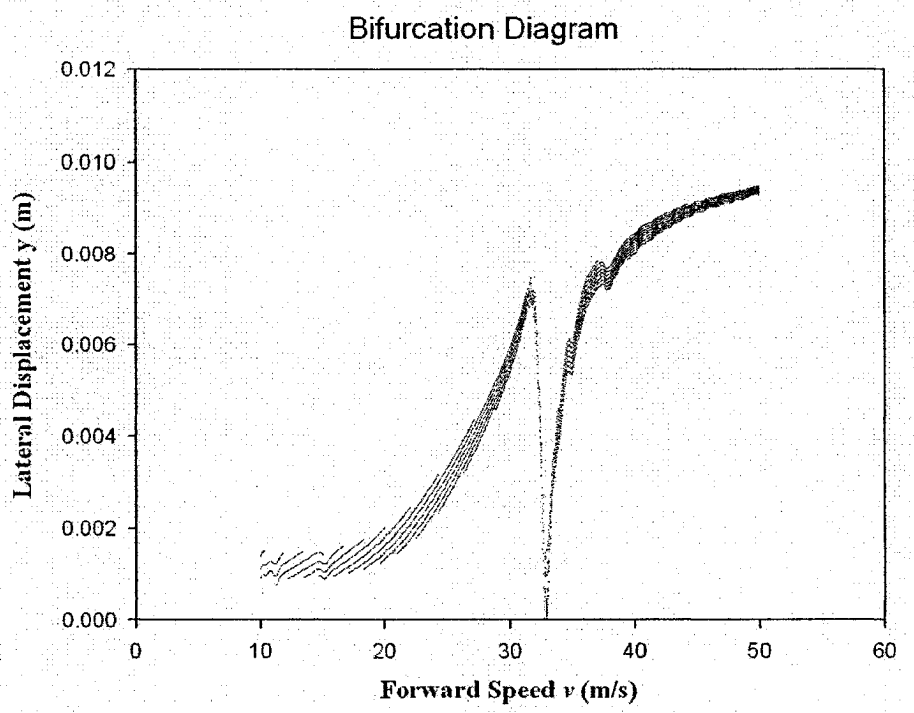

Figure 5.17 Bifurcation diagram, semi-active control, $S_0 = 0.01$

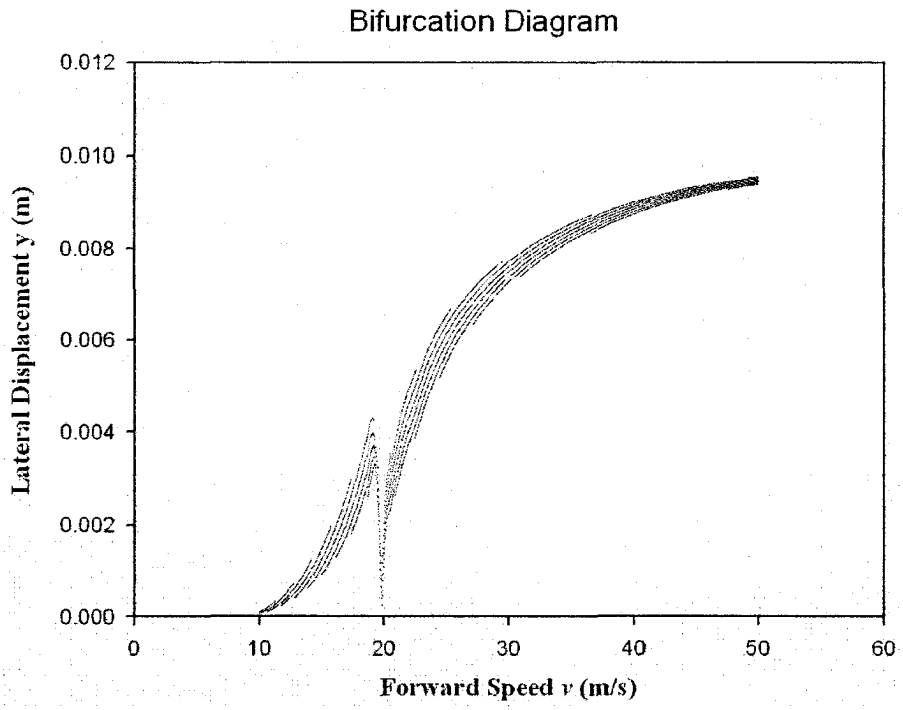

Figure 5.18 Bifurcation diagram, active control, $S_0 = 0.01$

(5) Figures 5.16 through 5.18 show the dynamic behaviours of railway wheelsets when spectral intensity is 0.01. Figure 5.16 illustrates that randomness gives rise to a blurry bifurcation diagram. Chaos is observed for $v > 33$ m/s. However, period tripling is broken into two halves, with chaos occurring at speeds in the mid-20s range. For the cases of semi-active and active control shown in Figures 5.17 and 5.18, respectively, there is no evidence of chaos. Instead, stable periodic solutions with different amplitudes seem to develop, which suggests that the control strategies can suppress the occurrence of chaos even when randomness is present. An interesting observation is that there is a "dip" to zero lateral displacement for both cases. The speed at which the dip occurs is the speed at which lateral displacement reaches the dead band in the deterministic case (that is, 33 m/s

in Figure 5.14, or 20 m/s in Figure 5.15). Since both speeds represent transition from one path to another, the "dip" may suggest sensitivity to small variation in speed around the transition point. The "dip" may also suggest a possibility of developing chaos when larger randomness is present. It should be pointed out that Reference [5.12] reported a similar blurring effect in its investigation of the Hénon map.

(6) In the case of moderate-to-large randomness, Figure 5.19 shows a bifurcation diagram that is further blurred, suggesting chaos may develop over a wider speed range. Bifurcation diagrams for semi-active and active control are shown in Figures 5.20 and 5.21, respectively. The lateral displacements for these cases are much smaller compared with their respective counterparts for $S_0 = 0$ and 0.01 shown in Figures 5.14, 5.15, 5.17 and 5.18. In all cases there seems to be no chaos. Stable periodic solutions are still present, in particular at higher speed values.

5.4 Conclusions

In this chapter, two control strategies are discussed that involve the semi-active and active control of the primary longitudinal stiffness. The main results may be summarized as follows:

(1) The critical hunting velocity of the wheelset can be increased by using semi-active or active control strategy. The semi-active strategy gives rise to an abrupt yaw profile at the threshold value. However, this abruptness can be eliminated by using the active control strategy;

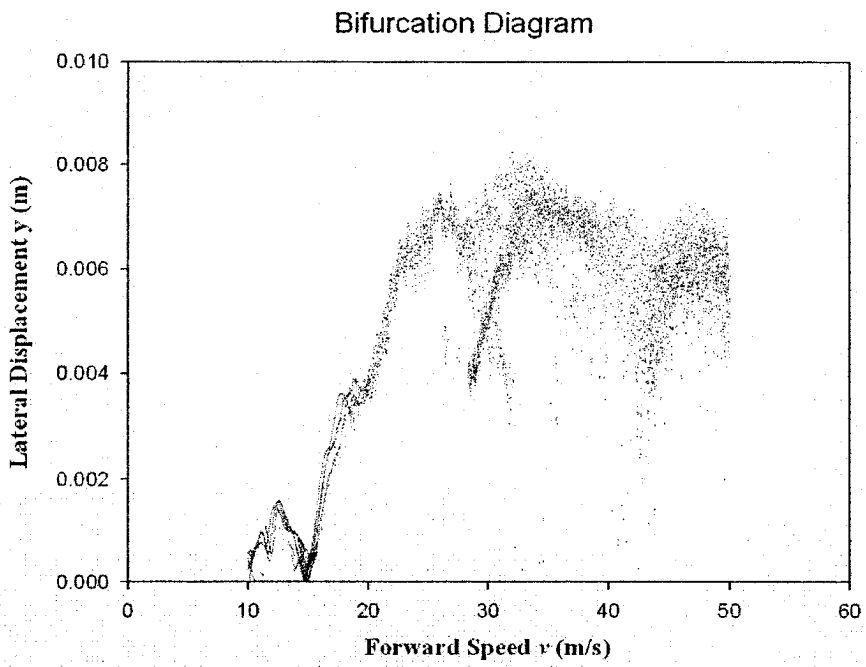

Figure 5.19 Bifurcation diagram, no control, $S_0 = 1$

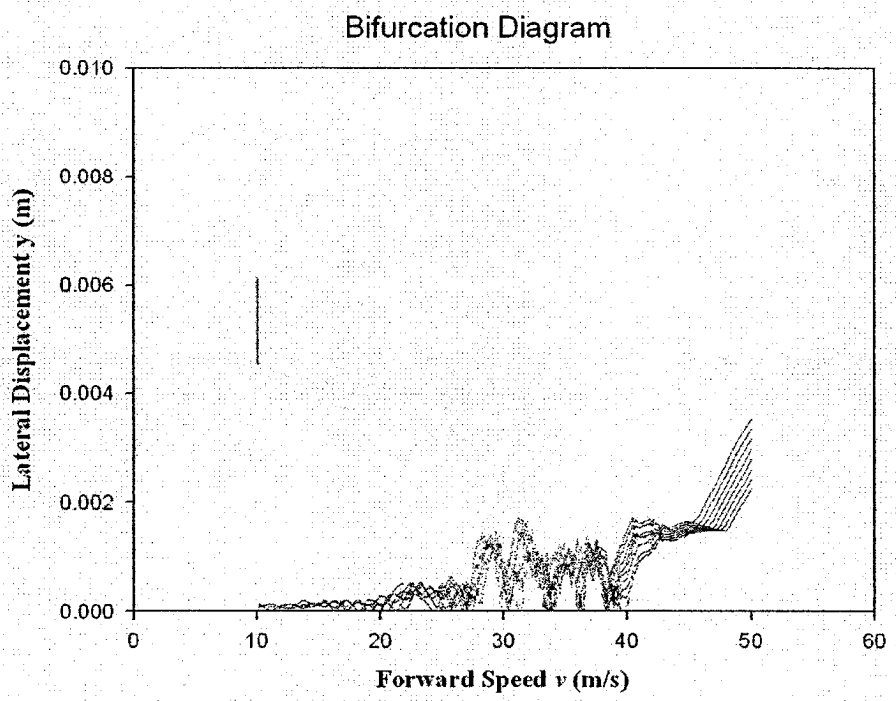

Figure 5.20 Bifurcation diagram, semi-active control, $S_0 = 1$

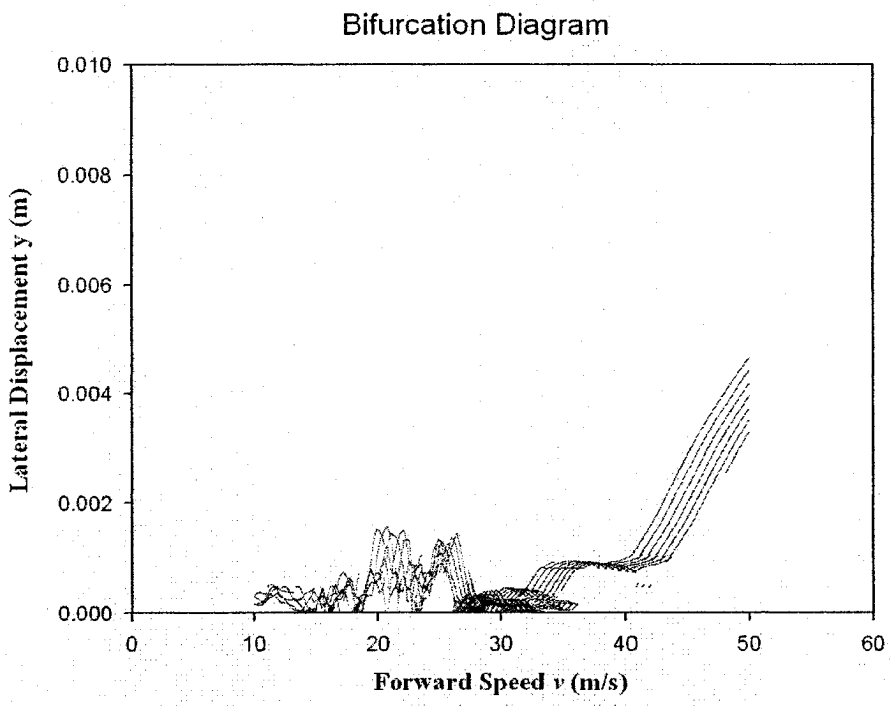

Figure 5.21 Bifurcation diagram, active control, $S_0 = 1$

(2) In the case of randomness in speed, the plots of information dimensions for no control, semi-active control, and active control are different for all spectral intensity considered; However, with randomness in dead band, or both speed and dead band, the information dimensions plots look almost identical except for the deterministic case;

(3) Active control strategy seems to be more effective than the semi-active counterpart when forward speed is low ($v < 14.5$ m/s) and when randomness is present only in forward speed. If randomness is associated with dead band, or with both speed and dead band, neither control strategy seems to be able to suppress the occurrence of chaos;

(4) For the deterministic case, increasing speed v can lead to chaos in the system. The two control strategies are effective in suppressing chaos, regardless of the speed. Since

implementing the control strategies means increasing the yaw stiffness, the present study also shows that increasing yaw stiffness can suppress chaotic oscillations in the single-axle wheelset;

(5) With the absence of any control strategy, randomness has a blurring effect on the bifurcation diagrams. However, once a control strategy is implemented, the blurring effect is not apparent; instead stable periodic solutions are developed, especially in the higher speed range.

Chapter 6

CONCLUSIONS AND RECOMMENDATIONS FOR FUTURE WORK

This chapter presents a summary of major conclusions reached during the course of the study documented here, followed by some recommendations for future work.

6.1 Summary of Major Conclusions

Major conclusions are summarized as follows, on a chapter basis.

Chapter 2:

Three models, their expansions and combinations are presented.

(1) The three original models are Models I, II and III. Model II expands on Model I. The main difference between Models II and III is that Model III does not include gravitational stiffnesses and gyroscopic couple, but applies the nonlinear creepage-creep force theory.

(2) Expanded models are Models IIa, IIb, IIIa and IIIb. Model IIa is obtained from Model II by removing the gravitational stiffnesses and gyroscopic couple. Model IIb is Model II with its linear creep forces and moments replaced by the nonlinear creep forces. Model IIIa is derived from Model III by linearizing the creep forces. Model IIIb is obtained by adding the effect due to spin creep to Model IIIa.

(3) These models are studied in three different combinations to determine how different effects affect the motion. The first combination is comprised of Models III, IIIa, and IIIb, where the effects due to the different ways of modeling creep forces and moments are

studied. The second combination consists of Models II and IIa. These models are used to examine the effect of gravitational stiffnesses and gyroscopic couple. The third combination consists of Models IIb and III and investigates the effect of the nonlinear creep forces and moments in conjunction with gravitational stiffnesses and gyroscopic moment. All of them are numerically studied in Chapter 4.

Chapter 4:

In this Chapter the wheelset models and combinations are investigated, with the aim of comparing the models and combinations for further examination. The means used for this preliminary investigation are: time history, phase portraits, Lyapunov exponents and information dimension. Based on these investigations the following conclusions may be given:

(1) Kalker's linear theory of creep forces and moments are not recommended. This is especially true when dealing with higher level of randomness ($S_0 > 1$).

(2) The effects of gravitational stiffnesses and gyroscopic couple are in general not negligible.

(3) From the point of view of modeling, Model IIb is the best model. It employs the Vermeulen and Johnson's nonlinear creep theory and includes the gravitational stiffnesses and gyroscopic couple. Model III is also a good choice, in particular when lacking wheelset data such as I_{wy}.

(4) The presence of small randomness ($S_0 < 1$) in forward speed seems not to alter the wheelset's dynamic behaviour. Namely, the motion does not change from non-chaotic to chaotic, or vice versa.

(5) Randomness in dead band dominates over randomness in forward speed. This means, reducing the unevenness in dead band is more effective in controlling the wheelset's behaviour than attempting to travel with constant, or almost constant, forward speed.

(6) Large randomness ($S_0 \geq 100$) in forward speed, or dead band, or both forward speed and dead band, seems not to change the value of information dimensions over the range of velocity considered. It also seems to universally push the wheelset's response into the chaotic realm.

Chapter 5:

In direct contrast to the control of dynamical systems there is no obvious way to define the "control of chaos". Chaos and bifurcation control can be achieved by nonlinear controllers or by control strategies. In this study two control strategies are employed: semi-active control and active control. These control strategies are aimed at the nonlinear dynamics of the wheelset. Model III is chosen to be the model to be investigated in two parts. The first part of the numerical investigation focuses on phase portraits and information dimensions. The second part is comprised of bifurcation diagrams of the wheelset. The main results may be summarized as follows:

(1) Semi-active and active control strategies increase the critical hunting velocity of the wheelset. The semi-active strategy gives rise to an abrupt yaw profile at the threshold

value. Such abrupt changes in displacements are due to the abrupt changes in stiffness k_2, but can be eliminated by using the active control strategy. In addition, a lower threshold value gives rise to a smaller range of yaw velocity, hence a lower value for the extreme yaw velocity.

(2) Compared with the no control case, the application of control strategies alters the information dimension plots substantially. But the two control strategies do not give rise to the same or close information dimensions, regardless of the spectral intensity S_0 in speed. However, with randomness in dead band, or both speed and dead band, the information dimensions plots look almost identical except for the deterministic case.

(3) Active control strategy seems to be more effective than the semi-active counterpart when forward speed is low ($v < 14.5$ m/s) and when randomness is present only in forward speed. If randomness is associated with dead band, or with both speed and dead band, the wheelset will experience chaotic motion, regardless of whether and what control strategy is applied.

(4) For the deterministic case, increasing the speed v can lead to chaos of the system. The two control strategies are effective in suppressing chaos, regardless of the speed. It is shown that the chaotic oscillations can be suppressed with increasing yaw stiffness, because implementing the control strategies means increasing the yaw stiffness.

(5) Randomness has blurring effect on the bifurcation diagrams for the no control case. However, once a control strategy is carried out, the blurring effect is not apparent; instead stable periodic solutions are developed, especially in the higher speed range.

(6) Although the control strategies can suppress the occurrence of chaos even with the presence of randomness, there remains a tendency of developing chaos when larger randomness is present.

Finally, two remarks may be in order. First, it should be pointed out that, to the author's best knowledge, no data for comparison is available in the literature. Second, a number of Fortran codes have been developed, during the course of the study presented in this thesis, to perform all the computations presented here, with the exception of zufall.f which is incorporated into the developed codes.

6.2 Recommendations for Future Work

A few recommendations for future work are,

(1) to seek more methods such as power spectrum, return maps and Poincaré maps to investigate the chaotic existence in railway wheelsets.

(2) to extend the research to two-axle wheelsets, and subsequently to the assembly of wheelsets and trucks, and the assembly of wheelsets, trucks and car body.

(3) to investigate the alternative of using time series analysis to save computing time or to conduct analysis in finer detail.

(4) to devise a control strategy that is effective in both the low and high speed ranges.

Appendix A

WHEEL- AXLE SET EQUATIONS OF MOTION

In this appendix, the equations of motion of a single-axle wheelset are given. The derivation of the equations follows closely that of [2.3]. The derivation and resulting equations are presented here chiefly for two reasons, the first being completeness in presenting materials, and the second being that certain equations are needed to expand one of the models introduced in Chapter 2.

A.1 Kinematics

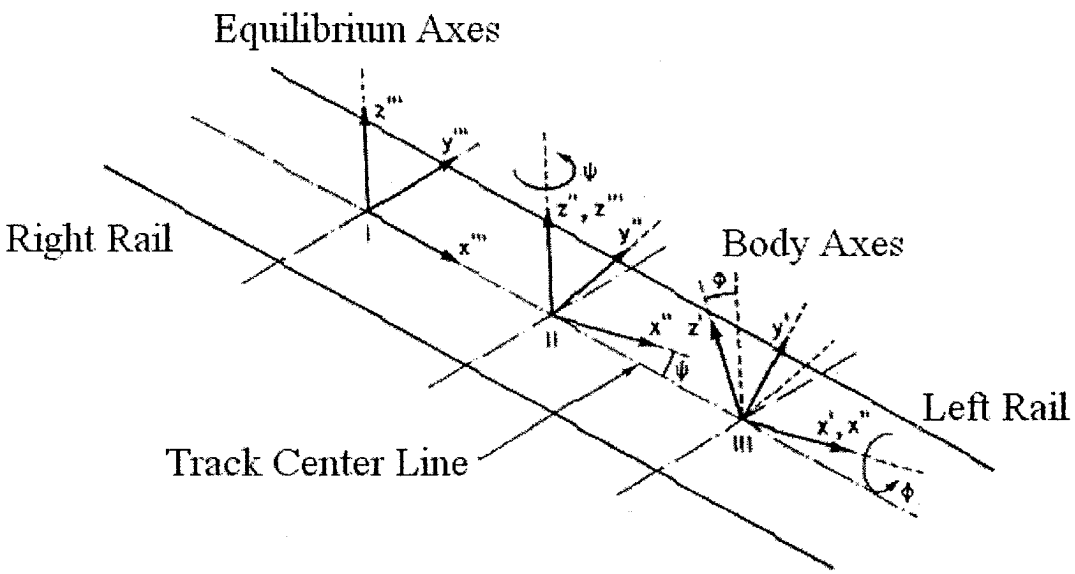

Figure A.1 Axes systems

Three sets of Cartesian coordinate systems are shown in Figure A.1. The coordinate system x''', y''', z''' has its origin at the track center line and moves at a constant forward velocity v with respect to a fixed inertial reference frame. The coordinate system x'', y'', z'' is an intermediate frame that is rotated by an angle ψ about the z''' axis. The

axes x', y', z' make up the wheelset body coordinate system, which has its origin at the center of mass. The coordinate system x', y', z' is also referred to as the body axes because the axes are attached to, and translate and rotate with the wheelset body. The coordinate system x''', y''', z''', on the other hand, is called the equilibrium axes in which Newton's laws of motion can apply.

In addition, two coordinate systems are attached to the left and right instantaneous wheel-rail contact points, (e_{1L}, e_{2L}, e_{3L}) and (e_{1R}, e_{2R}, e_{3R}), see Figure A.2. These coordinate systems are used to represent the directions of the wheel-rail contact forces.

The transformation equations between the coordinate axes are

$$\begin{Bmatrix} \mathbf{i}' \\ \mathbf{j}' \\ \mathbf{k}' \end{Bmatrix} = \begin{bmatrix} 1 & 0 & 0 \\ 0 & \cos\phi & \sin\phi \\ 0 & -\sin\phi & \cos\phi \end{bmatrix} \begin{Bmatrix} \mathbf{i}'' \\ \mathbf{j}'' \\ \mathbf{k}'' \end{Bmatrix} \tag{A.1}$$

$$\begin{Bmatrix} \mathbf{i}'' \\ \mathbf{j}'' \\ \mathbf{k}'' \end{Bmatrix} = \begin{bmatrix} \cos\psi & \sin\psi & 0 \\ -\sin\psi & \cos\psi & 0 \\ 0 & 0 & 1 \end{bmatrix} \begin{Bmatrix} \mathbf{i}''' \\ \mathbf{j}''' \\ \mathbf{k}''' \end{Bmatrix} \tag{A.2}$$

$$\begin{Bmatrix} \mathbf{i}' \\ \mathbf{j}' \\ \mathbf{k}' \end{Bmatrix} = \begin{bmatrix} \cos\psi & \sin\psi & 0 \\ -\cos\phi\sin\psi & \cos\phi\cos\psi & \sin\phi \\ \sin\phi\sin\psi & -\sin\phi\cos\psi & \cos\phi \end{bmatrix} \begin{Bmatrix} \mathbf{i}''' \\ \mathbf{j}''' \\ \mathbf{k}''' \end{Bmatrix} \tag{A.3}$$

For small roll φ and pitch ψ, Eq. (A.3) becomes

$$\begin{Bmatrix} \mathbf{i}' \\ \mathbf{j}' \\ \mathbf{k}' \end{Bmatrix} = \begin{bmatrix} 1 & \psi & 0 \\ -\psi & 1 & \phi \\ 0 & -\phi & 1 \end{bmatrix} \begin{Bmatrix} \mathbf{i}''' \\ \mathbf{j}''' \\ \mathbf{k}''' \end{Bmatrix} \tag{A.4}$$

where $\mathbf{i}', \mathbf{j}', \mathbf{k}'$, $\mathbf{i}'', \mathbf{j}'', \mathbf{k}''$ and $\mathbf{i}''', \mathbf{j}''', \mathbf{k}'''$ represent the unit vectors that correspond to the three coordinate systems.

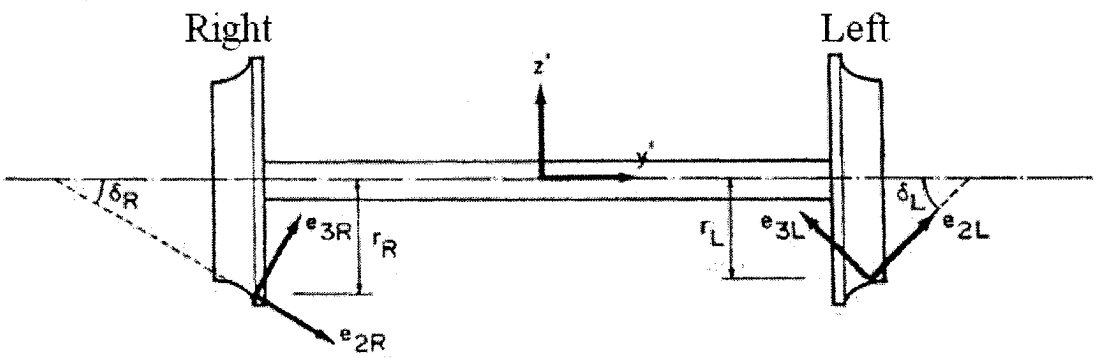

Figure A.2 Contact plane axes

In Figure A.2, δ_R and δ_L refer to the right and left contact angles, and r_R and r_L are the right and left rolling radii. The transformation equations between the contact-point axes and the wheelset body axes are

$$\begin{Bmatrix} \mathbf{e_{1R}} \\ \mathbf{e_{2R}} \\ \mathbf{e_{3R}} \end{Bmatrix} = \begin{bmatrix} 1 & 0 & 0 \\ 0 & \cos\delta_R & -\sin\delta_R \\ 0 & \sin\delta_R & \cos\delta_R \end{bmatrix} \begin{Bmatrix} \mathbf{i}' \\ \mathbf{j}' \\ \mathbf{k}' \end{Bmatrix} \tag{A.5}$$

$$\begin{Bmatrix} \mathbf{e_{1L}} \\ \mathbf{e_{2L}} \\ \mathbf{e_{3L}} \end{Bmatrix} = \begin{bmatrix} 1 & 0 & 0 \\ 0 & \cos\delta_L & \sin\delta_L \\ 0 & -\sin\delta_L & \cos\delta_L \end{bmatrix} \begin{Bmatrix} \mathbf{i}' \\ \mathbf{j}' \\ \mathbf{k}' \end{Bmatrix} \tag{A.6}$$

A.2 Degrees of Freedom and Constraints

The wheelset has in total six degrees of freedom. A description of the degrees of freedom is given in Table A.1 below, where $\Omega = v/r_0$ and r_0 is the nominal wheelset rolling radius.

Table A.1 Description of Variables

Variable	Description
x	longitudinal displacement of the wheelset mass center
y	lateral displacement of the wheelset mass center
z	vertical displacement of the wheelset mass center
φ	roll displacement about the x" axis
ψ	yaw displacement about the z" axis
β	angular displacement from a nominal value of Ω about the y' axis

It is assumed that there is no wheel lift and that the wheels are always in contact with the rails. With these assumptions, the vertical and roll displacement of the wheelset are related to its lateral and yaw displacement. The dependence of vertical and roll motions on the yaw motion is of second order* and is generally omitted. Therefore, vertical and roll displacements are considered functions of lateral displacement only. Consequently, two constraint equations are needed. They and their time derivatives are expressed as follows.

$$\begin{aligned} z &= z(y) \\ \dot{z} &= z'\dot{y} \\ \ddot{z} &= z''\dot{y}^2 + z'\ddot{y} \end{aligned} \tag{A.7}$$

and

$$\begin{aligned} \phi &= \phi(y) \\ \dot{\phi} &= \phi'\dot{y} \\ \ddot{\phi} &= \phi''\dot{y}^2 + \phi'\ddot{y} \end{aligned} \tag{A.8}$$

* N.K. Cooperrider and E.H. Law, Data Book – Wheel/Rail Geometry for Five Wheel Profiles and Three Rail Profiles, Report ERC-R_T5015, Arizona State University, Tempe, Arizona,1975.

where a over-dot and double over-dot represent differentiation with respect to time and a

prime and double prime denote differentiation with respect to y.

A.3 General Equations of Motion

The general wheelset equations of motion are derived in terms of the equilibrium axes x''', y''', z'''. The angular velocity vector $\mathbf{w}$ of the wheelset is

$$\mathbf{w} = \dot{\phi}\mathbf{i}'' + (\Omega + \dot{\beta})\mathbf{j}' + \dot{\psi}\mathbf{k}'' \tag{A.9}$$

From Eq. (A.1), $\mathbf{w}$ is expressed in body axes as

$$\begin{aligned} \mathbf{w} &= \dot{\phi}\mathbf{i}' + (\Omega + \dot{\beta} + \dot{\psi}\sin\phi)\mathbf{j}' + \dot{\psi}\cos\phi\mathbf{k}' \\ &= \omega_x\mathbf{i}' + \omega_y\mathbf{j}' + \omega_z\mathbf{k}' \end{aligned} \tag{A.10}$$

where

$$\begin{aligned} \omega_x &= \dot{\phi} \\ \omega_y &= \Omega + \dot{\beta} + \dot{\psi}\sin\phi \\ \omega_z &= \dot{\psi}\cos\phi \end{aligned}$$

The angular momentum of the wheelset in body axes is

$$\mathbf{H} = I_{wx}\omega_x\mathbf{i}' + I_{wy}\omega_y\mathbf{j}' + I_{wz}\omega_z\mathbf{k}' \tag{A.11}$$

where I_{wx}, I_{wy}, and I_{wz} are the principal mass moments of inertia of the wheelset. Note that $I_{wx} = I_{wz}$ because of symmetry.

The angular velocity of the body axes is

$$\mathbf{w}_{\mathbf{axis}} = \dot{\phi}\mathbf{i}' + \dot{\psi}\mathbf{k}'' = \dot{\phi}\mathbf{i}' + \dot{\psi}\sin\phi\mathbf{j}' + \dot{\psi}\cos\phi\mathbf{k}' \tag{A.12}$$

The time-rate of change of angular momentum can be written as

$$d\mathbf{H}/dt = I_{wx}\dot{\omega}_x\mathbf{i}' + I_{wy}\dot{\omega}_y\mathbf{j}' + I_{wz}\dot{\omega}_z\mathbf{k}' + \mathbf{w}_{\mathbf{axis}} \times \mathbf{H} \tag{A.13}$$

where "×" indicates cross product. Substituting Eqs. (A.11) and (A.12) into (A.13) yields

$$d\mathbf{H}/dt = (I_{wx}\ddot{\phi} - I_{wy}\Omega\dot{\psi})\mathbf{i}''' + I_{wy}\ddot{\beta}\mathbf{j}''' + (I_{wy}\Omega\dot{\phi} + I_{wx}\ddot{\psi})\mathbf{k}''' \tag{A.14}$$

The equations of motion are written in the equilibrium axes, from Newton's law, as

$$m\ddot{\mathbf{r}} = \sum \mathbf{F},\ d\mathbf{H}/dt = \sum \mathbf{M} \tag{A.15}$$

where m is the mass of the wheelset and $\mathbf{r}$ the position vector of the mass center of the wheelset. To express the moment vectors $\mathbf{M}$, the position vectors of the right and left contact points are needed. In terms of the body axes, they are

$$\begin{aligned} \mathbf{R_L} &= (a - \Delta_L)\mathbf{j}' - r_L\mathbf{k}' \\ \mathbf{R_R} &= -(a + \Delta_R)\mathbf{j}' - r_R\mathbf{k}' \end{aligned} \tag{A.16}$$

where Δ_L and Δ_R denote the lateral displacements of the left and right contact points from their respective equilibrium positions (see Figure A.3). a is one-half the track gauge, and r_L and r_R are the rolling radii. The components of the position vectors, in terms of the equilibrium axes, are, using Eq. (A.4):

$$\begin{aligned} R_{Lx} &= -(a - \Delta_L)\cos\phi\sin\psi - r_L\sin\phi\sin\psi \\ R_{Ly} &= (a - \Delta_L)\cos\phi\cos\psi + r_L\sin\phi\cos\psi \\ R_{Lz} &= (a - \Delta_L)\sin\phi - r_L\cos\phi \end{aligned} \tag{A.17}$$

and

$$\begin{aligned} R_{Rx} &= (a + \Delta_R)\cos\phi\sin\psi - r_R\sin\phi\sin\psi \\ R_{Ry} &= -(a + \Delta_R)\cos\phi\cos\psi + r_R\sin\phi\cos\psi \\ R_{Rz} &= -(a + \Delta_R)\sin\phi - r_R\cos\phi \end{aligned} \tag{A.18}$$

The summations of the forces and moments due to the axle load, creep, normal, and suspension forces shown in Figure A.3 are

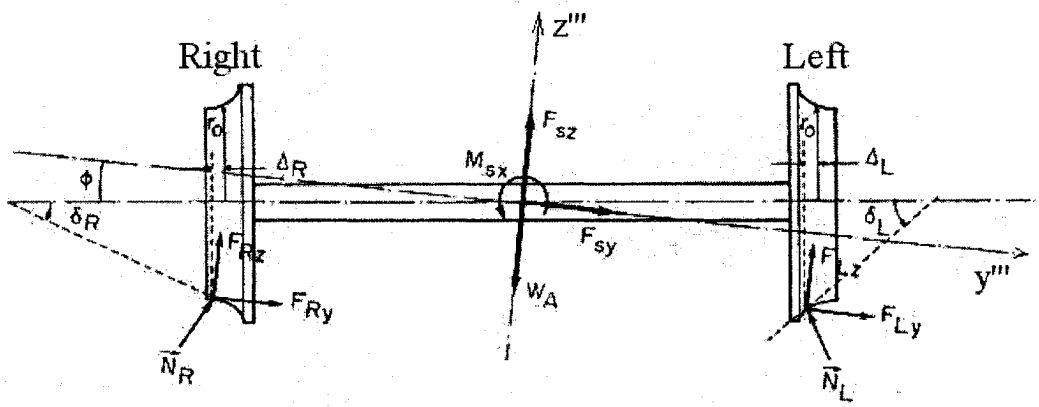

Figure A.3 Free-body diagram of a wheelset

$$\sum \mathbf{F} = \mathbf{F_L} + \mathbf{F_R} + \mathbf{N_L} + \mathbf{N_R} + \mathbf{F_s} + W_A\mathbf{k}'''$$
$$\sum \mathbf{M} = \mathbf{R_R} \times (\mathbf{F_R}+\mathbf{N_R}) + \mathbf{R_L} \times (\mathbf{F_L}+\mathbf{N_L}) + \mathbf{M_L} + \mathbf{M_R} + \mathbf{M_s} \quad \text{(A.19)}$$

A description of forces and moments appearing in Eq. (A.19) can be seen in Table A.2.

Table A.2 Definition of Forces

Forces variables	Definition
$\mathbf{F_L}$, $\mathbf{F_R}$	creep forces at left and right contact points, respectively
$\mathbf{M_L}$, $\mathbf{M_R}$	creep moments at left and right contact points, respectively
$\mathbf{F_s}$	suspension forces
$\mathbf{M_s}$	suspension moments
W_A	axle load
$\mathbf{N_L}$, $\mathbf{N_R}$	normal forces at left and right contact points, respectively

The components of Eq. (A.19) yield equations that govern the six degrees of freedom (see Table A.1) of the wheelset.

a) Longitudinal equation of motion

$$m\ddot{x} = F_{Lx} + F_{Rx} + N_{Lx} + N_{Rx} + F_{sx} \quad \text{(A.20)}$$

b) Lateral equation of motion

$$m\ddot{y} = F_{Ly} + F_{Ry} + N_{Ly} + N_{Ry} + F_{sy} \tag{A.21}$$

c) Vertical equation of motion

$$m\ddot{z} = F_{Lz} + F_{Rz} + N_{Lz} + N_{Rz} + F_{sz} - W_A \tag{A.22}$$

d) Roll equation of motion

$$\begin{aligned} I_{wx}\ddot{\phi} = {} & I_{wy}(v/r_0)\dot{\psi} + R_{Ry}(F_{Rz} + N_{Rz}) - R_{Rz}(F_{Ry} + N_{Ry}) \\ & + R_{Ly}(F_{Lz} + N_{Lz}) - R_{Lz}(F_{Ly} + N_{Ly}) + M_{Lx} + M_{Rx} + M_{sx} \end{aligned} \tag{A.23}$$

e) Spin equation of motion

$$\begin{aligned} I_{wy}\ddot{\beta} = {} & R_{Rz}F_{Rx} - R_{Rx}(F_{Rz} + N_{Rz}) + R_{Lz}F_{Lx} \\ & - R_{Lx}(F_{Lz} + N_{Lz}) + M_{Ly} + M_{Ry} + M_{sy} \end{aligned} \tag{A.24}$$

f) Yaw equation of motion

$$\begin{aligned} I_{wx}\ddot{\psi} = {} & -I_{wy}(v/r_0)\dot{\phi} + R_{Rx}(F_{Ry} + N_{Ry}) - R_{Ry}F_{Rx} \\ & + R_{Lx}(F_{Ly} + N_{Ly}) - R_{Ly}F_{Lx} + M_{Lz} + M_{Rz} + M_{sz} \end{aligned} \tag{A.25}$$

A.4 Normal Forces

The normal forces at the left and right contact points can be expressed in terms of their components in the equilibrium axes as follows

$$\begin{aligned} \mathbf{N_L} &= N_L\mathbf{e_{3L}} = N_L(-\sin\delta_L\mathbf{j}' + \cos\delta_L\mathbf{k}') \\ &= N_L[\sin(\delta_L + \phi)\sin\psi\mathbf{i}''' - \sin(\delta_L + \phi)\cos\psi\mathbf{j}''' + \cos(\delta_L + \phi)\mathbf{k}'''] \end{aligned} \tag{A.26}$$

$$\mathbf{N_R} = N_R[-\sin(\delta_R - \phi)\sin\psi\mathbf{i}''' + \sin(\delta_R - \phi)\cos\psi\mathbf{j}''' + \cos(\delta_R - \phi)\mathbf{k}'''] \tag{A.27}$$

The magnitudes of normal forces can be obtained from Eqs. (A.22) and (A.23), the vertical and roll equations, as

$$N_R \cos(\delta_R - \phi) = \frac{[R_{Ly} + R_{Lz}\tan(\delta_L + \phi)\cos\psi]F_z^* - M_\phi^*}{R_{Ly} - R_{Ry} + [R_{Lz}\tan(\delta_L + \phi) + R_{Rz}\tan(\delta_R - \phi)]\cos\psi} \tag{A.28}$$

$$N_L \cos(\delta_L + \phi) = \frac{[-R_{Ry} + R_{Rz}\tan(\delta_R - \phi)\cos\psi]F_z^* + M_\phi^*}{R_{Ly} - R_{Ry} + [R_{Lz}\tan(\delta_L + \phi) + R_{Rz}\tan(\delta_R - \phi)]\cos\psi} \tag{A.29}$$

where

$$F_z^* = m\ddot{z} + W_A - F_{Rz} - F_{Lz} - F_{sz} \tag{A.30}$$

$$\begin{aligned} M_\phi^* = {} & I_{wx}\ddot{\phi} - I_{wy}\Omega\dot{\psi} + R_{Rz}F_{Ry} - R_{Ry}F_{Rz} + R_{Lz}F_{Ly} - R_{Ly}F_{Lz} \\ & -M_{Lx} - M_{Rx} - M_{sx} \end{aligned} \tag{A.31}$$

Assuming small contact angles δ_L and δ_R and neglecting the inertia forces due to the vertical and roll motions (they are small compared to the axle load and lateral creep forces), Eqs. (A.28) and (A.29) are simplified to

$$\begin{aligned} N_L \cos(\delta_L + \phi) &\doteq \frac{1}{2}W_A - \frac{1}{2}F_{sz} - \frac{1}{2a}(r_R F_{Ry} + r_L F_{Ly}) \\ N_R \cos(\delta_R - \phi) &\doteq \frac{1}{2}W_A - \frac{1}{2}F_{sz} + \frac{1}{2a}(r_R F_{Ry} + r_L F_{Ly}) \end{aligned} \tag{A.32}$$

A.5 Creep Forces and Moments

The creep forces, in general, are defined with respect to the contact planes. However, after coordinate transformations, creep forces and moments are expressed in the equilibrium axes as follows.

$$\begin{aligned} F_{Lx} &= F'_{Lx}\cos\psi - F'_{Ly}\cos(\delta_L + \phi)\sin\psi \\ F_{Ly} &= F'_{Lx}\sin\psi + F'_{Ly}\cos(\delta_L + \phi)\cos\psi \\ F_{Lz} &= F'_{Ly}\sin(\delta_L + \phi) \\ M_{Lx} &= M'_{Lz}\sin(\delta_L + \phi)\sin\psi \\ M_{Ly} &= -M'_{Lz}\sin(\delta_L + \phi)\cos\psi \\ M_{Lz} &= M'_{Lz}\cos(\delta_L + \phi) \end{aligned} \tag{A.33}$$

and

$$
\begin{aligned}
F_{Rx} &= F'_{Rx}\cos\psi - F'_{Ry}\cos(\delta_R-\phi)\sin\psi \\
F_{Ry} &= F'_{Rx}\sin\psi + F'_{Ry}\cos(\delta_R-\phi)\cos\psi \\
F_{Rz} &= -F'_{Ry}\sin(\delta_R-\phi) \\
M_{Rx} &= -M'_{Rz}\sin(\delta_R-\phi)\sin\psi \\
M_{Ry} &= M'_{Rz}\sin(\delta_R-\phi)\cos\psi \\
M_{Rz} &= M'_{Rz}\cos(\delta_R-\phi)
\end{aligned}
\tag{A.34}
$$

In Eqs. (A.33) and (A.34), quantities that are primed are in terms of the contact plane axes (Figure A.2). These creep forces and moments are functions of the creepages. Each wheel experiences longitudinal, lateral and spin creepages, which are defined as the relative linear and angular motions between the wheel and rail. The longitudinal ξ'_x, lateral ξ'_y and spin ξ'_{sp} creepages are defined as

ξ'_x = (wheel longitudinal velocity – rail longitudinal velocity) at contact point / nominal velocity

ξ'_y = (lateral velocity of wheel- lateral velocity of rail) at contact point / nominal velocity

ξ'_{sp} = (angular velocity of wheel- angular velocity of rail) at contact point / nominal velocity

Now let R'_L and R'_R be the position vectors of the left and right contact points in the equilibrium axes. They are

$$
\begin{aligned}
\mathbf{R'_L} &= x\mathbf{i}''' + y\mathbf{j}''' + z\mathbf{k}''' + (a-\Delta_L)\mathbf{j}' - r_L\mathbf{k}' \\
&= [x-(a-\Delta_L)\cos\phi\sin\psi - r_L\sin\phi\sin\psi]\mathbf{i}''' \\
&\quad +[y+(a-\Delta_L)\cos\phi\cos\psi + r_L\sin\phi\cos\psi]\mathbf{j}''' \\
&\quad +[z+(a-\Delta_L)\sin\phi - r_L\cos\phi]\mathbf{k}'''
\end{aligned}
\tag{A.35}
$$

and

$$
\begin{aligned}
\mathbf{R}'_{\mathbf{R}} &= x\mathbf{i}''' + y\mathbf{j}''' + z\mathbf{k}''' - (a+\Delta_R)\mathbf{j}' - r_R\mathbf{k}' \\
&= [x + (a+\Delta_R)\cos\phi\sin\psi - r_R\sin\phi\sin\psi]\mathbf{i}''' \\
&+[y - (a+\Delta_R)\cos\phi\cos\psi + r_R\sin\phi\cos\psi]\mathbf{j}''' \\
&+[z - (a+\Delta_R)\sin\phi - r_R\cos\phi]\mathbf{k}'''
\end{aligned}
\tag{A.36}
$$

Applying the definitions of creeps leads

$$
\begin{aligned}
\xi'_{xL} &= [\dot{\mathbf{R}}'_{\mathbf{L}}\cdot\mathbf{e_{1L}} - v(r_L/r_0)\cos\psi]/v \\
\xi'_{yL} &= (\dot{\mathbf{R}}'_{\mathbf{L}}\cdot\mathbf{e_{2L}})/v \\
\xi'_{spL} &= (\mathbf{w}\cdot\mathbf{e_{3L}})/v
\end{aligned}
\tag{A.37}
$$

Applying Eqs. (A.6), (A.12) and (A.35) and neglecting higher-order terms results in

$$
\begin{aligned}
\xi'_{xL} &= (1/v)\left\{v[1-(r_L/r_0)] - \dot{\psi}[(a-\Delta_L)\cos\phi\cos\psi]\right\}\cos\psi \\
\xi'_{yL} &= (1/v)[\dot{y}\cos\psi + r_L\dot{\phi}\cos\phi\cos^2\psi - v\sin\psi]\cos(\delta_L+\phi) \\
&+(1/v)[\dot{z} + \dot{\phi}(a-\Delta_L)\cos\phi]\sin(\delta_L+\phi) \\
\xi'_{spL} &= (1/v)[\dot{\psi}\cos(\delta_L+\phi) - \Omega\sin\delta_L]
\end{aligned}
\tag{A.38}
$$

Similarly, one has

$$
\begin{aligned}
\xi'_{xR} &= [\dot{\mathbf{R}}'_{\mathbf{R}}\cdot\mathbf{e_{1R}} - v(r_R/r_0)\cos\psi]/v \\
\xi'_{yR} &= (\dot{\mathbf{R}}'_{\mathbf{R}}\cdot\mathbf{e_{2R}})/v \\
\xi'_{spR} &= (\mathbf{w}\cdot\mathbf{e_{3R}})/v
\end{aligned}
\tag{A.39}
$$

and

$$
\begin{aligned}
\xi'_{xR} &= (1/v)\left\{v[1-(r_R/r_0)] + \dot{\psi}[(a+\Delta_R)\cos\phi\cos\psi]\right\}\cos\psi \\
\xi'_{yR} &= (1/v)[\dot{y}\cos\psi + r_R\dot{\phi}\cos\phi\cos^2\psi - v\sin\psi]\cos(\delta_R-\phi) \\
&-(1/v)[\dot{z} - \dot{\phi}(a+\Delta_R)\cos\phi]\sin(\delta_R-\phi) \\
\xi'_{spL} &= (1/v)[\dot{\psi}\cos(\delta_R-\phi) + \Omega\sin\delta_R]
\end{aligned}
\tag{A.40}
$$

Small roll φ and yaw ψ angles reduce Eqs. (A.38) and (A.40) to

$$\begin{aligned}
\xi'_{xL} &= (1/v)\left\{v[1-(r_L/r_0)] - a\dot{\psi}\right\} \\
\xi'_{yL} &= (1/v)[\dot{y} + r_L\dot{\phi} - v\psi]\cos(\delta_L + \phi) \\
\xi'_{spL} &= (1/v)[\dot{\psi}\cos(\delta_L + \phi) - \Omega\sin\delta_L]
\end{aligned} \tag{A.41}$$

and

$$\begin{aligned}
\xi'_{xR} &= (1/v)\left\{v[1-(r_R/r_0)] + a\dot{\psi}\right\} \\
\xi'_{yR} &= (1/v)[\dot{y} + r_R\dot{\phi} - v\psi]\cos(\delta_R - \phi) \\
\xi'_{spR} &= (1/v)[\dot{\psi}\cos(\delta_R - \phi) + \Omega\sin\delta_R]
\end{aligned} \tag{A.42}$$

Further assuming small contact angles δ_L and δ_R reduces the creepages to

$$\begin{aligned}
\xi'_{xL} &= (1/v)\left\{v[1-(r_L/r_0)] - a\dot{\psi}\right\} \\
\xi'_{yL} &= (1/v)[\dot{y} + r_L\dot{\phi} - v\psi] \\
\xi'_{spL} &= (1/v)[\dot{\psi} - \Omega\delta_L]
\end{aligned} \tag{A.43}$$

and

$$\begin{aligned}
\xi'_{xR} &= (1/v)\left\{v[1-(r_R/r_0)] + a\dot{\psi}\right\} \\
\xi'_{yR} &= (1/v)[\dot{y} + r_R\dot{\phi} - v\psi] \\
\xi'_{spR} &= (1/v)[\dot{\psi} + \Omega\delta_R]
\end{aligned} \tag{A.44}$$

Employing Kalker's linear creep theory, the creep forces and moment are

$$\begin{aligned}
F'_x &= -f_{33}\xi'_x \\
F'_y &= -f_{11}\xi'_y - f_{12}\xi'_{sp} \\
M'_z &= f_{12}\xi'_y - f_{22}\xi'_{sp}
\end{aligned} \tag{A.45}$$

where f_{11}, f_{12}, f_{22} and f_{33} are the creep coefficients which are defined as:

$$\begin{aligned}
f_{11} &= (ab)GC_{22}, \qquad f_{12} = (ab)^{3/2}GC_{23} \\
f_{22} &= (ab)^2GC_{33}, \qquad f_{33} = (ab)GC_{11}
\end{aligned} \tag{A.46}$$

In Eq. (A.46),

a = semiaxis of the contact ellipse in the rolling direction

b = semiaxis of the contact ellipse in the lateral direction

G = modulus of rigidity

C_{ij} = creepage and spin coefficients which depend only on Poisson's ratio υ and the ratio of the semiaxes of the contact ellipse, a/b.

The substitution of creepages of Eqs. (A.43) and (A.44) into Eq. (A.45) yields the following expressions for creep forces and moments:

$$\begin{aligned} F'_{Lx} &= -(f_{33}/v)\left\{v[1-(r_L/r_0)] - a\dot{\psi}\right\} \\ F'_{Ly} &= -(f_{11}/v)[\dot{y} + r_L\dot{\phi} - v\psi] - (f_{12}/v)[\dot{\psi} - \Omega\delta_L] \\ M'_{Lz} &= (f_{12}/v)[\dot{y} + r_L\dot{\phi} - v\psi] - (f_{22}/v)[\dot{\psi} - \Omega\delta_L] \end{aligned} \tag{A.47}$$

$$\begin{aligned} F'_{Rx} &= -(f_{33}/v)\left\{v[1-(r_R/r_0)] + a\dot{\psi}\right\} \\ F'_{Ry} &= -(f_{11}/v)[\dot{y} + r_R\dot{\phi} - v\psi] - (f_{12}/v)[\dot{\psi} + \Omega\delta_R] \\ M'_{Rz} &= (f_{12}/v)[\dot{y} + r_R\dot{\phi} - v\psi] - (f_{22}/v)[\dot{\psi} + \Omega\delta_R] \end{aligned} \tag{A.48}$$

Next, components of creep forces and moments in the equilibrium axes are obtained by substituting Eq. (A. 47) into (A.33):

$$\begin{aligned} F_{Lx} &= -(f_{33}/v)\left\{v[1-(r_L/r_0)] - a\dot{\psi}\right\}\cos\psi \\ &\quad +(f_{11}/v)[\dot{y} + r_L\dot{\phi} - v\psi]\cos(\delta_L+\phi)\sin\psi \\ &\quad +(f_{12}/v)[\dot{\psi} - \Omega\delta_L]\cos(\delta_L+\phi)\sin\psi \\ F_{Ly} &= -(f_{33}/v)\left\{v[1-(r_L/r_0)] - a\dot{\psi}\right\}\sin\psi \\ &\quad -(f_{11}/v)[\dot{y} + r_L\dot{\phi} - v\psi]\cos(\delta_L+\phi)\cos\psi \\ &\quad -(f_{12}/v)[\dot{\psi} - \Omega\delta_L]\cos(\delta_L+\phi)\cos\psi \\ M_{Lz} &= (f_{12}/v)[\dot{y} + r_L\dot{\phi} - v\psi]\cos(\delta_L+\phi) \\ &\quad -(f_{22}/v)[\dot{\psi} - \Omega\delta_L]\cos(\delta_L+\phi) \end{aligned} \tag{A.49}$$

and Eq. (A.48) into (A.34):

$$
\begin{aligned}
F_{Rx} &= -(f_{33}/v)\left\{v[1-(r_R/r_0)]+a\dot{\psi}\right\}\cos\psi \\
&\quad +(f_{11}/v)[\dot{y}+r_R\dot{\phi}-v\psi]\cos(\delta_R-\phi)\sin\psi \\
&\quad +(f_{12}/v)[\dot{\psi}+\Omega\delta_R]\cos(\delta_R-\phi)\sin\psi \\
F_{Ry} &= -(f_{33}/v)\left\{v[1-(r_R/r_0)]+a\dot{\psi}\right\}\sin\psi \\
&\quad -(f_{11}/v)[\dot{y}+r_R\dot{\phi}-v\psi]\cos(\delta_R-\phi)\cos\psi \\
&\quad -(f_{12}/v)[\dot{\psi}+\Omega\delta_R]\cos(\delta_R-\phi)\cos\psi \\
M_{Rz} &= (f_{12}/v)[\dot{y}+r_R\dot{\phi}-v\psi]\cos(\delta_R-\phi) \\
&\quad -(f_{22}/v)[\dot{\psi}+\Omega\delta_R]\cos(\delta_R-\phi)
\end{aligned}
\tag{A.50}
$$

A.6 Lateral and Yaw Equations of Motion

By substituting N_{Ly} and N_{Ry}, from Eqs. (A.26) and (A.27), into Eqs. (A.22) and (A.25), the lateral and yaw equations of motion for the wheelset become

$$
m\ddot{y} = F_{Ly}+F_{Ry}+F_{sy}+N_R\sin(\delta_R-\phi)-N_L\sin(\delta_L+\phi) \tag{A.51}
$$

and

$$
\begin{aligned}
I_{wx}\ddot{\psi} &= -I_{wy}(v/r_0)\dot{\phi}+(R_{Rx}F_{Ry}-R_{Ry}F_{Rx})+(R_{Lx}F_{Ly}-R_{Ly}F_{Lx}) \\
&\quad +R_{Rx}N_R\sin(\delta_R-\phi)-R_{Lx}N_L\sin(\delta_L+\phi)+M_{Lz}+M_{Rz}+M_{sz}
\end{aligned}
\tag{A.52}
$$

where the normal forces N_R and N_L are given by Eqs. (A.28) and (A.29) or in their simplified form by Eq. (A.32).

A.7 Lateral and Yaw Gravitational Stiffnesses

The lateral gravitational stiffness is defined as

$$
F_g = -N_R\sin(\delta_R-\phi)+N_L\sin(\delta_L+\phi)
$$

It is termed lateral gravitational stiffness due to the fact that, when the terms $-N_R \sin(\delta_R - \phi)$ and $N_L \sin(\delta_L + \phi)$ are moved to the left side of Eq. (A.51), they contribute a restoring force because of gravity.

The lateral gravitational stiffness can be obtained by substituting Eq. (A.28) and Eq.(A.29) for N_L and N_R. However, the expression can be considerably simplified. Assuming small yaw and roll angles in Eqs. (A.28), (A.29) and (A.31), one obtains

$$F_g = F_z^* \Delta_L(y) + (F_z^* / a)\Delta_c(y) + (M_\phi^* / a)\Delta_\psi(y)$$

where

$$F_z^* = m\ddot{z} + W_A - F_{sz} - [F'_{Ly} \sin(\delta_L + \phi) - F'_{Ry} \sin(\delta_R - \phi)]$$

$$\begin{aligned} M_\phi^* = {} & I_{wx}\ddot{\phi} - I_{wy}\Omega\dot{\psi} - \psi[r_R F'_{Rx} + r_L F'_{Lx}] \\ & -[r_R F'_{Ry} \cos(\delta_R - \phi) + r_L F'_{Ly} \cos(\delta_L + \phi)] \\ & +\psi[M'_{Lz} \sin(\delta_L + \phi) - M'_{Rz} \sin(\delta_R - \phi)] - M_{sx} \end{aligned}$$

$$\Delta_L(y) = \frac{\tan(\delta_L + \phi) - \tan(\delta_R - \phi)}{2 - a^{-1}[r_L \tan(\delta_L + \phi) + r_R \tan(\delta_R - \phi)]}$$

$$\Delta_c(y) = \frac{(r_L - r_R)\tan(\delta_L + \phi)\tan(\delta_R - \phi)}{2 - a^{-1}[r_L \tan(\delta_L + \phi) + r_R \tan(\delta_R - \phi)]}$$

$$\Delta_\psi(y) = \frac{\tan(\delta_L + \phi) + \tan(\delta_R - \phi)}{2 - a^{-1}[r_L \tan(\delta_L + \phi) + r_R \tan(\delta_R - \phi)]}$$

At equilibrium, $F_{sz} = M_{sx} = 0$. Furthermore, assuming equilibrium about the roll axis gives rise to $M_\phi^* = 0$. Finally, neglecting the vertical inertia force $m\ddot{z}$ and the vertical components of the creep forces leads

$$F_g = W_A \left[\frac{\tan(\delta_L + \phi) - \tan(\delta_R - \phi)}{2 - a^{-1}[r_L \tan(\delta_L + \phi) + r_R \tan(\delta_R - \phi)]} \right] = W_A \Delta_L(y) \qquad \text{(A.53)}$$

where W_A is the axle load of the wheelset. It is then assumed that the angles δ_L, δ_R and φ are small so that the "tan" functions in the numerator of Eq. (A.53) can be replaced by the angles and the denominator replaced by 2. Hence, the simplified expression becomes

$$F_g = W_A\left[\frac{1}{2}(\delta_L - \delta_R) + \phi\right] \tag{A.54}$$

Similarly, the yaw gravitational stiffness is defined as

$$\begin{aligned} M_g &= -R_{Rx}N_R\sin(\delta_R - \phi) + R_{Lx}N_L\sin(\delta_L + \phi) \\ &= -a\psi[F_z^*\Delta_\psi(y) + (M_\phi^*/a)\Delta_L(y)] \\ &\quad + a\psi F_z^*\left[\frac{(r_L + r_R)\tan(\delta_L + \phi)\tan(\delta_R - \phi)}{2a - [r_L\tan(\delta_L + \phi) + r_R\tan(\delta_R - \phi)]}\right] \end{aligned} \tag{A.55}$$

This expression can also be simplified by neglecting the creep forces and by assuming equilibrium about the roll axis. The simplified expression for the yaw gravitational stiffness is

$$M_g = -a\psi W_A\left[\frac{\tan(\delta_L + \phi) + \tan(\delta_R - \phi)}{2 - a^{-1}[r_L\tan(\delta_L + \phi) + r_R\tan(\delta_R - \phi)]}\right] \tag{A.56}$$

Now applying the small angle assumption to obtain the further simplified expression

$$M_g = -a\psi W_A\left[\frac{1}{2}(\delta_L + \delta_R)\right] \tag{A.57}$$

A.8 Simplified Lateral and Yaw Equations of Motion

By using Eqs. (A.49) and (A.50) for creep forces and moments, Eqs. (A.54) and (A.57) for lateral and yaw gravitational stiffnesses, and Eqs. (A.18) and (A.19) for the components of the position vectors, the simplified lateral and yaw equations of motion of a wheelset are, from Eqs. (A.51) and (A.52)

$$m\ddot{y} + 2\frac{f_{11}}{v}\left[\dot{y} + \frac{r_L + r_R}{2}\dot{\phi} - v\psi\right] + 2f_{33}\left[1 - \frac{r_L + r_R}{2r_0}\right]\psi + 2f_{12}\left[\frac{\dot{\psi}}{v} - \frac{\delta_L - \delta_R}{2r_0}\right] + W_A\left[\frac{\delta_L - \delta_R}{2} + \phi\right] = F_{sy} \tag{A.58}$$

$$I_{wx}\ddot{\psi} + I_{wy}\frac{v}{r_0}\dot{\phi} + \frac{2a^2 f_{33}}{r_0}\left(\frac{r_L - r_R}{2a}\right) - \frac{2f_{12}}{v}\left[\dot{y} + \frac{r_L + r_R}{2}\dot{\phi} - v\psi\right] + 2a^2 f_{33}\frac{\dot{\psi}}{v} - 2f_{22}\frac{\delta_L - \delta_R}{2r_0} - aW_A\frac{\delta_L + \delta_R}{2}\psi + 2f_{22}\frac{\dot{\psi}}{v} = M_{sz} \tag{A.59}$$

These equations of motion are nonlinear. The left and right rolling radii r_L and r_R, the left and right contact angles δ_L and δ_R, and the roll angle φ are, in general, nonlinear functions of the lateral displacement y. They depend on the wheel and rail profiles and the points of contact. In addition, the suspension force F_{sy} and moment M_{sz} can be nonlinear functions of the variables.

The functions of rolling radii, contact angles and roll angle, in terms of lateral displacement, have been evaluated by Cooperrider and Law* for several wheel-rail profiles in a combined analytical and experimental study. Their approach involved a polynomial fit for the wheel and rail profiles, a computer program for the determination of the points of contact as the wheelset was moved laterally on the rail, and the computation of the relation functions. They have also validated experimentally some of their results.

These functions become linear for a conical wheel on a knife-edged rail. Let λ be the conical angle, it can be shown that:

* N.K. Cooperrider and E.H. Law, Data Book – Wheel/Rail Geometry for Five Wheel Profiles and Three Rail Profiles, Report ERC-R_T5015, Arizona State University, Tempe, Arizona,1975.

$$\frac{1}{2}(r_L - r_R) = \lambda y, \quad \frac{1}{2}(r_L + r_R) = r_0$$
$$\frac{1}{2}(\delta_L - \delta_R) = 0, \quad \frac{1}{2}(\delta_L + \delta_R) = \lambda \tag{A.60}$$

and

$$\phi = (\lambda / a) y \tag{A.61}$$

The equations of motion of the wheelset are reduced to

$$m\ddot{y} + 2\frac{f_{11}}{v}\left[\dot{y} + r_0\frac{\lambda}{a}\dot{y} - v\psi\right] + \frac{2f_{12}}{v}\dot{\psi} + W_A\frac{\lambda}{a}y = F_{sy}$$
$$I_{wx}\ddot{\psi} + I_{wy}\frac{v}{r_0}\frac{\lambda}{a}\dot{y} + \frac{2af_{33}\lambda}{r_0}y - \frac{2f_{12}}{v}\left[\dot{y} + r_0\frac{\lambda}{a}\dot{y} - v\psi\right] \tag{A.62}$$
$$+ 2a^2 f_{33}\frac{\dot{\psi}}{v} - aW_A\lambda\psi + 2f_{22}\frac{\dot{\psi}}{v} = M_{sz}$$

Appendix B

SAMPLE PLOTS OF MEANS, ROOT MEAN SQUARES AND VARIANCES OF LYAPUNOV EXPONENTS

The following plots are pertaining to Model III (as in Combination 1 using data from Table 2.5), randomness in forward speed and $S_0 = 1$.

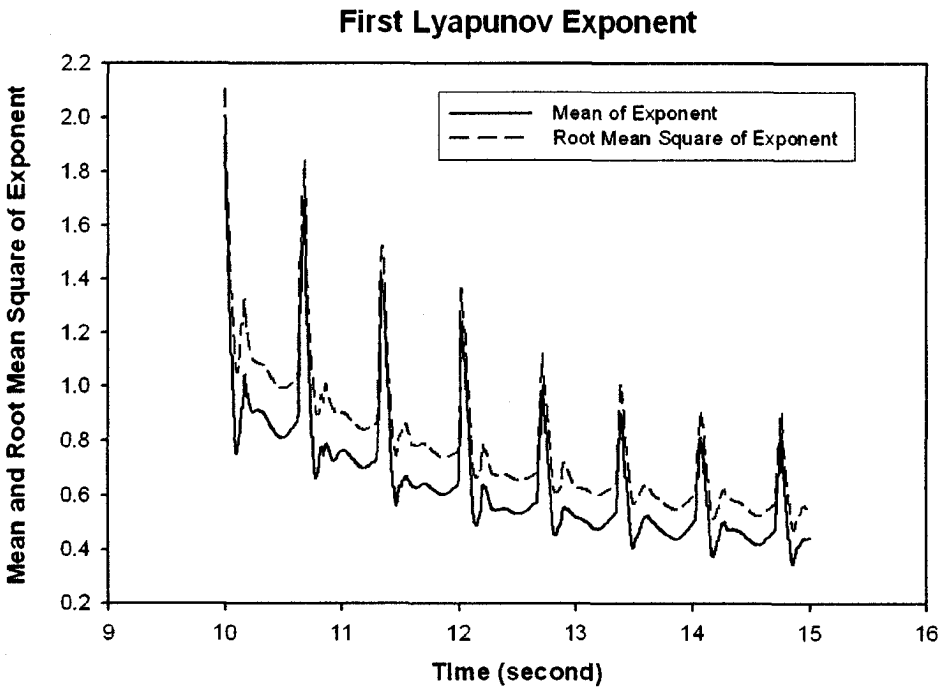

Figure B.1 Mean and root mean square of λ_1 versus time

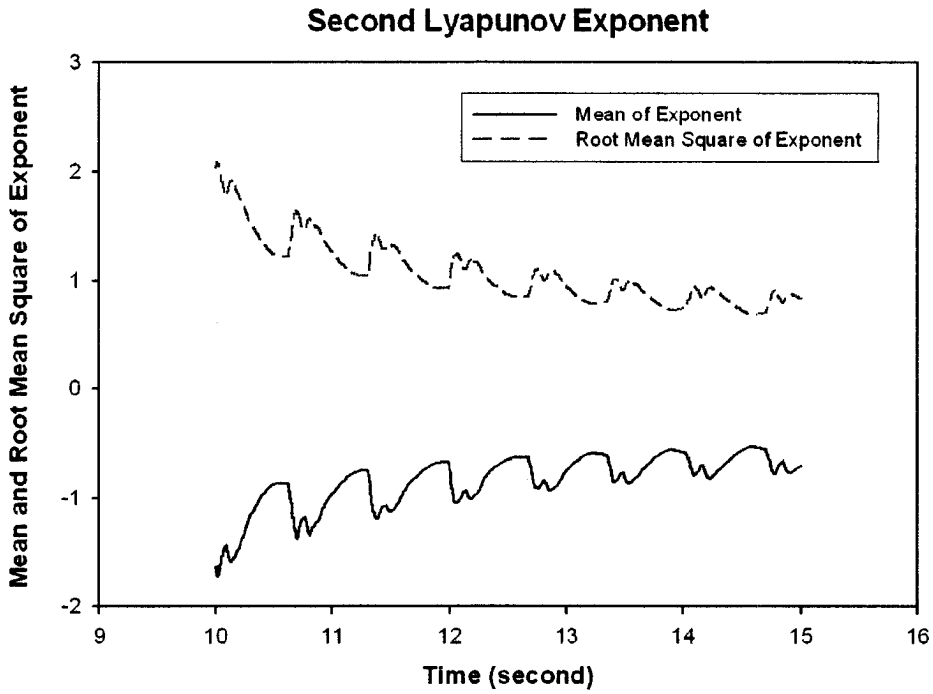

Figure B.2 Mean and root mean square of λ_2 versus time

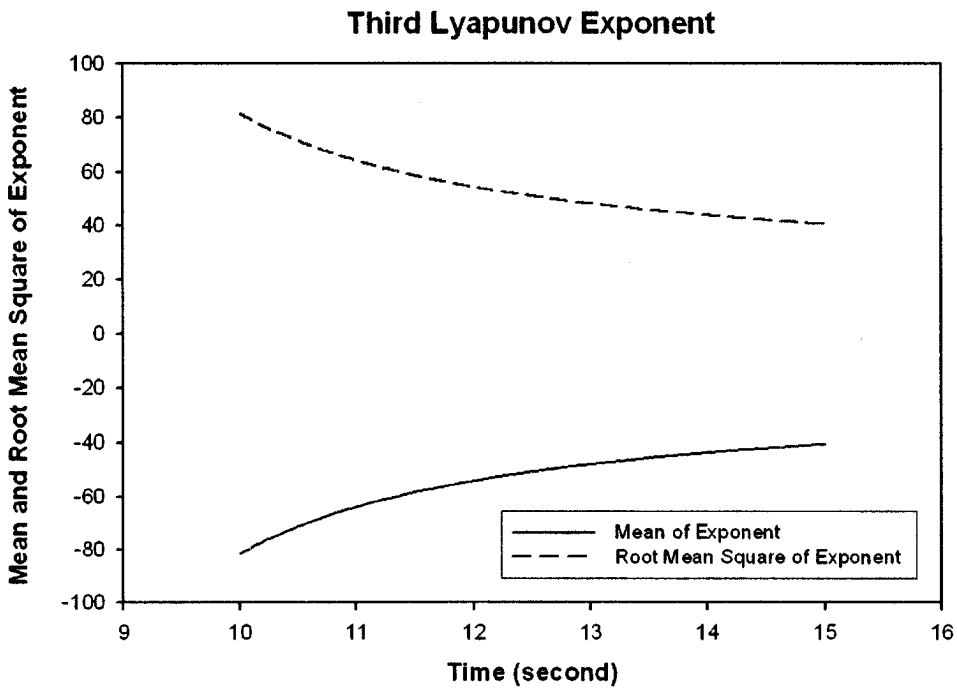

Figure B.3 Mean and root mean square of λ_3 versus time

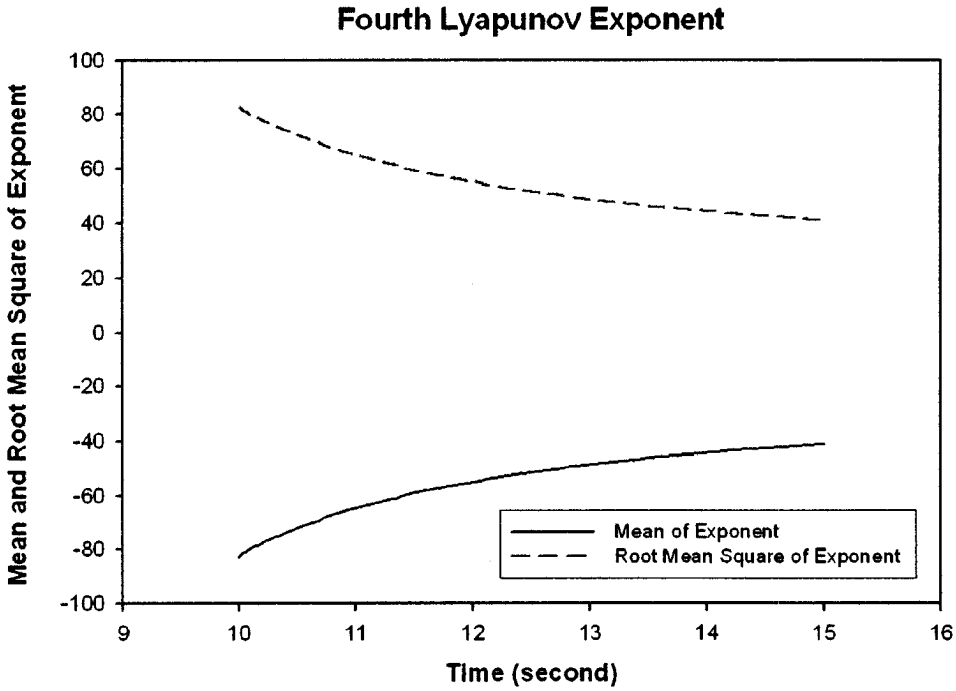

Figure B.4 Mean and root mean square of λ_4 versus time

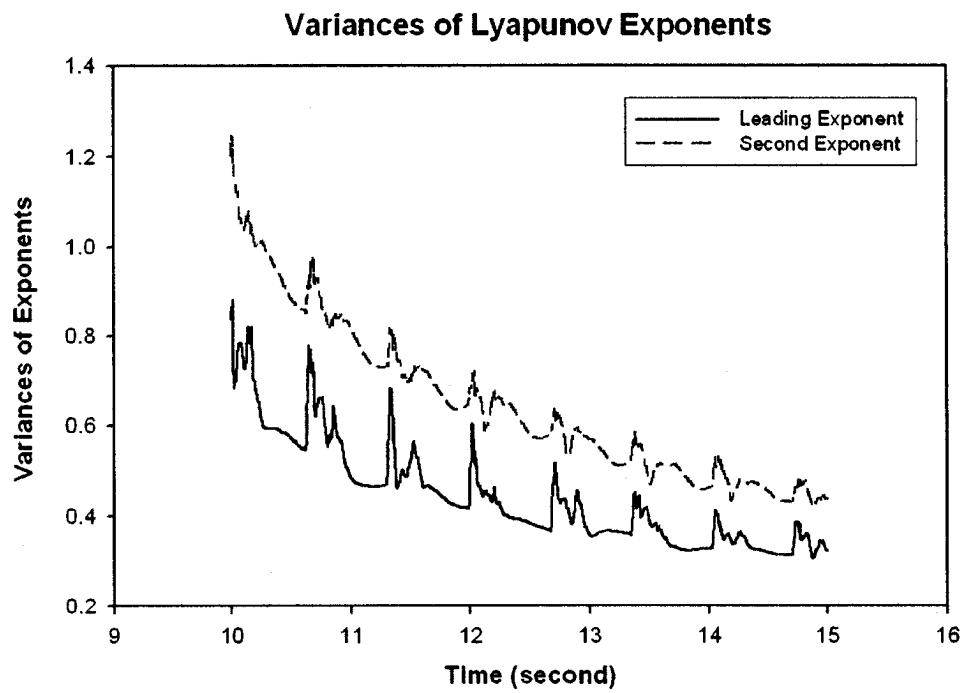

Figure B.5 Variances of λ_1 and λ_2 versus time

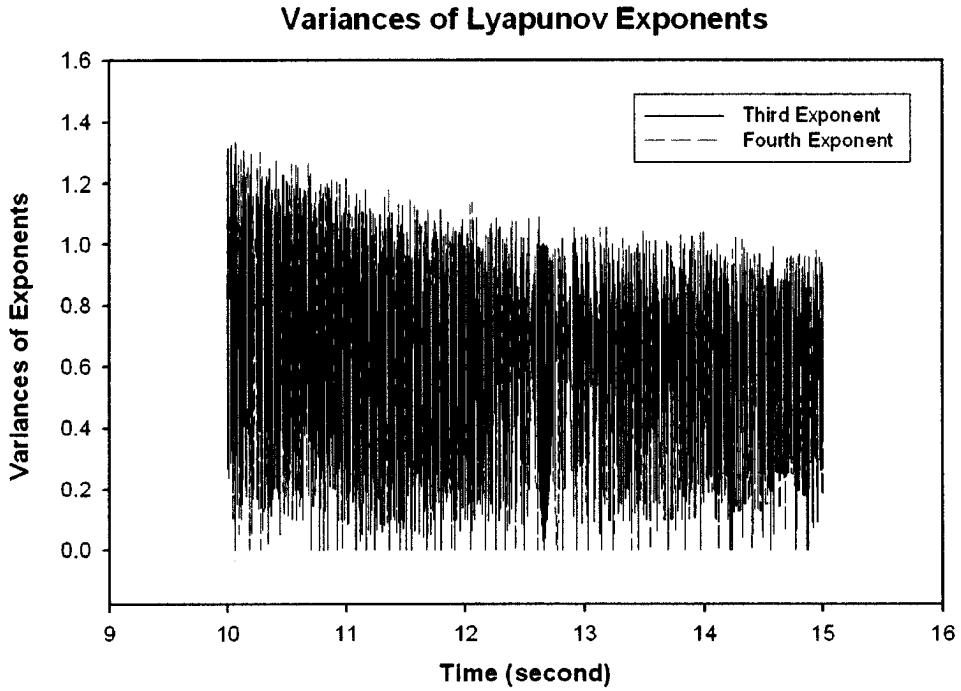

Figure B.6 Variances of λ_3 and λ_4 versus time

Note that the "waviness" seen in Figure B.6 can be minimized by using (1) a longer transient response period; and (2) a larger time step size.

Appendix C

SAMPLE RESULTS OF LYAPUNOV EXPONENTS AND INFORMATION DIMENSIONS

Table C.1 Lyapunov Exponents & Information Dimension (Model III + Table 2.5)

Deterministic Forward Speed					
v	λ_1	λ_2	λ_3	λ_4	D_I
1.00E+01	3.14E+00	8.90E-01	-3.05E+02	-3.06E+02	2.01E+00
1.01E+01	3.15E+00	1.27E+00	-3.02E+02	-3.03E+02	2.01E+00
1.02E+01	4.38E+00	2.99E+00	-2.98E+02	-3.05E+02	2.02E+00
1.03E+01	3.85E+00	2.81E+00	-2.91E+02	-3.05E+02	2.02E+00
1.04E+01	3.41E+00	2.85E+00	-2.87E+02	-3.03E+02	2.02E+00
1.05E+01	1.38E+00	-8.33E-02	-2.84E+02	-2.96E+02	2.00E+00
1.06E+01	1.24E+00	-4.64E+00	-2.78E+02	-2.91E+02	1.27E+00
1.07E+01	7.23E-02	-2.09E-01	-2.75E+02	-2.92E+02	1.35E+00
1.08E+01	2.09E+00	-2.06E+00	-2.72E+02	-2.90E+02	2.00E+00
1.09E+01	4.02E-01	-3.04E+00	-2.69E+02	-2.85E+02	1.13E+00
1.10E+01	-2.34E-01	-5.99E+00	-2.64E+02	-2.81E+02	0.00E+00
1.11E+01	-1.14E+00	-1.01E+01	-2.58E+02	-2.77E+02	0.00E+00
1.12E+01	-3.50E+00	-1.82E+01	-2.48E+02	-2.72E+02	0.00E+00
1.13E+01	-2.96E+00	-2.70E+01	-2.39E+02	-2.68E+02	0.00E+00
1.14E+01	-2.12E+00	-2.37E+01	-2.40E+02	-2.66E+02	0.00E+00
1.15E+01	-2.24E+00	-3.98E+01	-2.23E+02	-2.62E+02	0.00E+00
1.16E+01	-1.78E+00	-4.75E+01	-2.14E+02	-2.60E+02	0.00E+00
1.17E+01	-5.52E-01	-5.56E+01	-2.06E+02	-2.56E+02	0.00E+00
1.18E+01	-5.40E-01	-4.66E+01	-2.13E+02	-2.54E+02	0.00E+00
1.19E+01	-4.48E-01	-4.57E+01	-2.14E+02	-2.49E+02	0.00E+00
1.20E+01	-1.32E+00	-2.42E+01	-2.37E+02	-2.43E+02	0.00E+00
1.21E+01	-2.75E-01	-3.48E+01	-2.22E+02	-2.45E+02	0.00E+00
1.22E+01	-3.67E-01	-3.19E+01	-2.29E+02	-2.36E+02	0.00E+00
1.23E+01	4.55E-01	-3.27E+01	-2.19E+02	-2.42E+02	1.01E+00
1.24E+01	9.74E-01	-2.45E+01	-2.29E+02	-2.37E+02	1.04E+00
1.25E+01	6.96E-01	-1.90E+01	-2.33E+02	-2.34E+02	1.04E+00
1.26E+01	2.52E-02	-2.07E+01	-2.27E+02	-2.34E+02	1.00E+00
1.27E+01	1.95E-01	-1.71E+01	-2.29E+02	-2.31E+02	1.01E+00

1.28E+01	8.92E-01	-1.94E+01	-2.25E+02	-2.31E+02	1.05E+00
1.29E+01	3.45E+00	-1.85E+01	-2.26E+02	-2.29E+02	1.19E+00
1.30E+01	2.33E+00	-1.38E+01	-2.27E+02	-2.28E+02	1.17E+00
1.31E+01	1.83E+00	-1.30E+01	-2.26E+02	-2.26E+02	1.14E+00
1.32E+01	7.57E-01	-8.65E+00	-2.25E+02	-2.26E+02	1.09E+00
1.33E+01	7.39E-01	-1.20E+01	-2.22E+02	-2.23E+02	1.06E+00
1.34E+01	1.75E+00	-1.07E+01	-2.21E+02	-2.22E+02	1.16E+00
1.35E+01	6.60E-01	-6.84E+00	-2.21E+02	-2.22E+02	1.10E+00
1.36E+01	3.11E+00	-1.23E+01	-2.17E+02	-2.19E+02	1.25E+00
1.37E+01	2.65E+00	-6.79E+00	-2.18E+02	-2.20E+02	1.39E+00
1.38E+01	1.19E+00	-2.59E+00	-2.18E+02	-2.20E+02	1.46E+00
1.39E+01	2.58E+00	-4.63E+00	-2.16E+02	-2.17E+02	1.56E+00
1.40E+01	4.36E+00	-5.99E+00	-2.16E+02	-2.16E+02	1.73E+00
1.41E+01	2.02E+00	-1.23E+00	-2.13E+02	-2.18E+02	2.00E+00
1.42E+01	3.62E+00	-1.75E+00	-2.10E+02	-2.18E+02	2.01E+00
1.43E+01	7.44E+00	1.14E+00	-2.14E+02	-2.18E+02	2.04E+00
1.44E+01	9.72E+00	-1.81E-01	-2.14E+02	-2.17E+02	2.04E+00
1.45E+01	4.19E+00	1.96E+00	-2.11E+02	-2.12E+02	2.03E+00
1.46E+01	2.52E+00	7.02E-03	-2.07E+02	-2.10E+02	2.01E+00
1.47E+01	8.40E+00	1.12E+00	-2.08E+02	-2.13E+02	2.05E+00
1.48E+01	3.15E+00	2.79E+00	-2.06E+02	-2.09E+02	2.03E+00
1.49E+01	2.73E+00	2.41E+00	-2.06E+02	-2.06E+02	2.03E+00
1.50E+01	6.04E-01	-3.55E+00	-1.96E+02	-2.04E+02	1.17E+00
1.51E+01	3.65E+00	2.32E-01	-2.02E+02	-2.03E+02	2.02E+00
1.52E+01	3.37E+00	3.17E+00	-1.99E+02	-2.06E+02	2.03E+00
1.53E+01	2.80E+00	-3.30E+00	-1.92E+02	-2.03E+02	1.85E+00
1.54E+01	5.58E+00	-7.94E-01	-1.99E+02	-1.99E+02	2.02E+00
1.55E+01	1.67E+00	-8.63E+00	-1.86E+02	-1.98E+02	1.19E+00
1.56E+01	5.03E-01	-1.08E+00	-1.91E+02	-1.96E+02	1.47E+00
1.57E+01	1.45E+00	-2.41E+00	-1.89E+02	-1.95E+02	1.60E+00
1.58E+01	1.83E+00	-4.61E+00	-1.89E+02	-1.91E+02	1.40E+00
1.59E+01	1.67E+00	-7.96E+00	-1.85E+02	-1.89E+02	1.21E+00
1.60E+01	2.04E+00	-9.20E+00	-1.84E+02	-1.87E+02	1.22E+00
1.61E+01	2.41E+00	-1.04E+01	-1.83E+02	-1.85E+02	1.23E+00
1.62E+01	3.91E+00	-1.03E+01	-1.78E+02	-1.89E+02	1.38E+00
1.63E+01	2.74E+00	-2.55E+01	-1.67E+02	-1.81E+02	1.11E+00
1.64E+01	4.08E+00	-1.34E+01	-1.78E+02	-1.81E+02	1.30E+00
1.65E+01	4.44E+00	-2.14E+01	-1.70E+02	-1.80E+02	1.21E+00
1.66E+01	4.53E+00	-9.35E+00	-1.76E+02	-1.83E+02	1.48E+00

1.67E+01	7.80E+00	-1.91E+01	-1.66E+02	-1.84E+02	1.41E+00
1.68E+01	6.62E+00	-1.46E+01	-1.68E+02	-1.84E+02	1.45E+00
1.69E+01	3.15E+00	-5.05E+00	-1.66E+02	-1.90E+02	1.62E+00
1.70E+01	4.60E+00	-1.61E+01	-1.55E+02	-1.89E+02	1.29E+00
1.71E+01	3.40E+00	-8.74E+00	-1.67E+02	-1.81E+02	1.39E+00
1.72E+01	3.32E+00	-1.68E+00	-1.74E+02	-1.79E+02	2.01E+00
1.73E+01	4.22E+00	2.42E+00	-1.74E+02	-1.82E+02	2.04E+00
1.74E+01	3.28E+00	3.13E+00	-1.73E+02	-1.80E+02	2.04E+00
1.75E+01	3.31E+00	2.86E+00	-1.73E+02	-1.79E+02	2.04E+00
1.76E+01	3.28E+00	2.24E+00	-1.72E+02	-1.77E+02	2.03E+00
1.77E+01	2.49E+00	-1.36E+00	-1.69E+02	-1.74E+02	2.01E+00
1.78E+01	-1.34E+00	-3.06E+00	-1.65E+02	-1.70E+02	0.00E+00
1.79E+01	-1.09E+00	-2.94E+00	-1.63E+02	-1.70E+02	0.00E+00
1.80E+01	1.59E+00	-2.42E+00	-1.65E+02	-1.70E+02	1.66E+00
1.81E+01	7.06E-01	-3.37E+00	-1.62E+02	-1.69E+02	1.21E+00
1.82E+01	3.32E+00	-2.70E+00	-1.64E+02	-1.69E+02	2.00E+00
1.83E+01	3.05E+00	-6.01E+00	-1.59E+02	-1.68E+02	1.51E+00
1.84E+01	-1.15E+00	-5.13E+00	-1.59E+02	-1.63E+02	0.00E+00
1.85E+01	-1.80E+00	-7.45E+00	-1.55E+02	-1.62E+02	0.00E+00
1.86E+01	2.53E+00	-3.68E+00	-1.59E+02	-1.65E+02	1.69E+00
1.87E+01	1.18E+00	-4.82E+00	-1.58E+02	-1.61E+02	1.24E+00
1.88E+01	3.11E+00	-7.76E+00	-1.53E+02	-1.63E+02	1.40E+00
1.89E+01	1.41E-01	-8.68E+00	-1.52E+02	-1.59E+02	1.02E+00
1.90E+01	3.16E+00	-5.53E+00	-1.55E+02	-1.60E+02	1.57E+00
1.91E+01	5.84E-01	-8.65E+00	-1.50E+02	-1.58E+02	1.07E+00
1.92E+01	2.58E+00	-9.67E+00	-1.50E+02	-1.57E+02	1.27E+00
1.93E+01	1.04E+00	-1.20E+01	-1.47E+02	-1.54E+02	1.09E+00
1.94E+01	3.15E+00	-8.04E+00	-1.48E+02	-1.58E+02	1.39E+00
1.95E+01	3.02E+00	-7.68E+00	-1.48E+02	-1.57E+02	1.39E+00
1.96E+01	4.21E+00	-7.79E+00	-1.48E+02	-1.56E+02	1.54E+00
1.97E+01	3.76E+00	-8.91E+00	-1.47E+02	-1.54E+02	1.42E+00
1.98E+01	5.50E+00	-6.34E+00	-1.49E+02	-1.55E+02	1.87E+00
1.99E+01	2.55E+00	-1.01E+01	-1.47E+02	-1.49E+02	1.25E+00
2.00E+01	2.78E+00	-1.09E+01	-1.42E+02	-1.52E+02	1.25E+00

Table C.2 Lyapunov Exponents & Information Dimension (Model III + Table 2.5)

Random Forward Speed, S_0 = 1					
v	λ_1	λ_2	λ_3	λ_4	D_l
1.00E+01	1.93E-01	-1.65E+00	-3.52E+02	-3.99E+02	1.12E+00
1.01E+01	8.49E-01	-1.83E+00	-3.53E+02	-3.86E+02	1.46E+00
1.02E+01	1.37E+00	-1.70E+00	-3.49E+02	-3.70E+02	1.81E+00
1.03E+01	1.07E+00	-1.19E+00	-3.45E+02	-3.62E+02	1.90E+00
1.04E+01	1.05E+00	-9.51E-01	-3.44E+02	-3.61E+02	2.00E+00
1.05E+01	1.10E+00	-7.65E-01	-3.41E+02	-3.57E+02	2.00E+00
1.06E+01	9.78E-01	-5.95E-01	-3.41E+02	-3.50E+02	2.00E+00
1.07E+01	1.28E+00	-1.74E-01	-3.34E+02	-3.40E+02	2.00E+00
1.08E+01	1.75E+00	2.71E-02	-3.27E+02	-3.33E+02	2.01E+00
1.09E+01	2.19E+00	1.27E-01	-3.22E+02	-3.25E+02	2.01E+00
1.10E+01	2.50E+00	1.89E-01	-3.22E+02	-3.26E+02	2.01E+00
1.11E+01	2.44E+00	1.40E-01	-3.23E+02	-3.25E+02	2.01E+00
1.12E+01	3.00E+00	1.50E-01	-3.17E+02	-3.17E+02	2.01E+00
1.13E+01	3.16E+00	4.08E-01	-3.13E+02	-3.15E+02	2.01E+00
1.14E+01	2.63E+00	6.73E-01	-3.07E+02	-3.09E+02	2.01E+00
1.15E+01	3.09E+00	1.16E+00	-3.05E+02	-3.10E+02	2.01E+00
1.16E+01	2.62E+00	1.65E+00	-3.01E+02	-3.05E+02	2.01E+00
1.17E+01	1.77E+00	1.69E+00	-2.96E+02	-3.02E+02	2.01E+00
1.18E+01	1.02E+00	4.37E-01	-2.89E+02	-2.97E+02	2.01E+00
1.19E+01	3.41E-01	-2.00E+00	-2.82E+02	-2.93E+02	1.17E+00
1.20E+01	-6.59E-01	-2.92E+00	-2.79E+02	-2.93E+02	0.00E+00
1.21E+01	-4.23E-01	-5.70E+00	-2.72E+02	-2.88E+02	0.00E+00
1.22E+01	1.06E+00	-9.63E+00	-2.66E+02	-2.85E+02	1.11E+00
1.23E+01	6.51E-01	-1.12E+01	-2.62E+02	-2.82E+02	1.06E+00
1.24E+01	-1.51E+00	-1.26E+01	-2.57E+02	-2.76E+02	0.00E+00
1.25E+01	-2.33E+00	-1.72E+01	-2.49E+02	-2.72E+02	0.00E+00
1.26E+01	-2.76E+00	-2.06E+01	-2.45E+02	-2.68E+02	0.00E+00
1.27E+01	-2.11E+00	-2.47E+01	-2.40E+02	-2.64E+02	0.00E+00
1.28E+01	-1.91E+00	-2.78E+01	-2.35E+02	-2.60E+02	0.00E+00
1.29E+01	-1.77E+00	-2.86E+01	-2.33E+02	-2.58E+02	0.00E+00
1.30E+01	-1.26E+00	-2.98E+01	-2.31E+02	-2.54E+02	0.00E+00
1.31E+01	-9.42E-01	-2.92E+01	-2.30E+02	-2.50E+02	0.00E+00
1.32E+01	-6.94E-01	-2.88E+01	-2.29E+02	-2.46E+02	0.00E+00
1.33E+01	-4.66E-01	-2.75E+01	-2.28E+02	-2.43E+02	0.00E+00
1.34E+01	-2.26E-01	-2.53E+01	-2.29E+02	-2.40E+02	0.00E+00

1.35E+01	2.38E-01	-2.31E+01	-2.29E+02	-2.38E+02	1.01E+00
1.36E+01	3.62E-01	-2.18E+01	-2.29E+02	-2.37E+02	1.02E+00
1.37E+01	6.39E-01	-2.05E+01	-2.28E+02	-2.34E+02	1.03E+00
1.38E+01	1.14E+00	-1.89E+01	-2.27E+02	-2.32E+02	1.06E+00
1.39E+01	1.16E+00	-1.68E+01	-2.27E+02	-2.31E+02	1.07E+00
1.40E+01	1.63E+00	-1.57E+01	-2.26E+02	-2.30E+02	1.10E+00
1.41E+01	2.24E+00	-1.51E+01	-2.25E+02	-2.28E+02	1.15E+00
1.42E+01	1.87E+00	-1.41E+01	-2.24E+02	-2.27E+02	1.13E+00
1.43E+01	1.19E+00	-1.26E+01	-2.23E+02	-2.25E+02	1.09E+00
1.44E+01	9.57E-01	-1.15E+01	-2.21E+02	-2.23E+02	1.08E+00
1.45E+01	1.31E+00	-1.00E+01	-2.20E+02	-2.21E+02	1.13E+00
1.46E+01	1.71E+00	-9.56E+00	-2.19E+02	-2.20E+02	1.18E+00
1.47E+01	1.92E+00	-8.64E+00	-2.19E+02	-2.20E+02	1.22E+00
1.48E+01	2.24E+00	-7.69E+00	-2.17E+02	-2.18E+02	1.29E+00
1.49E+01	2.47E+00	-6.21E+00	-2.16E+02	-2.17E+02	1.40E+00
1.50E+01	2.73E+00	-4.69E+00	-2.15E+02	-2.17E+02	1.58E+00
1.51E+01	2.98E+00	-3.14E+00	-2.14E+02	-2.16E+02	1.95E+00
1.52E+01	3.15E+00	-2.26E+00	-2.13E+02	-2.15E+02	2.00E+00
1.53E+01	3.31E+00	-9.38E-01	-2.11E+02	-2.14E+02	2.01E+00
1.54E+01	3.61E+00	-4.07E-01	-2.10E+02	-2.13E+02	2.02E+00
1.55E+01	3.89E+00	-1.01E-02	-2.09E+02	-2.12E+02	2.02E+00
1.56E+01	3.69E+00	2.15E-01	-2.07E+02	-2.10E+02	2.02E+00
1.57E+01	4.05E+00	6.25E-01	-2.06E+02	-2.09E+02	2.02E+00
1.58E+01	3.91E+00	7.67E-01	-2.05E+02	-2.07E+02	2.02E+00
1.59E+01	4.09E+00	5.88E-01	-2.03E+02	-2.06E+02	2.02E+00
1.60E+01	3.87E+00	2.08E-01	-2.01E+02	-2.04E+02	2.02E+00
1.61E+01	4.17E+00	8.85E-02	-1.99E+02	-2.03E+02	2.02E+00
1.62E+01	3.84E+00	-2.39E-01	-1.97E+02	-2.02E+02	2.02E+00
1.63E+01	3.38E+00	-1.06E+00	-1.95E+02	-2.00E+02	2.01E+00
1.64E+01	3.59E+00	-1.31E+00	-1.94E+02	-1.99E+02	2.01E+00
1.65E+01	2.82E+00	-2.39E+00	-1.91E+02	-1.97E+02	2.00E+00
1.66E+01	2.76E+00	-3.19E+00	-1.89E+02	-1.95E+02	1.87E+00
1.67E+01	2.32E+00	-3.86E+00	-1.88E+02	-1.93E+02	1.60E+00
1.68E+01	2.57E+00	-5.05E+00	-1.86E+02	-1.91E+02	1.51E+00
1.69E+01	2.90E+00	-6.55E+00	-1.83E+02	-1.90E+02	1.44E+00
1.70E+01	3.24E+00	-6.86E+00	-1.82E+02	-1.89E+02	1.47E+00
1.71E+01	3.48E+00	-7.78E+00	-1.80E+02	-1.88E+02	1.45E+00
1.72E+01	4.08E+00	-7.27E+00	-1.79E+02	-1.88E+02	1.56E+00
1.73E+01	4.61E+00	-7.34E+00	-1.77E+02	-1.87E+02	1.63E+00

1.74E+01	4.81E+00	-7.00E+00	-1.76E+02	-1.87E+02	1.69E+00
1.75E+01	5.12E+00	-6.23E+00	-1.75E+02	-1.86E+02	1.82E+00
1.76E+01	4.96E+00	-5.90E+00	-1.74E+02	-1.86E+02	1.84E+00
1.77E+01	4.82E+00	-5.23E+00	-1.73E+02	-1.84E+02	1.92E+00
1.78E+01	4.59E+00	-4.72E+00	-1.73E+02	-1.83E+02	1.97E+00
1.79E+01	4.23E+00	-4.29E+00	-1.71E+02	-1.82E+02	1.99E+00
1.80E+01	3.83E+00	-4.21E+00	-1.70E+02	-1.81E+02	1.91E+00
1.81E+01	3.43E+00	-3.11E+00	-1.70E+02	-1.80E+02	2.00E+00
1.82E+01	2.94E+00	-2.96E+00	-1.69E+02	-1.78E+02	1.99E+00
1.83E+01	3.18E+00	-2.57E+00	-1.68E+02	-1.77E+02	2.00E+00
1.84E+01	2.74E+00	-2.43E+00	-1.67E+02	-1.76E+02	2.00E+00
1.85E+01	2.17E+00	-2.69E+00	-1.66E+02	-1.74E+02	1.81E+00
1.86E+01	1.61E+00	-3.49E+00	-1.65E+02	-1.72E+02	1.46E+00
1.87E+01	1.53E+00	-3.62E+00	-1.64E+02	-1.71E+02	1.42E+00
1.88E+01	1.53E+00	-3.18E+00	-1.64E+02	-1.69E+02	1.48E+00
1.89E+01	1.56E+00	-4.19E+00	-1.62E+02	-1.68E+02	1.37E+00
1.90E+01	1.73E+00	-4.99E+00	-1.60E+02	-1.67E+02	1.35E+00
1.91E+01	1.86E+00	-5.51E+00	-1.59E+02	-1.66E+02	1.34E+00
1.92E+01	1.82E+00	-5.74E+00	-1.58E+02	-1.65E+02	1.32E+00
1.93E+01	2.16E+00	-5.86E+00	-1.58E+02	-1.64E+02	1.37E+00
1.94E+01	2.01E+00	-6.52E+00	-1.56E+02	-1.63E+02	1.31E+00
1.95E+01	2.12E+00	-6.70E+00	-1.55E+02	-1.61E+02	1.32E+00
1.96E+01	2.24E+00	-7.14E+00	-1.54E+02	-1.61E+02	1.31E+00
1.97E+01	2.22E+00	-7.44E+00	-1.53E+02	-1.60E+02	1.30E+00
1.98E+01	2.38E+00	-7.55E+00	-1.52E+02	-1.59E+02	1.32E+00
1.99E+01	2.45E+00	-7.94E+00	-1.51E+02	-1.58E+02	1.31E+00
2.00E+01	2.39E+00	-8.49E+00	-1.50E+02	-1.57E+02	1.28E+00

Table C.3 Information Dimension (Model III + Table 2.5)

speed	Information Dimension					
	S_0=0	S_0=0.0025	S_0=0.01	S_0=1	S_0=25	S_0=100
1.00E+01	2.01E+00	2.01E+00	2.01E+00	1.12E+00	2.49E+00	3.19E+00
1.01E+01	2.01E+00	2.01E+00	2.01E+00	1.46E+00	2.48E+00	3.09E+00
1.02E+01	2.02E+00	2.03E+00	2.03E+00	1.81E+00	2.51E+00	3.09E+00
1.03E+01	2.02E+00	2.03E+00	2.04E+00	1.90E+00	2.47E+00	3.12E+00
1.04E+01	2.02E+00	2.03E+00	2.02E+00	2.00E+00	2.46E+00	3.11E+00
1.05E+01	2.00E+00	1.41E+00	2.00E+00	2.00E+00	2.44E+00	3.13E+00
1.06E+01	1.27E+00	0.00E+00	0.00E+00	2.00E+00	2.44E+00	3.15E+00
1.07E+01	1.35E+00	1.15E+00	1.60E+00	2.00E+00	2.49E+00	3.16E+00
1.08E+01	2.00E+00	1.56E+00	1.58E+00	2.01E+00	2.51E+00	3.12E+00
1.09E+01	1.13E+00	1.09E+00	1.10E+00	2.01E+00	2.48E+00	3.16E+00
1.10E+01	0.00E+00	0.00E+00	0.00E+00	2.01E+00	2.51E+00	3.14E+00
1.11E+01	0.00E+00	0.00E+00	0.00E+00	2.01E+00	2.54E+00	3.19E+00
1.12E+01	0.00E+00	0.00E+00	0.00E+00	2.01E+00	2.55E+00	3.21E+00
1.13E+01	0.00E+00	0.00E+00	0.00E+00	2.01E+00	2.51E+00	3.23E+00
1.14E+01	0.00E+00	0.00E+00	0.00E+00	2.01E+00	2.51E+00	3.22E+00
1.15E+01	0.00E+00	0.00E+00	0.00E+00	2.01E+00	2.51E+00	3.24E+00
1.16E+01	0.00E+00	0.00E+00	0.00E+00	2.01E+00	2.49E+00	3.19E+00
1.17E+01	0.00E+00	0.00E+00	0.00E+00	2.01E+00	2.48E+00	3.26E+00
1.18E+01	0.00E+00	0.00E+00	0.00E+00	2.01E+00	2.43E+00	3.26E+00
1.19E+01	0.00E+00	0.00E+00	0.00E+00	1.17E+00	2.44E+00	3.28E+00
1.20E+01	0.00E+00	0.00E+00	0.00E+00	0.00E+00	2.44E+00	3.24E+00
1.21E+01	0.00E+00	0.00E+00	0.00E+00	0.00E+00	2.48E+00	3.17E+00
1.22E+01	0.00E+00	0.00E+00	0.00E+00	1.11E+00	2.48E+00	3.14E+00
1.23E+01	1.01E+00	0.00E+00	1.00E+00	1.06E+00	2.49E+00	3.19E+00
1.24E+01	1.04E+00	1.01E+00	1.01E+00	0.00E+00	2.44E+00	3.17E+00
1.25E+01	1.04E+00	1.03E+00	1.02E+00	0.00E+00	2.45E+00	3.20E+00
1.26E+01	1.00E+00	1.04E+00	1.04E+00	0.00E+00	2.45E+00	3.24E+00
1.27E+01	1.01E+00	1.05E+00	1.06E+00	0.00E+00	2.45E+00	3.19E+00
1.28E+01	1.05E+00	1.08E+00	1.09E+00	0.00E+00	2.44E+00	3.22E+00
1.29E+01	1.19E+00	1.19E+00	1.18E+00	0.00E+00	2.42E+00	3.17E+00
1.30E+01	1.17E+00	1.14E+00	1.14E+00	0.00E+00	2.40E+00	3.18E+00
1.31E+01	1.14E+00	1.11E+00	1.12E+00	0.00E+00	2.42E+00	3.18E+00
1.32E+01	1.09E+00	1.08E+00	1.08E+00	0.00E+00	2.43E+00	3.19E+00
1.33E+01	1.06E+00	1.05E+00	1.06E+00	0.00E+00	2.47E+00	3.18E+00
1.34E+01	1.16E+00	1.10E+00	1.10E+00	0.00E+00	2.49E+00	3.19E+00

1.35E+01	1.10E+00	1.19E+00	1.16E+00	1.01E+00	2.41E+00	3.17E+00
1.36E+01	1.25E+00	1.23E+00	1.24E+00	1.02E+00	2.40E+00	3.14E+00
1.37E+01	1.39E+00	1.30E+00	1.28E+00	1.03E+00	2.41E+00	3.15E+00
1.38E+01	1.46E+00	1.37E+00	1.40E+00	1.06E+00	2.42E+00	3.18E+00
1.39E+01	1.56E+00	1.53E+00	1.47E+00	1.07E+00	2.41E+00	3.09E+00
1.40E+01	1.73E+00	1.98E+00	1.81E+00	1.10E+00	2.40E+00	3.12E+00
1.41E+01	2.00E+00	2.02E+00	2.02E+00	1.15E+00	2.36E+00	3.12E+00
1.42E+01	2.01E+00	2.03E+00	2.02E+00	1.13E+00	2.38E+00	3.15E+00
1.43E+01	2.04E+00	2.03E+00	2.03E+00	1.09E+00	2.37E+00	3.12E+00
1.44E+01	2.04E+00	2.04E+00	2.03E+00	1.08E+00	2.39E+00	3.13E+00
1.45E+01	2.03E+00	2.03E+00	2.03E+00	1.13E+00	2.38E+00	3.05E+00
1.46E+01	2.01E+00	2.04E+00	2.04E+00	1.18E+00	2.36E+00	3.01E+00
1.47E+01	2.05E+00	2.05E+00	2.04E+00	1.22E+00	2.34E+00	3.02E+00
1.48E+01	2.03E+00	2.03E+00	2.03E+00	1.29E+00	2.28E+00	3.06E+00
1.49E+01	2.03E+00	2.02E+00	2.02E+00	1.40E+00	2.33E+00	3.06E+00
1.50E+01	1.17E+00	2.01E+00	2.01E+00	1.58E+00	2.32E+00	3.06E+00
1.51E+01	2.02E+00	2.01E+00	2.01E+00	1.95E+00	2.29E+00	3.03E+00
1.52E+01	2.03E+00	2.02E+00	2.02E+00	2.00E+00	2.33E+00	3.05E+00
1.53E+01	1.85E+00	2.02E+00	2.03E+00	2.01E+00	2.35E+00	3.04E+00
1.54E+01	2.02E+00	2.03E+00	2.03E+00	2.02E+00	2.33E+00	3.05E+00
1.55E+01	1.19E+00	2.00E+00	2.01E+00	2.02E+00	2.34E+00	3.03E+00
1.56E+01	1.47E+00	1.73E+00	1.69E+00	2.02E+00	2.35E+00	3.10E+00
1.57E+01	1.60E+00	1.44E+00	1.29E+00	2.02E+00	2.34E+00	3.08E+00
1.58E+01	1.40E+00	1.25E+00	1.32E+00	2.02E+00	2.32E+00	3.09E+00
1.59E+01	1.21E+00	1.31E+00	1.29E+00	2.02E+00	2.33E+00	3.03E+00
1.60E+01	1.22E+00	1.31E+00	1.28E+00	2.02E+00	2.39E+00	2.98E+00
1.61E+01	1.23E+00	1.20E+00	1.21E+00	2.02E+00	2.35E+00	2.90E+00
1.62E+01	1.38E+00	1.17E+00	1.21E+00	2.02E+00	2.33E+00	2.91E+00
1.63E+01	1.11E+00	1.18E+00	1.20E+00	2.01E+00	2.35E+00	2.99E+00
1.64E+01	1.30E+00	1.21E+00	1.19E+00	2.01E+00	2.30E+00	2.94E+00
1.65E+01	1.21E+00	1.25E+00	1.24E+00	2.00E+00	2.29E+00	2.97E+00
1.66E+01	1.48E+00	1.29E+00	1.28E+00	1.87E+00	2.28E+00	2.93E+00
1.67E+01	1.41E+00	1.53E+00	1.49E+00	1.60E+00	2.26E+00	2.97E+00
1.68E+01	1.45E+00	1.52E+00	1.56E+00	1.51E+00	2.26E+00	2.95E+00
1.69E+01	1.62E+00	1.91E+00	1.79E+00	1.44E+00	2.24E+00	2.98E+00
1.70E+01	1.29E+00	1.91E+00	1.87E+00	1.47E+00	2.25E+00	2.97E+00
1.71E+01	1.39E+00	2.02E+00	2.01E+00	1.45E+00	2.23E+00	2.95E+00
1.72E+01	2.01E+00	2.02E+00	2.02E+00	1.56E+00	2.25E+00	3.00E+00
1.73E+01	2.04E+00	2.01E+00	2.02E+00	1.63E+00	2.24E+00	3.00E+00

1.74E+01	2.04E+00	2.02E+00	2.02E+00	1.69E+00	2.25E+00	2.98E+00
1.75E+01	2.04E+00	2.02E+00	2.02E+00	1.82E+00	2.24E+00	2.96E+00
1.76E+01	2.03E+00	2.02E+00	2.02E+00	1.84E+00	2.24E+00	2.95E+00
1.77E+01	2.01E+00	2.01E+00	2.01E+00	1.92E+00	2.26E+00	2.92E+00
1.78E+01	0.00E+00	2.01E+00	2.00E+00	1.97E+00	2.28E+00	2.85E+00
1.79E+01	0.00E+00	1.33E+00	1.59E+00	1.99E+00	2.28E+00	2.86E+00
1.80E+01	1.66E+00	1.97E+00	1.94E+00	1.91E+00	2.26E+00	2.83E+00
1.81E+01	1.21E+00	1.45E+00	1.51E+00	2.00E+00	2.27E+00	2.81E+00
1.82E+01	2.00E+00	1.73E+00	1.90E+00	1.99E+00	2.27E+00	2.83E+00
1.83E+01	1.51E+00	1.38E+00	1.60E+00	2.00E+00	2.25E+00	2.84E+00
1.84E+01	0.00E+00	1.36E+00	1.52E+00	2.00E+00	2.26E+00	2.81E+00
1.85E+01	0.00E+00	1.30E+00	1.43E+00	1.81E+00	2.25E+00	2.81E+00
1.86E+01	1.69E+00	1.51E+00	1.51E+00	1.46E+00	2.26E+00	2.87E+00
1.87E+01	1.24E+00	1.43E+00	1.54E+00	1.42E+00	2.23E+00	2.86E+00
1.88E+01	1.40E+00	1.57E+00	1.45E+00	1.48E+00	2.25E+00	2.82E+00
1.89E+01	1.02E+00	1.38E+00	1.50E+00	1.37E+00	2.23E+00	2.89E+00
1.90E+01	1.57E+00	1.45E+00	1.36E+00	1.35E+00	2.24E+00	2.88E+00
1.91E+01	1.07E+00	1.39E+00	1.39E+00	1.34E+00	2.25E+00	2.86E+00
1.92E+01	1.27E+00	1.44E+00	1.43E+00	1.32E+00	2.23E+00	2.91E+00
1.93E+01	1.09E+00	1.42E+00	1.42E+00	1.37E+00	2.24E+00	2.91E+00
1.94E+01	1.39E+00	1.31E+00	1.32E+00	1.31E+00	2.21E+00	2.87E+00
1.95E+01	1.39E+00	1.32E+00	1.35E+00	1.32E+00	2.22E+00	2.91E+00
1.96E+01	1.54E+00	1.34E+00	1.35E+00	1.31E+00	2.23E+00	2.89E+00
1.97E+01	1.42E+00	1.35E+00	1.35E+00	1.30E+00	2.24E+00	2.90E+00
1.98E+01	1.87E+00	1.36E+00	1.40E+00	1.32E+00	2.23E+00	2.87E+00
1.99E+01	1.25E+00	1.25E+00	1.32E+00	1.31E+00	2.24E+00	2.86E+00
2.00E+01	1.25E+00	1.35E+00	1.35E+00	1.28E+00	2.22E+00	2.88E+00

Table C.4 Information Dimensions of Model III with Randomness in Forward Speed

speed	Information Dimension					
	S_0=0	S_0=0.0025	S_0=0.01	S_0=1	S_0=100	S_0=900
1.00E+01	2.01E+00	2.01E+00	2.01E+00	2.00E+00	3.18E+00	3.85E+00
1.01E+01	2.01E+00	2.01E+00	2.01E+00	1.81E+00	3.11E+00	3.82E+00
1.02E+01	2.02E+00	2.03E+00	2.03E+00	1.81E+00	3.06E+00	3.89E+00
1.03E+01	2.02E+00	2.03E+00	2.03E+00	2.00E+00	3.11E+00	3.82E+00
1.04E+01	2.02E+00	2.03E+00	2.02E+00	2.00E+00	3.14E+00	3.83E+00
1.05E+01	2.00E+00	1.38E+00	2.00E+00	2.00E+00	3.17E+00	3.84E+00
1.06E+01	1.27E+00	0.00E+00	0.00E+00	2.00E+00	3.12E+00	3.77E+00
1.07E+01	1.35E+00	1.02E+00	1.21E+00	2.01E+00	3.17E+00	3.79E+00
1.08E+01	2.00E+00	1.56E+00	1.61E+00	2.01E+00	3.22E+00	3.78E+00
1.09E+01	1.13E+00	1.11E+00	1.11E+00	2.01E+00	3.17E+00	3.83E+00
1.10E+01	0.00E+00	0.00E+00	0.00E+00	2.01E+00	3.27E+00	3.83E+00
1.11E+01	0.00E+00	0.00E+00	0.00E+00	2.01E+00	3.24E+00	3.84E+00
1.12E+01	0.00E+00	0.00E+00	0.00E+00	2.01E+00	3.21E+00	3.78E+00
1.13E+01	0.00E+00	0.00E+00	0.00E+00	2.01E+00	3.20E+00	3.81E+00
1.14E+01	0.00E+00	0.00E+00	0.00E+00	2.01E+00	3.21E+00	3.85E+00
1.15E+01	0.00E+00	0.00E+00	0.00E+00	2.02E+00	3.26E+00	3.81E+00
1.16E+01	0.00E+00	0.00E+00	0.00E+00	2.02E+00	3.20E+00	3.81E+00
1.17E+01	0.00E+00	0.00E+00	0.00E+00	2.01E+00	3.19E+00	3.83E+00
1.18E+01	0.00E+00	0.00E+00	0.00E+00	0.00E+00	3.17E+00	3.83E+00
1.19E+01	0.00E+00	0.00E+00	0.00E+00	1.14E+00	3.16E+00	3.85E+00
1.20E+01	0.00E+00	0.00E+00	0.00E+00	1.17E+00	3.17E+00	3.83E+00
1.21E+01	0.00E+00	0.00E+00	0.00E+00	0.00E+00	3.14E+00	3.89E+00
1.22E+01	0.00E+00	0.00E+00	0.00E+00	0.00E+00	3.14E+00	3.87E+00
1.23E+01	1.01E+00	0.00E+00	0.00E+00	0.00E+00	3.14E+00	3.89E+00
1.24E+01	1.04E+00	1.01E+00	1.01E+00	0.00E+00	3.14E+00	3.88E+00
1.25E+01	1.04E+00	1.03E+00	1.02E+00	0.00E+00	3.12E+00	3.92E+00
1.26E+01	1.00E+00	1.04E+00	1.04E+00	0.00E+00	3.11E+00	3.86E+00
1.27E+01	1.01E+00	1.07E+00	1.05E+00	0.00E+00	3.12E+00	3.83E+00
1.28E+01	1.05E+00	1.09E+00	1.08E+00	0.00E+00	3.10E+00	3.83E+00
1.29E+01	1.19E+00	1.19E+00	1.19E+00	0.00E+00	3.10E+00	3.81E+00
1.30E+01	1.17E+00	1.14E+00	1.13E+00	0.00E+00	3.05E+00	3.80E+00
1.31E+01	1.14E+00	1.11E+00	1.11E+00	0.00E+00	3.06E+00	3.78E+00
1.32E+01	1.09E+00	1.06E+00	1.09E+00	0.00E+00	3.14E+00	3.81E+00
1.33E+01	1.06E+00	1.05E+00	1.04E+00	0.00E+00	3.12E+00	3.73E+00

1.34E+01	1.16E+00	1.12E+00	1.10E+00	0.00E+00	3.17E+00	3.71E+00
1.35E+01	1.10E+00	1.15E+00	1.16E+00	1.01E+00	3.11E+00	3.76E+00
1.36E+01	1.25E+00	1.25E+00	1.22E+00	1.03E+00	3.08E+00	3.77E+00
1.37E+01	1.39E+00	1.29E+00	1.30E+00	1.05E+00	3.09E+00	3.78E+00
1.38E+01	1.46E+00	1.37E+00	1.37E+00	1.07E+00	3.08E+00	3.78E+00
1.39E+01	1.56E+00	1.45E+00	1.45E+00	1.08E+00	3.01E+00	3.79E+00
1.40E+01	1.73E+00	1.77E+00	1.86E+00	1.10E+00	2.99E+00	3.79E+00
1.41E+01	2.00E+00	2.01E+00	2.01E+00	1.11E+00	3.05E+00	3.76E+00
1.42E+01	2.01E+00	2.03E+00	2.03E+00	1.08E+00	3.04E+00	3.77E+00
1.43E+01	2.04E+00	2.02E+00	2.03E+00	1.06E+00	3.00E+00	3.75E+00
1.44E+01	2.04E+00	2.04E+00	2.03E+00	1.08E+00	3.00E+00	3.72E+00
1.45E+01	2.03E+00	2.03E+00	2.03E+00	1.15E+00	3.07E+00	3.76E+00
1.46E+01	2.01E+00	2.04E+00	2.03E+00	1.20E+00	3.08E+00	3.75E+00
1.47E+01	2.05E+00	2.05E+00	2.04E+00	1.28E+00	3.12E+00	3.69E+00
1.48E+01	2.03E+00	2.03E+00	2.03E+00	1.39E+00	3.10E+00	3.72E+00
1.49E+01	2.03E+00	2.01E+00	2.02E+00	1.59E+00	3.13E+00	3.75E+00
1.50E+01	1.17E+00	2.01E+00	2.01E+00	1.87E+00	3.16E+00	3.73E+00

Table C.5 Information Dimensions of Model III with Randomness in Dead Band

speed	Information Dimension					
	S_0=0	S_0=0.0025	S_0=0.01	S_0=1	S_0=100	S_0=900
1.00E+01	2.01E+00	2.87E+00	2.94E+00	3.66E+00	3.89E+00	3.91E+00
1.01E+01	2.01E+00	2.87E+00	2.97E+00	3.67E+00	3.89E+00	3.92E+00
1.02E+01	2.02E+00	2.88E+00	2.92E+00	3.67E+00	3.89E+00	3.92E+00
1.03E+01	2.02E+00	2.87E+00	2.96E+00	3.66E+00	3.89E+00	3.91E+00
1.04E+01	2.02E+00	2.87E+00	2.93E+00	3.67E+00	3.88E+00	3.92E+00
1.05E+01	2.00E+00	2.81E+00	2.94E+00	3.65E+00	3.90E+00	3.91E+00
1.06E+01	1.27E+00	2.90E+00	2.96E+00	3.67E+00	3.88E+00	3.91E+00
1.07E+01	1.35E+00	2.86E+00	2.92E+00	3.67E+00	3.90E+00	3.92E+00
1.08E+01	2.00E+00	2.86E+00	2.96E+00	3.66E+00	3.89E+00	3.92E+00
1.09E+01	1.13E+00	2.87E+00	2.93E+00	3.69E+00	3.89E+00	3.92E+00
1.10E+01	0.00E+00	2.87E+00	2.95E+00	3.65E+00	3.90E+00	3.92E+00
1.11E+01	0.00E+00	2.88E+00	2.94E+00	3.69E+00	3.88E+00	3.92E+00
1.12E+01	0.00E+00	2.86E+00	2.95E+00	3.66E+00	3.90E+00	3.91E+00
1.13E+01	0.00E+00	2.87E+00	2.97E+00	3.67E+00	3.88E+00	3.92E+00
1.14E+01	0.00E+00	2.87E+00	2.93E+00	3.67E+00	3.90E+00	3.92E+00
1.15E+01	0.00E+00	2.86E+00	2.97E+00	3.66E+00	3.89E+00	3.92E+00
1.16E+01	0.00E+00	2.88E+00	2.94E+00	3.68E+00	3.89E+00	3.93E+00

1.17E+01	0.00E+00	2.84E+00	2.96E+00	3.66E+00	3.90E+00	3.92E+00
1.18E+01	0.00E+00	2.90E+00	2.96E+00	3.68E+00	3.88E+00	3.93E+00
1.19E+01	0.00E+00	2.88E+00	2.95E+00	3.67E+00	3.90E+00	3.92E+00
1.20E+01	0.00E+00	2.89E+00	2.96E+00	3.67E+00	3.89E+00	3.92E+00
1.21E+01	0.00E+00	2.90E+00	2.94E+00	3.68E+00	3.90E+00	3.93E+00
1.22E+01	0.00E+00	2.86E+00	2.95E+00	3.66E+00	3.90E+00	3.92E+00
1.23E+01	1.01E+00	2.91E+00	2.94E+00	3.68E+00	3.89E+00	3.93E+00
1.24E+01	1.04E+00	2.87E+00	2.97E+00	3.65E+00	3.91E+00	3.92E+00
1.25E+01	1.04E+00	2.89E+00	2.95E+00	3.68E+00	3.88E+00	3.92E+00
1.26E+01	1.00E+00	2.88E+00	2.98E+00	3.68E+00	3.91E+00	3.92E+00
1.27E+01	1.01E+00	2.91E+00	2.97E+00	3.66E+00	3.89E+00	3.93E+00
1.28E+01	1.05E+00	2.91E+00	2.94E+00	3.69E+00	3.90E+00	3.93E+00
1.29E+01	1.19E+00	2.88E+00	2.97E+00	3.67E+00	3.91E+00	3.92E+00
1.30E+01	1.17E+00	2.91E+00	2.96E+00	3.69E+00	3.89E+00	3.93E+00
1.31E+01	1.14E+00	2.88E+00	2.96E+00	3.65E+00	3.90E+00	3.92E+00
1.32E+01	1.09E+00	2.91E+00	2.97E+00	3.69E+00	3.89E+00	3.93E+00
1.33E+01	1.06E+00	2.89E+00	2.97E+00	3.67E+00	3.91E+00	3.93E+00
1.34E+01	1.16E+00	2.87E+00	2.96E+00	3.66E+00	3.90E+00	3.93E+00
1.35E+01	1.10E+00	2.90E+00	2.98E+00	3.68E+00	3.89E+00	3.93E+00
1.36E+01	1.25E+00	2.88E+00	2.94E+00	3.66E+00	3.91E+00	3.93E+00
1.37E+01	1.39E+00	2.89E+00	2.99E+00	3.69E+00	3.88E+00	3.93E+00
1.38E+01	1.46E+00	2.88E+00	2.97E+00	3.66E+00	3.91E+00	3.93E+00
1.39E+01	1.56E+00	2.90E+00	2.98E+00	3.68E+00	3.89E+00	3.93E+00
1.40E+01	1.73E+00	2.90E+00	2.95E+00	3.68E+00	3.91E+00	3.93E+00
1.41E+01	2.00E+00	2.88E+00	2.96E+00	3.67E+00	3.90E+00	3.93E+00
1.42E+01	2.01E+00	2.88E+00	2.99E+00	3.68E+00	3.89E+00	3.93E+00
1.43E+01	2.04E+00	2.87E+00	2.96E+00	3.66E+00	3.91E+00	3.93E+00
1.44E+01	2.04E+00	2.89E+00	3.00E+00	3.68E+00	3.89E+00	3.93E+00
1.45E+01	2.03E+00	2.88E+00	2.99E+00	3.69E+00	3.91E+00	3.93E+00
1.46E+01	2.01E+00	2.88E+00	2.99E+00	3.67E+00	3.90E+00	3.93E+00
1.47E+01	2.05E+00	2.89E+00	2.97E+00	3.69E+00	3.90E+00	3.94E+00
1.48E+01	2.03E+00	2.87E+00	2.97E+00	3.68E+00	3.91E+00	3.93E+00
1.49E+01	2.03E+00	2.91E+00	2.99E+00	3.68E+00	3.89E+00	3.93E+00
1.50E+01	1.17E+00	2.89E+00	2.99E+00	3.67E+00	3.91E+00	3.93E+00

Table C.6 Information Dimensions of Model III with Randomness in Both Forward Speed and Dead Band

speed	Information Dimension					
	S_0=0	S_0=0.0025	S_0=0.01	S_0=1	S_0=100	S_0=900
1.00E+01	2.01E+00	2.90E+00	3.19E+00	3.82E+00	3.94E+00	3.96E+00
1.01E+01	2.01E+00	2.89E+00	3.17E+00	3.82E+00	3.94E+00	3.96E+00
1.02E+01	2.02E+00	2.92E+00	3.19E+00	3.82E+00	3.94E+00	3.96E+00
1.03E+01	2.02E+00	2.85E+00	3.16E+00	3.82E+00	3.94E+00	3.96E+00
1.04E+01	2.02E+00	2.91E+00	3.17E+00	3.83E+00	3.95E+00	3.96E+00
1.05E+01	2.00E+00	2.93E+00	3.19E+00	3.82E+00	3.94E+00	3.96E+00
1.06E+01	1.27E+00	2.89E+00	3.18E+00	3.82E+00	3.95E+00	3.96E+00
1.07E+01	1.35E+00	2.93E+00	3.21E+00	3.82E+00	3.94E+00	3.96E+00
1.08E+01	2.00E+00	2.90E+00	3.16E+00	3.82E+00	3.95E+00	3.96E+00
1.09E+01	1.13E+00	2.94E+00	3.17E+00	3.83E+00	3.95E+00	3.96E+00
1.10E+01	0.00E+00	2.92E+00	3.19E+00	3.82E+00	3.95E+00	3.96E+00
1.11E+01	0.00E+00	2.92E+00	3.18E+00	3.83E+00	3.95E+00	3.96E+00
1.12E+01	0.00E+00	2.91E+00	3.20E+00	3.82E+00	3.94E+00	3.96E+00
1.13E+01	0.00E+00	2.91E+00	3.16E+00	3.82E+00	3.95E+00	3.96E+00
1.14E+01	0.00E+00	2.93E+00	3.20E+00	3.83E+00	3.95E+00	3.97E+00
1.15E+01	0.00E+00	2.94E+00	3.19E+00	3.82E+00	3.95E+00	3.96E+00
1.16E+01	0.00E+00	2.91E+00	3.20E+00	3.83E+00	3.95E+00	3.96E+00
1.17E+01	0.00E+00	2.94E+00	3.20E+00	3.82E+00	3.95E+00	3.96E+00
1.18E+01	0.00E+00	2.91E+00	3.19E+00	3.83E+00	3.95E+00	3.96E+00
1.19E+01	0.00E+00	2.94E+00	3.20E+00	3.82E+00	3.95E+00	3.97E+00
1.20E+01	0.00E+00	2.91E+00	3.18E+00	3.83E+00	3.95E+00	3.96E+00
1.21E+01	0.00E+00	2.96E+00	3.20E+00	3.82E+00	3.95E+00	3.97E+00
1.22E+01	0.00E+00	2.90E+00	3.17E+00	3.82E+00	3.95E+00	3.96E+00
1.23E+01	1.01E+00	2.96E+00	3.17E+00	3.83E+00	3.95E+00	3.97E+00
1.24E+01	1.04E+00	2.95E+00	3.21E+00	3.82E+00	3.95E+00	3.97E+00
1.25E+01	1.04E+00	2.91E+00	3.18E+00	3.83E+00	3.95E+00	3.96E+00
1.26E+01	1.00E+00	2.95E+00	3.20E+00	3.83E+00	3.95E+00	3.97E+00
1.27E+01	1.01E+00	2.92E+00	3.20E+00	3.82E+00	3.95E+00	3.96E+00
1.28E+01	1.05E+00	2.92E+00	3.18E+00	3.83E+00	3.95E+00	3.97E+00
1.29E+01	1.19E+00	2.94E+00	3.19E+00	3.82E+00	3.95E+00	3.96E+00
1.30E+01	1.17E+00	2.90E+00	3.20E+00	3.83E+00	3.95E+00	3.97E+00
1.31E+01	1.14E+00	2.95E+00	3.20E+00	3.83E+00	3.95E+00	3.97E+00
1.32E+01	1.09E+00	2.88E+00	3.18E+00	3.83E+00	3.95E+00	3.96E+00
1.33E+01	1.06E+00	3.01E+00	3.22E+00	3.83E+00	3.95E+00	3.97E+00
1.34E+01	1.16E+00	2.94E+00	3.21E+00	3.82E+00	3.95E+00	3.97E+00

1.35E+01	1.10E+00	2.96E+00	3.20E+00	3.83E+00	3.95E+00	3.97E+00
1.36E+01	1.25E+00	2.98E+00	3.19E+00	3.83E+00	3.95E+00	3.97E+00
1.37E+01	1.39E+00	2.92E+00	3.21E+00	3.83E+00	3.95E+00	3.97E+00
1.38E+01	1.46E+00	2.99E+00	3.21E+00	3.83E+00	3.95E+00	3.97E+00
1.39E+01	1.56E+00	2.93E+00	3.20E+00	3.83E+00	3.95E+00	3.97E+00
1.40E+01	1.73E+00	3.01E+00	3.20E+00	3.83E+00	3.95E+00	3.97E+00
1.41E+01	2.00E+00	2.94E+00	3.20E+00	3.83E+00	3.95E+00	3.97E+00
1.42E+01	2.01E+00	2.98E+00	3.23E+00	3.83E+00	3.95E+00	3.97E+00
1.43E+01	2.04E+00	2.95E+00	3.18E+00	3.83E+00	3.95E+00	3.97E+00
1.44E+01	2.04E+00	2.96E+00	3.21E+00	3.83E+00	3.96E+00	3.97E+00
1.45E+01	2.03E+00	2.98E+00	3.21E+00	3.83E+00	3.95E+00	3.97E+00
1.46E+01	2.01E+00	2.94E+00	3.21E+00	3.83E+00	3.95E+00	3.97E+00
1.47E+01	2.05E+00	2.97E+00	3.20E+00	3.83E+00	3.95E+00	3.97E+00
1.48E+01	2.03E+00	2.93E+00	3.21E+00	3.83E+00	3.95E+00	3.97E+00
1.49E+01	2.03E+00	3.00E+00	3.20E+00	3.83E+00	3.95E+00	3.97E+00
1.50E+01	1.17E+00	2.98E+00	3.22E+00	3.83E+00	3.95E+00	3.97E+00

Appendix D

COMPUTED BIFURCATION DIAGRAMS FOR THE ENTIRE SPEED RANGE OF 1 TO 50 m/s

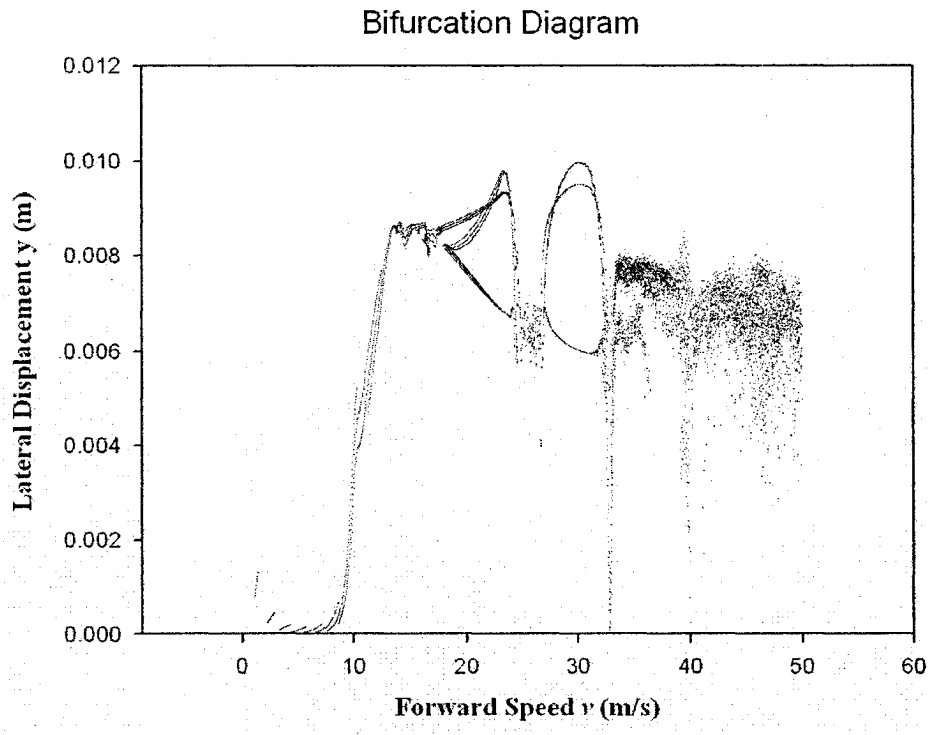

Figure D.1 Bifurcation diagram, no control, $S_0 = 0.01$

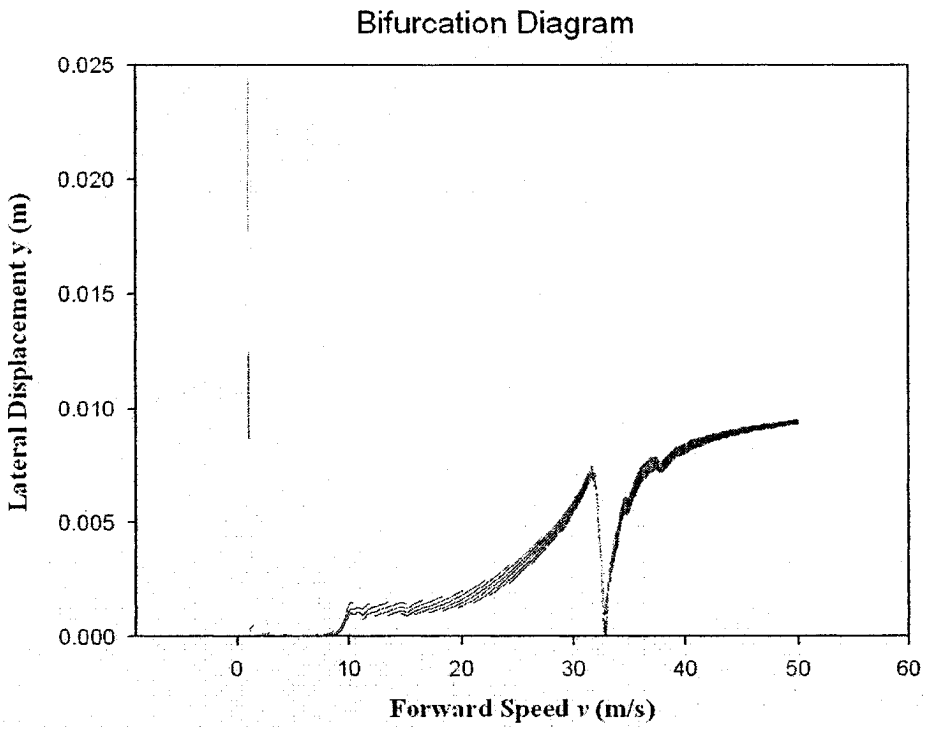

Figure D.2 Bifurcation diagram, semi-active control, $S_0 = 0.01$

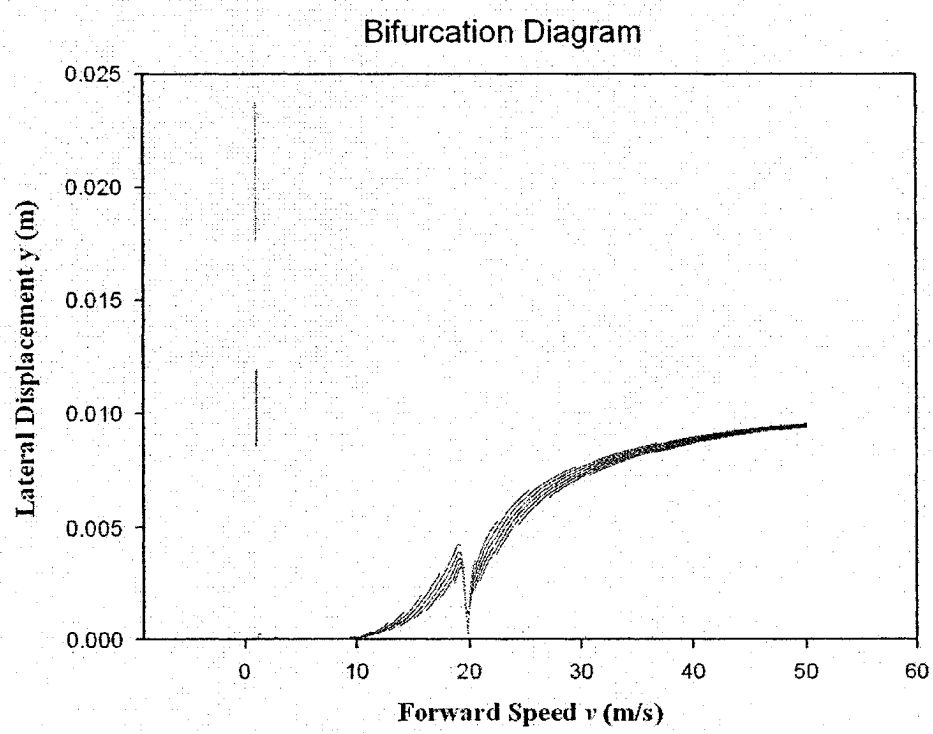

Figure D.3 Bifurcation diagram, active control, $S_0 = 0.01$

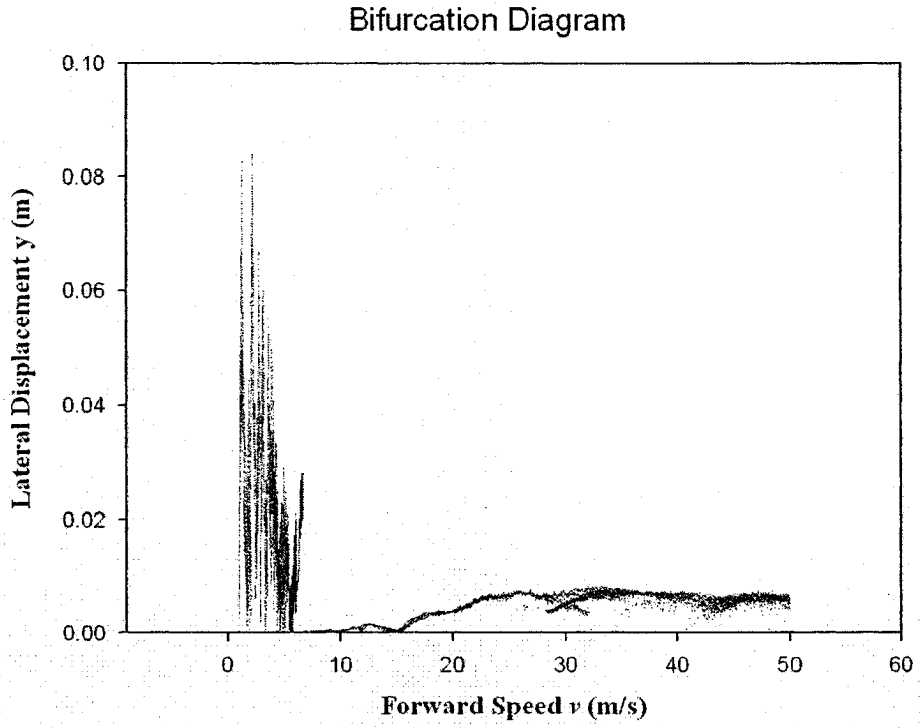

Figure D.4 Bifurcation diagram, no control, $S_0 = 1$

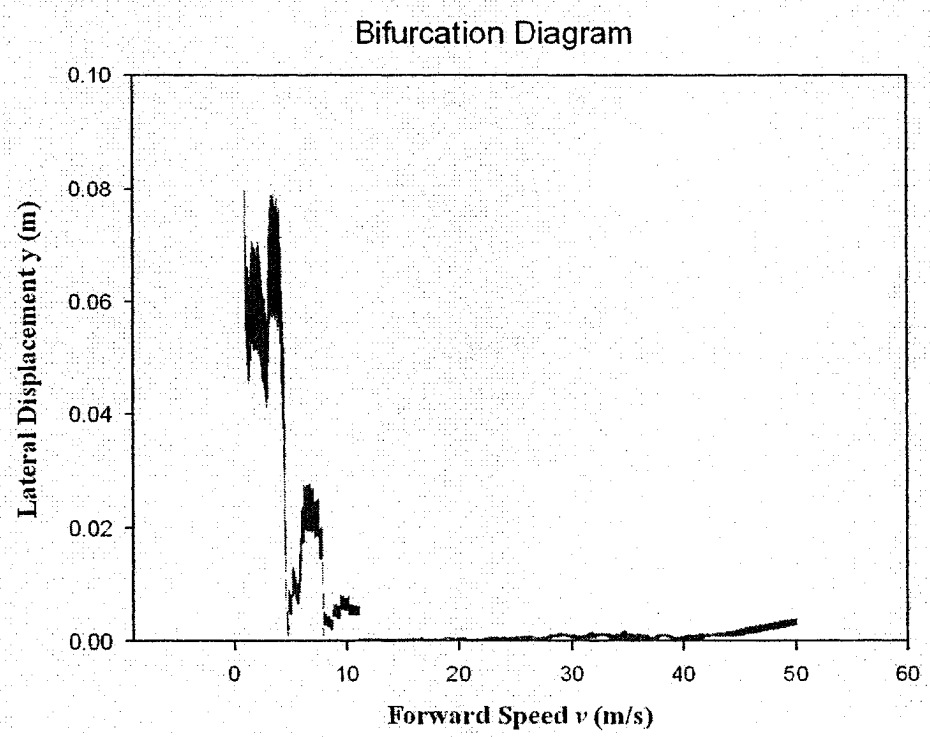

Figure D.5 Bifurcation diagram, semi-active control, $S_0 = 1$

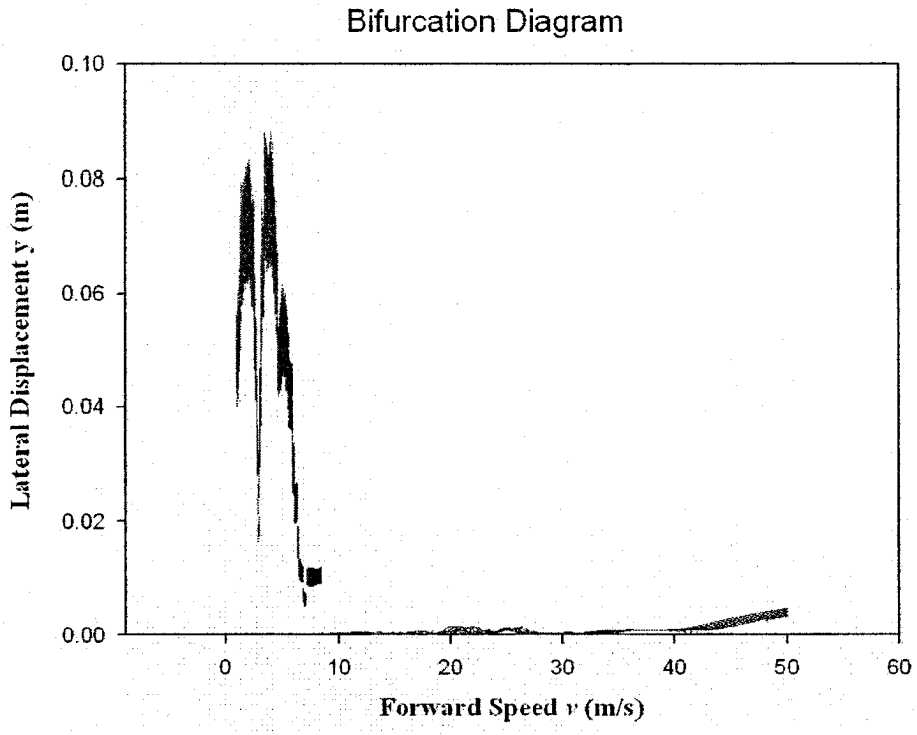

Figure D.6 Bifurcation diagram, active control, $S_0 = 1$

REFERENCES

Chapter 1

[1.1] D.E. Petersen and M. Hoffmann, *Dry Friction and Impact Dynamics in Railway Vehicles*, Master's Thesis, Technical University of Denmark, 2003.

[1.2] H. True, Some recent developments in nonlinear railway vehicle dynamics, in *Proc. 1st European Nonlinear Oscillation Conference*, Hamburg, Germany (1993), 129-148.

[1.3] H. True and R. Asmund, The dynamics of a railway freight wagon wheelset with dry friction damping, *Vehicle System Dynamics* (2002) **38**, 149-163.

[1.4] N.K. Cooperrider, The hunting behavior of conventional railway trucks, *Journal of Engineering for Industry* (1972) **94**, 752-762.

[1.5] A. A. Shabana and J.R. Sany, A survey of rail vehicle track simulations and flexible multibody dynamics, *Nonlinear Dynamics* (2006) **26**, 179-210.

[1.6] A.D. DePater, The approximate determination of the hunting movement of a railway vehicle by aid of the method of Krylov and Bogoljubow, *Applied Science Research* (1961) **A10**, 205-228.

[1.7] T. Matsudaira, Paper awarded prize in the competition sponsored by the Office of Research and Experiment (UIC) of the International Union of Railways (UIC), ORE report RP2/SVA-C9, UIC, Utrecht, 1960.

[1.8] A.H. Wickens, The dynamic stability of railway vehicle wheelsets and bogies having profiled wheels, *International Journal Solids Structures* (1965) **1**, 319-341.

[1.9] R.R. Huilgol, Hopf-Friedrichs bifurcation and the hunting of a railway axle, *Quarterly Journal Applied Mathematics* (1978) **36**, 85-94.

[1.10] F.W. Carter, *Railway Electric Traction*, London: Edward Arnold (1922), 57-70.

[1.11] K.L. Johnson, The effect of a tangential force upon the rolling motion of an elastic sphere upon a plane, *Journal Applied Mechanics* (1958) **25**, 339-346.

[1.12] P.J. Vermeulen and K.L. Johnson, Contact of non-spherical elastic bodies transmitting tangential forces, *Journal Applied Mechanics* (1964) **31**, 338-340.

[1.13] N.K. Cooperrider, The hunting behavior of conventional railway trucks, Contribution by Rail Transportation Division for Presentation at the ASME Winter Annual Meeting, New York 1970.

[1.14] L.M. Sweet and J.A. Sivak, Analysis of nonlinear wheelset forces in flange contact, *Journal of Dynamic Systems, Measurement and Control* (1979) **101**, 238-246.

[1.15] M.A. Lohe and R.R. Huilgol, Flange force effects on the motion of a train wheelset, *Vehicle System Dynamics* (1982) **11**, 283-303.

[1.16] J.P. Meizard and A.D. DePater, Railway vehicle systems dynamics and chaotic motions, *International Journal Nonlinear Mechanics* (1989) **24**, 1-17.

[1.17] C. Knudsen, R. Feldberg and H. True, Bifurcations and chaos in a model of a rolling railway wheelset, *Philosophical Transactions of the Royal Society A* (1992) **338**, 455-469.

[1.18] E. Silvsaard and H. True, Chaos in railway-vehicle dynamics, in *Nonlinearity and Chaos in Engineering Dynamics* (1994), 183-192.

[1.19] P. Carlbom, *Carbody and Passengers in Rail Vehicle Dynamics*, Ph.D. Dissertation, Department of Vehicle Engineering, Royal Institute of Technology, Sweden, 2000.

[1.20] A.H. Nayfeh and B. Balachandran, *Applied Nonlinear Dynamics*, John Wiley, New York, 1994.

[1.21] H.O. Wang and E. H. Abed, Bifurcation control of chaotic dynamical systems, in *the Second IFAC Nonlinear Control Symposium*, Bordeaux, France, (1992) **6**, 24-26.

[1.22] E. Ott, C. Grebogi and J.A. Yorke, Controlling chaos, *Physical Review Letters*, (1990) **64**, 1196-1199.

[1.23] F.J. Romeiras, E, Ott, C. Grebogi and W.P. Dayawansa, Controlling chaotic dynamical systems, in *Proc. 1991 American Control Conference*, Boston, MA, (1991).

[1.24] E. Ott, *Chaos in Dynamical Systems*, Cambridge University Press, Cambridge, England, 1993.

[1.25] E. Ott, C. Grebogi and J.A. Yorke, Controling chaotic dynamical systems, in *CHAOS: Soviet-American Perspectives on Nonlinear Science* (1990) **2a**, 153-172.

[1.26] A. Hubler, Adaptive control of chaotic systems, *Helvetica Physica Acta* (1989) **62**, 343-346.

[1.27] A. Hubler and E. Luscher, Resonant stimulation and control of nonlinear oscillators, *Natunwissenschaften* (1989) **76**, 67-69.

[1.28] E.A. Jackson, Control of dynamic flows with attractors, *Physical Review A* (1991) **A44**, 4839-4853.

[1.29] J. Singer, Y.Z. Wang and H.H. Bau, Controlling a chaotic system, *Physical Review Letters* (1991) **66**, 1123-1125.

[1.30] T.L. Vincent and J. Yu, Control of a chaotic system, *Dynamics and Control* (1991) **1**, 35-52.

[1.31] A.M. Harb and M.A. Zohdy, Chaos and bifurcation control using nonlinear recursive controller, *Nonlinear Analysis: Modeling and Control* (2002) **7**, 37-43.

[1.32] A. Mohan and M. Ahmadian, Nonlinear investigation of the effect of primary suspension on the hunting stability of a rail wheelset, *Proceedings of the 2004 ASME/IEEE Joint Rail Conference* (2004), 53-61.

Chapter 2

[2.1] P.J. Vermeulen and K.L. Johnson, Contact of non-spherical elastic bodies transmitting tangential forces, *Journal Applied Mechanics* (1964) **31**, 338-340.

[2.2] J.J. Kalker, *On the Rolling Contact of Two Elastic Bodied in the Presence of Dry Friction*, Ph.D. Dissertation, Delft University of Technology, The Netherlands, 1967.

[2.3] V.K. Garg and R.V. Dukkipati, *Dynamics of Railway Vehicle Systems*, Academic Press, 1984.

[2.4] M. Ahmadian and S.P. Yang, Hopf bifurcation and hunting behavior in a rail wheelset with flange contact, *Nonlinear Dynamics* (1998) **15**, 15-30.

[2.5] Y. Nath and K. Jayadev, Influence of yaw stiffness on the nonlinear dynamics of railway wheelset, *Communications in Nonlinear Science and Numerical Simulation* (2005) **10**, 179-190.

Chapter 3

[3.1] G. Marsaglia, A current view of random number generators, in *Computing Science and Statistics: Proceedings of the XVIth Symposium on the Interface* (1985), 3-10.

[3.2] J. Yu, Random vibration control for dual-shaker and multi-shaker for cross coupled systems, Post-Doctoral Report. (Private communication, 2000)

[3.3] http://www.netlib.org/random/zufall.f

[3.4] The Statistical Package for the Social Sciences, The SPSS Inc., Chicago, IL, U.S.A.

Chapter 4

[4.1] R.L. Devaney, *A First Course in Chaotic Dynamical Systems,* Westview Press, 1992.

[4.2] A. Wolf, J.B. Swift, H.L. Swiney and J.A. Vasano, Determining Lyapunov exponents from a time series, *Physica D* (1985) **16**, 285-317.

[4.3] F. Moon, *Chaotic and Fractal Dynamics*, Springer-Verlag, 1990.

[4.4] J.L. Kaplan and J.A. Yorke, Chaotic behavior of multidimensional difference equations, In *Functional Differential Equations and Approximations of Fixed Points, Lecture Notes in Mathematics* Vol 730, Springer, 1979, 228-237.

[4.5] M.A. Jafarizadeh and S. Behnia, Hierarchy of random chaotic maps with an invariant measure, *Journal of Mathematical Physics* (2003) **44**, 5386-5400.

[4.6] D. Nychka, S. Ellner, A.R. Gallant and D. McCaffrey, Finding chaos in noisy systems, *Journal of Royal Statistical Society B* (1992), **54**, 399-426.

[4.7] A. Serletis, A. Shahmoradi and D. Serletis, Effect of noise on estimation of Lyapunov exponents from a time series, *Chaos, Solitons and Fractals* (2007) **32**, 883-887.

[4.8] M. Shintani and O. Linton, Is there chaos in the world economy? A nonparametric test using consistent standard errors, *International Economics Review* (2003) **44**, 449-454.

[4.9] M. Shintani and O. Linton, Nonparametric neural network estimation of Lyapunov exponents and direct tests for chaos, *Journal of Econometrics* (2004) **120**, 1-33.

[4.10] Y.J. Whang and O. Linton, The asymptotic distribution of nonparametric estimates of the Lyapunov exponent for stochastic time series, *Journal of Econometrics* (1999) **91**, 1-42.

[4.11] C.W.S. To and M.L. Liu, Lyapunov exponents and information dimensions of multi-degree-of-freedom systems under deterministic and stationary random excitations, in *IUTAM Symposium on Advances in Nonlinear Stochastic Mechanics* (1995), 449-458.

[4.12] A.H. Wickens, The dynamics of railway vehicles on straight track: Fundamental considerations of lateral stability, *Proc. Institute of Mechanical Engineering* Part F (1965) **180**, 29-44.

[4.13] Y. Nath and K. Jayadev, Influence of yaw stiffness on the nonlinear dynamics of railway wheelset, *Communications in Nonlinear Science and Numerical Simulation* (2005) **10**, 179-190.

[4.14] M.L. Liu and J. Yu, Lyapunov exponents and information dimensions of nonlinear railway wheelsets incorporating randomness, in *The 2006 World Congress in Computer Science, Computer Engineering and Applied Computing* (2006), paper number CSC4093 (7p.) Las Vegas, Nevada, USA.

Chapter 5

[5.1] E. Ott, C. Grebogi and J.A. Yorke, Controlling chaos, *Physical Review Letters* (1990) **64**, 1196-1199.

[5.2] F.J. Romeiras, E, Ott, C. Grebogi and W.P. Dayawansa, Controlling chaotic dynamical systems, *Proc. 1991 American Control Conference*, Boston (1991).

[5.3] J. Singer, Y.Z. Wang and H.H. Bau, Controlling a chaotic system, *Physical Review Letters* (1991) **66**, 1123-1125.

[5.4] T.L. Vincent and J. Yu, Control of a chaotic system, *Dynamics and Control*, (1991) **1**, 35-52.

[5.5] A.I. Mees, *Dynamics of Feedback Systems*, Wiley, New York, 1981.

[5.6] J. Baillieul, R.W. Brockett and R.B. Washburn, Chaotic motion in nonlinear feedback systems, *IEEE Trans. Circuits and Systems* (1980) **CAS-27**, 990-997.

[5.7] R. Genesio and A. Tesi, Harmonic balance methods for the analysis of chaotic dynamics in nonlinear systems, *Automatica* (to appear).

[5.8] A. Mohan and M. Ahmadian, Nonlinear investigation of the effect of primary suspension on the hunting stability of a rail wheelset, *Proceedings of the 2004 ASME/IEEE Joint Rail Conference* (2004), 53-61.

[5.9] H. True, Some recent developments in nonlinear railway vehicle dynamics, in *Proc. 1st European Nonlinear Oscillation Conference*, Hamburg, Germany (1993), 129-148.

[5.10] H. True and R. Asmund, The dynamics of a railway freight wagon wheelset with dry friction damping, *Vehicle System Dynamics* (2002) **38**, 149-163.

[5.11] C. Knudsen, R. Feldberg and H. True, Bifurcations and chaos in a model of a rolling railway wheelset, *Philosophical Transactions of the Royal Society A* (1992) **338**, 455-469.

[5.12] H.G. Davies and K. Rangavajhula, Noisy parametric sweep through a period-doubling bifurcation of the Hénon map, *Chaos, Solitons and Fractals* (2002) **14**, 293-299.